

11

---

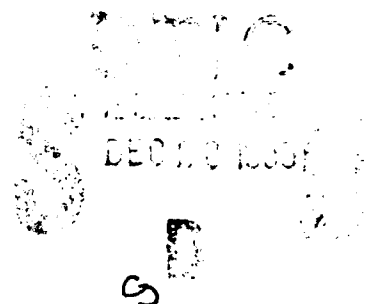
# Marine Physical Laboratory

DTIC FILE COPY

AD-A230 171

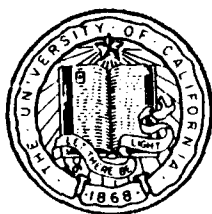
## Digital, One Way, Acoustic Communication in the Ocean

Amos A. Dotan



SIO Reference 90-30  
September 1990

*Approved for public release; distribution unlimited.*



University of California, San Diego  
Scripps Institution of Oceanography

---

UNCLASSIFIED

SECURITY CLASSIFICATION OF THIS PAGE

## REPORT DOCUMENTATION PAGE

Form Approved  
OMB No. 0704-0188

1a. REPORT SECURITY CLASSIFICATION UNCLASSIFIED			1b. RESTRICTIVE MARKINGS		
2a. SECURITY CLASSIFICATION AUTHORITY			3. DISTRIBUTION / AVAILABILITY OF REPORT Approved for public release; distribution unlimited.		
2b. DECLASSIFICATION / DOWNGRADING SCHEDULE					
4. PERFORMING ORGANIZATION REPORT NUMBER(S) SIO Reference 90-30			5. MONITORING ORGANIZATION REPORT NUMBER(S)		
6a. NAME OF PERFORMING ORGANIZATION University of California, San Diego		6b. OFFICE SYMBOL (If applicable) MPL	7a. NAME OF MONITORING ORGANIZATION Office of Naval Research Department of the Navy		
6c. ADDRESS (City, State, and ZIP Code) Marine Physical Laboratory Scripps Institution of Oceanography San Diego, California 92152			7b. ADDRESS (City, State, and ZIP Code) 800 North Quincy Street Arlington, VA 22217-5000		
8a. NAME OF FUNDING / SPONSORING ORGANIZATION Office of Naval Research		8b. OFFICE SYMBOL (If applicable) ONR	9. PROCUREMENT INSTRUMENT IDENTIFICATION NUMBER N00014-88-K-2040		
8c. ADDRESS (City, State, and ZIP Code) 800 North Quincy Street Arlington, VA 22217-5000			10. SOURCE OF FUNDING NUMBERS		
			PROGRAM ELEMENT NO.	PROJECT NO.	TASK NO.
					WORK UNIT ACCESSION NO.
11. TITLE (Include Security Classification) DIGITAL, ONE WAY, ACOUSTIC COMMUNICATION IN THE OCEAN					
12. PERSONAL AUTHOR(S) Amos A. Dotan					
13a. TYPE OF REPORT dissertation		13b. TIME COVERED FROM _____ TO _____		14. DATE OF REPORT (Year, Month, Day) September 1990	
15. PAGE COUNT 161					
16. SUPPLEMENTARY NOTATION					
17. COSATI CODES			18. SUBJECT TERMS (Continue on reverse if necessary and identify by block number)		
FIELD	GROUP	SUB-GROUP			
			underwater telemetry, acoustic communication, channel modeling, equalization		
19. ABSTRACT (Continue on reverse if necessary and identify by block number)					
<p>This dissertation summarizes the work done on developing methods for underwater telemetry, between two freely drifting stations, in the presence of a slowly time-varying, frequency-selective fading channel and strong multipath.</p> <p>At sea experiments conducted during 1989-90 show that the acoustic communication channel suffers from strong frequency-selective fading and strong multipath on the order of seconds. Moreover, most of the time, the intensity of the received signal due to the first multipath is much stronger than the received direct signal.</p> <p>In order to establish a reliable communication channel in the presence of strong fading, diversity must be used. DPSK chirp modulation proved to be superior over all other frequency diversity methods. Moreover, it is shown that a chirp QDPSK with bandwidth expansion of 5 has better performance than a combination of an error correcting code and frequency diversity method with similar bandwidth expansion. The achieved bit error rate when a chirp DPSK is used in the presence of frequency selective fading is the same as that of a conventional DPSK modulation in the presence of AWGN.</p>					
20. DISTRIBUTION / AVAILABILITY OF ABSTRACT <input type="checkbox"/> UNCLASSIFIED/UNLIMITED <input checked="" type="checkbox"/> SAME AS RPT. <input type="checkbox"/> DTIC USERS			21. ABSTRACT SECURITY CLASSIFICATION UNCLASSIFIED		
22a. NAME OF RESPONSIBLE INDIVIDUAL William S. Hodgkiss			22b. TELEPHONE (Include Area Code) (619) 534-1798		22c. OFFICE SYMBOL MPL

Both bit synchronization and equalization methods which take into consideration the multipath and fading effects, are proposed. The major problem with bit synchronization is the destructive effect of the micromultipath that causes large time jitter. A modified version of a method that uses time of arrival estimation is proposed. Two phenomena cause the equalizer for an underwater acoustic communication link to be totally different from all well-known equalizers. The first is the huge delays between the direct path and the multipaths which reach the order of thousands of bits. The second is that the first multipath is stronger than the direct path which causes the channel to have an unstable impulse response. The proposed equalizer is a combination of decision feedback and forward equalizer. This combination solves the problem of the instability on one hand and has the minimum number of taps on the other.

Real data modulated by the chirp DPSK modulation was transmitted through the ocean, received, and analyzed. The achieved bit error rate was almost the same as predicted theoretically.

UNIVERSITY OF CALIFORNIA, SAN DIEGO

Digital, One Way, Acoustic Communication  
in The Ocean

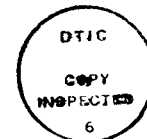
A dissertation submitted in partial satisfaction of the  
requirements for the degree Doctor of Philosophy  
in Electrical Engineering  
(Communication Theory and Systems)

by

Amos A. Dotan

Committee in charge:

Professor Victor C. Anderson  
Professor Lawrence B. Milstein  
Professor Jack K. Wolf  
Professor Andrew J. Viterbi  
Professor William S. Hodgkiss, Jr., Chairman



Accession For	
NTIS CRA&I	<input checked="checked" type="checkbox"/>
DTIC TAB	<input type="checkbox"/>
Unannounced	<input type="checkbox"/>
Justification	
By	
Distribution /	
Availability Codes	
Dist	Avail and/or Special
A-1	

1990

Copyright 1990

by

Amos A. Dotan

The dissertation of Amos A. Dotan is approved,  
and it is acceptable in quality and form for publication on  
microfilm:

---

---

---

---

---

Chair

University of California, San Diego

1990

**To my wife Yaffa and my kids Efrat and Omri**

## Table of Contents

Signature Page .....	iii
Dedication Page .....	iv
Table of Contents .....	v
List of Figures .....	viii
List of Tables .....	x
Acknowledgements .....	xi
Vita and Publications .....	xii
Field of Study .....	xiii
Abstract .....	xiv
<b>I Introduction .....</b>	<b>1</b>
I.1 General .....	1
I.2 Underwater acoustic telemetry - overview .....	2
<b>II Channel Characterization and modeling .....</b>	<b>9</b>
II.1 General .....	9
II.2 Channel characterization .....	12
II.3 Channel character - experimental results .....	14
II.3.1 The channel multipath characteristics .....	18
II.3.2 Time variation properties of the channel .....	23
II.3.3 The frequency selectivity properties of the channel .....	26
II.4 Channel modeling .....	34

<b>III Modulation approach .....</b>	<b>36</b>
III.1 Introduction .....	36
III.2 Frequency diversity techniques for selective fading channel .....	36
III.2.1 The combining method .....	37
III.2.2 Switch diversity .....	42
III.3 Special modulation techniques .....	44
III.3.1 Combined Modulation and coding .....	44
III.3.2 Chirp as a frequency diversity technique .....	45
III.3.3 Unequal bit error rate method .....	50
III.4 Do we need Error correction .....	54
III.5 Combined chirp DPSK and error correction .....	56
<b>IV Synchronization .....</b>	<b>58</b>
IV.1 Introduction .....	58
IV.2 The optimum bit synchronizer .....	61
IV.2.1 System performance .....	64
IV.3 Bit synchronization using time of arrival estimation method .....	70
<b>V Equalization .....</b>	<b>82</b>
V.1 Introduction .....	82
V.2 An LMS equalizer for underwater acoustic channel .....	85
V.2.1 Filter's weight calculation .....	89
V.3 Error propagation problem .....	91
V.4 Simulation results .....	95
<b>VI Examples and discussion of results .....</b>	<b>101</b>

VI.1 Real data analysis .....	107
Appendix-A - Chirp as a frequency diversity technique .....	110
Appendix B - Performance of several common error correction codes .....	132
Appendix C - Proof of equation 3.16 .....	136
Appendix D - Optimal power assignment .....	137
References .....	139

## List of Figures

### Chapter I

1.1 Attenuation of electromagnetic radiation in clear water .....	3
1.2 Low frequency acoustic attenuation coefficient .....	4

### Chapter II

2.1 Experiment setup .....	15
2.2 Projector and monitor hydrophone location .....	15
2.3 Time series and power spectrum of an 8 msec long chirp waveform .....	17
2.4 Typical received signal .....	19
2.5 Typical channel multipath character .....	19
2.6 Typical time variation of channel multipath character (first 20 msec). ....	21
2.7 Typical time variation of channel multipath character, (time slice between 370 and 530 msec) .....	22
2.8 The square magnitude coherency function of the channel as a function of time .....	24
2.9 The spectra of 28 -8 msec chirp, signals received sequentially (one every 4 second). ....	25
2.10 Amplitude variation of nine tones, 50 and 100 Hz apart .....	27
2.11 Amplitude variation of nine tones, 250 and 500 Hz apart .....	28
2.12 Amplitude variation of nine tones, 1 kHz apart .....	29
2.13 The correlation between the envelopes of nine tones and the central tone, for the five sets of tones .....	30
2.14 Histograms of the envelopes of the 250 Hz spaced tones .....	31
2.15 Histograms of the envelopes of the 1 kHz spaced tones .....	32
2.16 Histograms of the 15 kHz tone, at different time periods .....	33
2.17 A simplified model of an underwater acoustic communication channel. ....	34

### Chapter III

3.1 Coherent binary FSK receiver with L combined channels .....	38
3.2 Incoherent binary FSK receiver with L combined channels .....	39
3.3 BPSK receiver with L combined channels .....	39
3.4 Bit error probability of binary incoherent FSK with L order diversity as a function of SNR .....	41
3.5 Bit error probability of binary coherent FSK with L order diversity, as a function of SNR .....	42
3.6 Combining coding and modulation - block diagram. ....	44
3.7 Suboptimum binary DPSK demodulator. ....	46
3.8 Optimum binary DPSK demodulator. ....	46
3.9 Bit error rate of 2,4,8,16 and 32-ary DPSK .....	48
3.10 Comparison of 4-ary Chirp DPSK with various types of combined modulated and coded waveforms .....	49
3.11 Bit energy allocation that gives minimal M.S.E for 12 bits D/A converter and BDPSK modulation .....	52
3.12 Comparison of the M.S.E when equal bit energy is used and the optimal M.S.E, for 12 bit A/D converter. ....	53
3.13 Spectra of chirp signals with time-bandwidth product of 5 and 10. ....	57

## Chapter IV

4.1 Bit sy. chronization - Block diagram of a suboptimum scheme .....	62
4.2 Bit synchronizer - estimation error .....	66
4.3 The equivalent lowpass match filter output - $g(t)$ .....	69
4.4 The normalized error standard deviation as a function of the signal to noise ratio for different values of $K$ . ....	70
4.5 Bit synchronization - Spectrum of the lowpass filter output .....	71
4.6 Bit synchronization - Autocorrelation implementation .....	72
4.7 Error state diagram .....	76
4.8 $\Lambda$ as a function of Signal to Noise Ratio for various values of ' $k$ ', $\delta$ and for $\alpha=0$ .....	78
4.9 $\Lambda$ as a function of Signal to Noise Ratio for various values of ' $k$ ', $\delta$ and for $\alpha=0.25\pi$ .....	79
4.10 $\Lambda$ as a function of Signal to Noise Ratio for various values of ' $k$ ', $\delta$ and for $\alpha=\pi$ .....	80
4.11 $\Lambda$ as a function of Signal to Noise Ratio for various values of ' $k$ ', $\delta$ and for $\alpha$ changes very rapidly. ....	81

## Chapter V

5.1 A block diagram of an underwater channel equalizer. ....	87
5.2 The relationship between the decision of the present and the previous bits ....	94
5.3 Equalizer weights calculated directly from (5.36) and (5.37) .....	97
5.4 Equalizer weights calculated using the Wiener-Hopf equation (noiseless channel) .....	98
5.5 Equalizer weights calculated using the LMS algorithm (500 iterations), in noiseless channel. ....	99
5.6 Equalizer weights calculated using the LMS algorithm (500 iterations), ( $\frac{E_b}{N_0} = 10dB$ ). ....	100

## chapter VI

6.1 The spectrum and the phase of a chirp signal with $BT = 10$ . ....	103
6.2 Comparison between various diversity method and chirp DPSK modulation. ....	104
6.3 Implemented DPSK receiver - block diagram. ....	107
6.4 Power spectral density of the ambient noise (after bandpassing) .....	108
6.5 Comparison between theoretical and achieved bit error rate. ....	109

## Appendix A

A.1 incoherent "BFSK" Receiver .....	112
A.2 Binary Chirp DPSK Receiver. ....	118
A.3 The calculated probability density function of $\gamma$ for various values of $K$ and $\hat{\gamma}_b = 10 \text{ dB}$ . ....	122
A.4 The probability density function of $\gamma$ for $K = 4$ and $\hat{\gamma}_b = 10 \text{ dB}$ . Comparison between calculated and simulated results. ....	123
A.5 The bit error probability of a chirp DPSK as a function of $\hat{\gamma}$ for various values of $K$ . ....	124
A.6 The bit error probability of a 4-Phase chirp DPSK as a function of $\hat{\gamma}$ .....	125
A.7 Indirect path effect on the BER of chirp BDPSK modulation for $\alpha = 0.5$ and $\theta = \pi$ . ....	128

A.8 Motion effect on the BER of chirp BDPSK modulation. ....	131
--	-----

## Appendix B

B.1 Bit error probability versus channel error probability for block length $n=2^m-1$ Hamming codes with $m=3,4$ , and 5 .....	132
B.2 Block, and bit error probabilities versus channel error rate with extended Golay coding. ....	133
B.3 Bit error probability versus channel error rate performance of several block length 127, BCH codes .....	134
B.4 Bit error probability versus channel error rate performance of several convolutional coding systems. ....	135

## List of Tables

### Chapter 5

5.1 possible combinations of present, previous, and detected bits. ....	93
---	----

## ACKNOWLEDGEMENTS

I wish to thank Dr. Hodgkiss for supervising my work during the past three years with thoughtful advices and encouragements, and for his patience while dealing with my language difficulties. Without him, this study would not have been completed.

Throughout the three years at UCSD, I have been supported by RAFAEL. I appreciate the opportunity provided to me by this institution which enabled me to broaden my horizons and achieve the Ph.D degree. Special thanks to John McInerney and Eric Wolin for introducing me to the world of the MPL computer environment. Their continuous help significantly facilitated my research.

I enjoyed the company and insightful discussions with my colleagues Jean-Marie Tran and Gerald D'spain from MPL, and Sreenivasa Raghavan, Lynn Gotesman and Mooi-Choo Chuah with whom I spent many hours in preparing for exams, and with whom I shared and discussed ideas.

David Almagor and Shimon Tzukerman with whom I shared my office provided a friendly and pleasant environment. Special thanks to Marving Darling, Greg Edmonds, and Chris Nickles for preparing all the sea experiments and suffering with me while we were out at sea.

I would like to thank my parents; my mother Chava and my father Jacob who raised me, educated me and consistently encouraged me to go further.

Last, but not least, I am indebted to my wife Yaffa and my children Efrat and Omri. They were always supportive and encouraging in spite my endless working hours and occasional bad moods. To whom , with love, I dedicate this work.

This work was supported by the Office of Naval Research under contract N00014-88-K-2040.

## VITA

March 23, 1950 Born, Haifa, Israel

- |           |  |
|-----------|--|
| 1970      | Practical Engineer in Electrical Engineering,<br>vocational college "ORT Yad A. Singalovsky",<br>Tel-Aviv, Israel.         |
| 1974-1977 | working as a practical Engineer for the Israeli Defense<br>Forces.   |
| 1974-1977 | B.Sc in Electrical Engineering,<br>Tel-Aviv University.  |
| 1977-     | Employed by Rafael, A.D.A, as an Electrical Engineer.  |
| 1982      | M.Sc degree in Electrical Engineering,<br>Technion - Israel Institute of Technology, Haifa, Israel.                        |
| 1982      | Rafael, Advanced communication system research group leader  |
| 1988-1990 | Research Assistant at the Marine Physical Laboratory of the<br>Scripps Institution of Oceanography, San-Diego, California. |
| 1990      | Doctor of Philosophy in Electrical Engineering,<br>University of California, San-Diego.                                    |

## PUBLICATIONS

- I. Rusnak, A. Dotan, "Effectiveness of Repeater Jammer Against Noncoherent BFSK Demodulator". IEEE International Symposium on Information Theory, June 24-28, 1985.
- I. Rusnak, A. Dotan "Performance of Transponder Jammer against Noncoherent FSK Receiver". IEEE, The Fifteenth Convention of Electronics Engineers in Israel, Tel-Aviv, April 7-9, 1987.
- A. Dotan, W.S. Hodgkiss, "Coherence of transients",MPL TM-422, San-Diego, July 1990.
- A. Dotan, W.S. Hodgkiss, "Equalization of a non-minimum phase underwater acoustic communication channel" submitted for publication in the IEEE, Journal of Oceanic Engineering, special issue on Acoustic Telemetry.

## **FIELDS OF STUDY**

Major Field: Electrical Engineering

Studies in Communication Systems

Professors Lawrence B. Milstein

Studies in Digital Signal Processing and Array Processing.

Professor William S. Hodgkiss

Studies in Detection and Estimation Theory

Professor Carl W. Helstrom

## ABSTRACT OF THE DISSERTATION

Digital, One Way, Acoustic Communication  
in The Ocean

by

Amos A. Dotan

Doctor of Philosophy in Electrical Engineering

(Communication Theory and Systems)

University of California, San Diego, 1990

Professor William S. Hodgkiss, Jr., Chair

This dissertation summarizes the work done on developing methods for underwater telemetry, between two freely drifting stations, in the presense of a slowly time-varying, frequency-selective fading channel and strong multipath.

At sea experiments conducted during 1989-90 show that the acoustic communication channel suffers from strong frequency-selective fading and strong multipath on the order of seconds. Moreover, most of the time, the intensity of the received signal due to the first multipath is much stronger than the received direct signal.

In order to establish a reliable communication channel in the presense of strong fading, diversity must be used. DPSK chirp modulation proved to be superior over all other frequency diversity methods. Moreover, it is shown that a chirp QDPSK with bandwidth expansion of 5 has better performance than a combination of an error correcting code and frequency diversity method with similar bandwidth expansion. The achieved bit error rate when a chirp DPSK is used in the presense of frequency selective

fading is the same as that of a conventional DPSK modulation in the presense of AWGN.

Both bit synchronization and equalization methods which take into consideration the multipath and fading effects, are proposed. The major problem with bit synchronization is the destructive effect of the micromultipath that causes large time jitter. A modified version of a method that uses time of arrival estimation is proposed. Two phenomenon cause the equalizer for an underwater acoustic communication link to be totally different from all well-known equalizers. The first is the huge delays between the direct path and the multipaths which reach the order of thousands of bits. The second is that the first multipath is stronger than the direct path which causes the channel to have an unstable impulse response. The proposed equalizer is a combination of decision feedback and forward equalizer. This combination solves the problem of the instability on one hand and has the minimum number of taps on the other.

Real data modulated by the chirp DPSK modulation was transmitted through the ocean, received, and analyzed. The achieved bit error rate was almost the same as predicted theoretically.

# I INTRODUCTION

## I.1 General

During the last two decades, impressive success has been achieved in communicating and transmitting data between any two places on earth. Great success has been achieved in transmitting and receiving high quality video pictures from the moon and even from farther in the universe, but much less attention has been paid to underwater communication.

The major reason for the difficulties and the poor performance in underwater communication is due to the fact that the acoustic channel is very complex. High attenuation, strong multipath, and fading effects cause the underwater acoustic channel to be almost useless as a channel for transmitting acoustic data.

As part of a program undertaken at the Marine Physical Laboratory, an underwater communication link between two freely drifting sensors was required. The basic requirements of the link were the following:

- a) Operating frequency 10 - 20 kHz.
- b) Operating range 2 - 5 km
- c) Bit rate of 1 kbit/sec
- d) Source level 170 dB/1 $\mu$ Pa
- e) Water depth 4000 m
- d) Receiver depth 300 m
- e) Transmitter depth 500 m

The objective of this research was to develop an underwater acoustic link that gives reliable performance under the channel constraints.

Chapter 1 of this thesis gives a brief review of past and present efforts in developing underwater communication systems. In Chapter 2 we summarize the results of three at-sea experiments which were conducted during 1989-90. By using the experimental results, a simplified model of the underwater acoustic communication channel is obtained. Chapter 3 deals with modulation techniques that are efficient in a strong fading environment. It is shown that under the assumption of slowly time-varying, frequency-selective fading, the chirp DPSK modulation technique is a superior modulation scheme for combating the fading phenomena. Chapter 4 and 5 propose bit synchronization and equalization methods that are suitable to the assumed channel. Chapter 6 summarizes the results of at-sea experiments in which the proposed chirp DPSK modulation scheme was implemented.

## I.2 Underwater acoustic telemetry - overview

Two years before Columbus discovered America, Leonardo da Vinci wrote: *If you cause your ship to stop, and place the head of a long tube in the water and place the outer extremity to your ear you will hear ships at a great distance from you.* Until at the turn of this century, essentially no improvement was made in the science of underwater sound. Scientific research using diving bells and the beginning of the submarine generation motivated researches to seek better ways to communicate underwater.

Although underwater echo detection schemes emerged prior to World War I, World War II ushered in the modern age of underwater sound exploitation. But even then the water medium was used primarily for sound navigation and ranging (SONAR).

In the past, most of the incentive for underwater communication has come from the requirements associated with submarines. Now there are very rapidly growing requirements for commercial applications, wireless command and control of unmanned vehicles, high data rate video transmission, and communication with deep divers and scientific instruments moored deep in the ocean.

Conventional telemetry employs either electrical signals transmitted over closed wire systems or some form of electromagnetic radiation (radio wave, microwaves, etc.). The former method is inconvenient at sea and latter is impractical due to the high attenuation imposed upon the entire electromagnetic spectrum by sea water. Figure 1.1<sup>5</sup> shows that only the visible region holds any promise for underwater telemetry and even then in the practical environments, the measured values of the absorption coefficients far exceed the clean water values.

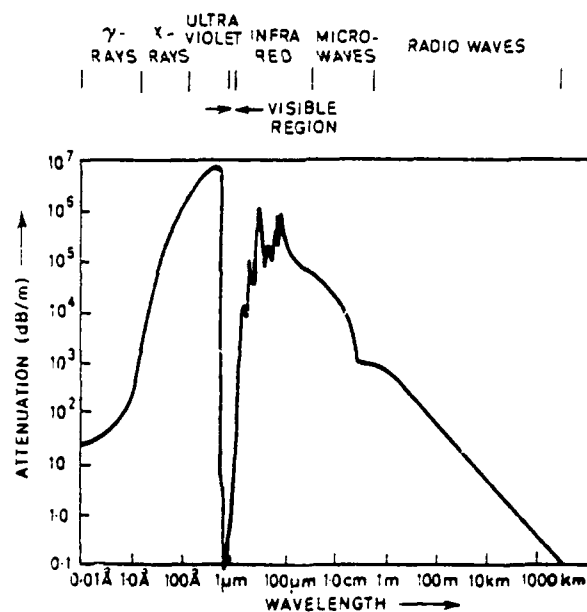
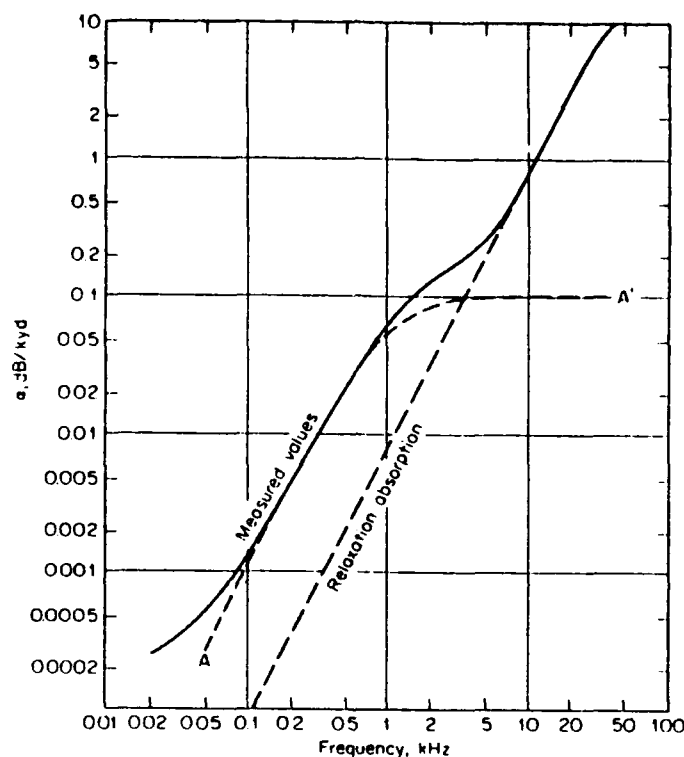


Figure 1.1 Attenuation of electromagnetic radiation in clear water<sup>5</sup>.

Therefore, it is clear that the carrier signal must be an acoustic transmission

since the attenuation imposed by sea water is much less severe provided that the frequency is restricted to below 100 kHz (See Figure 1.2 [ Urick<sup>85</sup> Fig 5.3 ])



**Figure 1.2** Low frequency acoustic attenuation coefficient<sup>85</sup>

Although prone to echo interference, signal spreading and Doppler frequency shift, acoustic signaling is the oldest and the most successful form of cableless underwater communication, because of the relatively low attenuation in the water.

The first underwater communication system was a telephone developed in 1945 at the Naval Underwater Sound Laboratory. This underwater telephone had been designed to communicate with submerged submarines and employed the upper sideband of an 8.3 kHz U.S.S.B system. In the subsequent 15 years, similar systems

appeared using the frequency range of 8-11 kHz with analog modulation, most of them using AM or SSB modulation. Considerable amount of transmitter power up to some hundreds of watts was employed to obtain a range of a few kilometers. From these first operational systems, military underwater acoustic communication has moved toward lower frequencies that permit transmission over longer ranges or higher frequencies which enable higher information rate.

Over the years, various forms of acoustic communication systems have been developed. These have included direct AM and SSB for underwater telephones, or FM for sensor data. The difficulties of AM in the presence of multipath and dispersion were recognized and experiments with frequency modulation, analog as well as digital, have been made. Before shifting to digital modulation techniques, researchers have partially succeeded in transmitting a wide variety of information. A direct-path FM acoustic television link was demonstrated by the Ball Brothers Company in 1968, where an information rate of tens of kHz was achieved for several kilometers of water path. Also, of the more secure command control links, with data rates as low as 1 bit/sec or less but with high reliability have been achieved in severe multipath environment.

At the same time, experiments in telemetry over a vertical path from sensors lowered down to a hydrophone suspended from a surface ship were in progress. As the phenomenon of multipath is less dominant in the vertical direction, reasonable results have been achieved. A 21 kHz carrier amplitude modulation was used in a system which was used to communicate between a surface ship and a 1800 foot deep hydrophone<sup>29</sup>. Tested in 1966, Performance of another system, using FSK modulation with a carrier frequency of 40 kHz and achieving data rate up to 45 bit/sec was reported by Hearn<sup>40</sup>.

Over the last several years, there have been many attempts at designing more reliable communication systems using digital modulation techniques. It became clear that analog as well as digital modulation techniques using amplitude modulation perform inadequately in most underwater applications because of the destructive nature of the underwater channel. Therefore most of the effort has been directed toward digital systems which use different kinds of frequency modulation.

When low data rate was required for control telemetry, undersea navigation, and positional systems, relatively simple underwater acoustic communication systems yielded reliable performance. Problems arise when data rates increase or transmission have long range multipath echos. The destructive nature of the acoustic channel causes significant interference which severely limits the achievable system performance. In the past, many techniques for combating the multipath problem have been proposed. At low data rates, careful selection of antimultipath scheme will suffice. High data rate telemetry, however, is a special case in that many of the conventional methods cannot be employed.

High data rates, on the order of several kbits/sec, require correspondingly high transmission bandwidths. This forces the use of high carrier frequency signals. Unfortunately, rapid attenuation of the acoustic signal limits these frequencies to no more than a couple of hundred of kHz. Over the last 15 years, digital techniques for underwater communication have been widely used and few underwater high data rate communication systems have been designed and developed for command and control, speech transmission, video data and telemetry information. Pioneering work has been done at the Woods Hole, Oceanographic Institute<sup>2,73</sup>

The nature of the underwater acoustic channel prevents the use of coherent modulation. Hence non-coherent FSK modulation is the most commonly used modulation method<sup>47</sup>. The MT-300, designed and built at Honeywell<sup>36</sup>. for a wireless high

security and high reliable control system, achieved good performance using FSK modulation with frequency diversity. Tested in 1982, the ATDL<sup>79</sup> is another acoustic telemetry system which uses noncoherent FSK modulation. This achieves high reliability by using a smart answer back communication protocol.

Significant progress in underwater communication systems is achieved when anti multipath modulation and coding techniques are used. In 1981, Wax<sup>88</sup> demonstrated an MFSK system using a 15 kHz carrier with a bandwidth of 3 kHz. A low data rate was achieved (40 bits/sec) over a long distance (up to three miles) with very low bit error rate ( $10^{-5}$ ). A method proposed by Pieper et al<sup>71</sup> is now under development at Woods Hole<sup>15,16</sup> where a data rate of 10 kbits/sec over 10 km in shallow water is expected to be achieved.

Another method of combating the multipath problem is by using spread spectrum techniques. A commercial telemetry system using frequency hopping has been proposed by Datasonics. A different spread spectrum technique implementation for underwater communication has been presented by W. Hill.<sup>42</sup> This system uses a chirp FSK modulation as a way to combat multipath and fading.

Less successful results have been achieved in developing systems for acoustic telemetry of video information. Since relatively high bit rate is required to transmit video information, reasonable performance is achieved only in limited scenarios.

The first attempt at sending TV pictures through the water appears to be the Cutlink experiments<sup>10</sup> performed in 1968-9. Both analog and digital FM signals modulated a carrier frequency of 15 kHz with a total bandwidth of 3 kHz. Using 15 watts radiated power, a data rate of 2.5 kbits/sec for a vertical path of up to 6 km was achieved. Collins<sup>23</sup> describes an acoustic telemetry system for video information which uses a narrow beam acoustic link to transmit slow scan video frames for a dis-

tance of up to 30 meters. The transducer projected the beam at an angle of  $10^\circ$  down from, horizontal with a source level of 234.5 dB @ 1  $\mu$  Pa at 1m. In the presence of weak multipath, good quality frames were received continuously at 8.5 seconds intervals.

R. M. Dunbar<sup>30</sup> reports experiments transmitting T.V pictures at very high data rate. A self-contained TV telemetry system which works in the vertical direction (from bottom to surface and vice versa) was presented by B. Leduc and G. Ayela<sup>51</sup> in 1990. This system works at 21 kHz and uses various kinds of PSK modulation. The operating range is up to 6 km depth and the maximum data rate is 9.6 kbit/sec (19.2 kbit/sec at 2 km depth). The effective source level is 165 dB @ 1 Pa at 1 m, 1 volt.

Underwater communication equipment has a wide variety of applications and many companies have developed specific products such as SONALINK<sup>50</sup> and PASTY<sup>33</sup>.

## II Channel characterization and modeling

### II.I General

The first step in designing a complete communication system is to characterize the medium through which the data is to be transmitted. From this knowledge, a model of a communication channel can be developed and thus an expression for the received signal can be found

The ocean is far from being the ideal medium for sound propagation. Its vertical velocity gradient causes the transmitted energy to be refracted. Some times, communication between two, points can be impossible due to the formation of shadow zones. Also, the carrier frequency is subject to a randomly fluctuating Doppler shift as a result of surface and internal waves. However, the signal is, most seriously distorted by multipath propagation. It describes a condition which causes the signals from a given transmitter to be received via a number of different paths with each path having a different time delay.

Two major factors contribute to this multipath propagation. First the ocean is inhomogeneous. Its own wave motion breaks up the surface layer and produces a turbulent and thermal microstructure consisting of a random distribution of small patches of water with slightly differing temperatures which are continually in motion. This inhomogenities yield variations in the acoustic refractive index. Thus it is possible for several signals each radiated in slightly different initial directions to be refracted in such a way that they all arrive at the receiver where interference occurs due to the multiplicity of signal transmit times and hence relative phases

involved. Often referred to as forward scattering or fading. This phenomenon produces random fluctuations in both the amplitude and phase of the carrier signal which become progressively more troublesome as range increases. Usually, the signal amplitude follows a Rayleigh distribution. In some special cases where a single multipath is particularly strong, the signal amplitude follows a Rayleigh Rice distribution.

The second factor is specular reflection from boundaries such as the ocean surface, bottom, and the interface between the water and man-made objects. Specular reflection can be strong approaching the strength of the direct signal or even more<sup>55</sup>. The transit time delays associated with these echoes also are often much longer than the direct signal. Particularly troublesome are the reflections from the surface which not only fluctuate greatly but, due to the instantaneous surface shapes, can have amplitude in excess of the direct signal. Multiple reflections also are possible and usually occur between the surface and the bottom in shallow water. Propagation delay also is produced by reflection from the boundaries of the ocean. Apart from the direct path it is also possible for sound to travel between the transmitter and the receiver after being reflected from a large number of favorable surfaces. The multipath phenomenon results in the reception of several delayed replicas of the original transmitted signal. These delayed replicas which often are stronger than the direct signal itself cause strong intersymbol interference (ISI).

The effect of multipath propagation on the signal pulse is to spread it in time, the pulse spreading being determined by the maximum difference in the transit delays associated with the various paths. Relative movement in parts of the medium which causes the multipath propagation to come about results in a difference in the frequencies of the signal arriving via different paths (Doppler-shift). Thus a modulated signal suffers a time spreading due to the differential time delays and a

frequency spreading due to different Doppler shifts arising on the various paths.

As mentioned previously, if a single sine wave is transmitted through such a channel, the received signal is the resultant of a number of sine waves of slightly different frequencies which have been subjected to different time delays. As a result, the amplitude and the phase of the received signal fluctuate in a random manner. The amplitude fluctuations (fading) of the sine waves of different frequencies transmitted through such a channel are correlated if the frequency difference is not greater than the inverse of the pulse spreading in the channel. Hence, a band limited signal with a bandwidth which does not exceed the inverse of the pulse-spreading in a multipath channel, retains its frequency spectrum (apart from an ambiguity arising from the Doppler shift and the Doppler spreading), when transmitted over such a channel. Therefore, the inverse of the pulse spreading can be termed as the coherent bandwidth of the channel. If the signal bandwidth increases beyond this value, the various frequency components of the signal fade in an uncorrelated manner, causing the signal to be distorted.

If all the spectral components of the signal fluctuate in a correlated manner flat fading of the signal occurs and the channel is defined as a frequency nonselective channel. Lack of correlation of the fluctuation characteristics of different frequency components signifies frequency selective fading of the signal. The underwater acoustic channel is a time varying channel. Fading and multipath behavior change with time. A channel in which the changes are very slow is defined as a slowly time-varying channel. A channel which changes its behavior rapidly is defined as a fast time varying channel.

The behavior of the channel in the time domain depends on the operating scenario and the environment of the communication system. If the receiver and the transmitter do not change their position during the operation, the channel is a very

slowly time-varying channel, and the time constant of the channel is in the order of some hundreds of milliseconds. If the receiver and /or the transmitter move and change their position during the operation, the channel becomes a fast time-varying channel.

## II.2 Channel characterization

The effect of fading on the transmitted signal is usually modeled as a linear time-varying filter. By employing a narrowband signal model, the input to the channel is given by

$$S(t) = \text{Re} \left\{ \bar{S}(t) \exp(j\omega_c t) \right\} . \quad (2.1)$$

when  $\text{Re}(\cdot)$  denotes the real part of  $(\cdot)$ . The output is given by:

$$Y(t) = \text{Re} \left\{ \bar{Y}(t) \exp(j\omega_c t) \right\} \quad (2.2)$$

where:

$$\bar{Y}(t) = \alpha \bar{S}(t) + \int_{-\infty}^{+\infty} h(t-\tau; t) \bar{S}(\tau) d\tau + \bar{n}(t) , \quad (2.3)$$

and,  $h(\tau; t)$  is the lowpass (complex) impulse response of the fading channel.  $\tau$  represents the usual filter response variable and the  $t$  - dependence indicates that the very structure of the impulse response changes with time<sup>84</sup>.  $h(\tau; t)$  is modeled as a complex, zero mean Gaussian random process. Hence it has Rayleigh amplitude and uniform phase distribution. The Fourier transform of  $h(\tau; t)$  with respect to  $\tau$ ,  $H(f; t)$ , is the time-varying equivalent lowpass transfer function of the channel.  $H(f; t)$  is also a zero mean, complex Gaussian random process. In addition to the transfer function,

the channel (or the fading process) is characterized by the ensemble autocovariance,  $R_T(\tau_1, \tau_2; t_1, t_2)$ , of the channel impulse response,  $h(\tau, t)$ . In most cases, the channel is assumed to be wide sense stationary in both dimensions, i.e.

$$R_T(\tau_1, \tau_2; t_1, t_2) = R_T(\tau; \Delta t)$$

where,  $\tau \equiv \tau_1 - \tau_2$  and  $\Delta t \equiv t_1 - t_2$ .

Another expression which is used to characterize the fading channel is the spaced-tone complex covariance which is defined as:

$$R_F(f_1, f_2; t_1, t_2) = E \left\{ H(f_1; t_1) H^*(f_2; t_2) \right\} . \quad (2.4)$$

This expression characterizes the relationships of values of the transfer function at different frequencies and at different times. Under the assumption of stationarity,

$$R_F(f_1, f_2; t_1, t_2) = R_F(\Delta f; \Delta t) .$$

A measure of the degree of frequency selectivity commonly employed in the literature is the distance  $\rho_H$  between the  $\frac{1}{e}$  points of the frequency correlation function<sup>35</sup>.

In most cases,

$$R_F(\Delta f; \Delta t) = R_f(\Delta f) R_t(\Delta t) . \quad (2.5)$$

For  $R_t(\Delta t)$  which is almost constant during the observation time, the fading is known as very slowly time varying fading. When  $R_f(\Delta f)$  is constant (i.e not frequency dependent), the fading is known as frequency nonselective fading. When  $R_f(\Delta f)$  is such that  $\rho_H$  is much smaller than the data bandwidth, the fading is known as frequency selective fading. The ratio between the available channel bandwidth and  $\rho_H$  is the amount of diversity that the channel provides and is defined as  $K$ . In the most general case of fading, the received signal  $Y(t)$  consists of two components: a single specular component and a diffuse Rayleigh distributed component. When  $\alpha$  in (2.3) is zero, only the diffuse component of fading exists. In this case,  $Y$  in (2.4) is a Rayleigh random process with the following distribution function:

$$P(y) = \frac{y}{\sigma^2} \exp\left[-\frac{y^2}{2\sigma^2}\right] U(y), \quad (2.6)$$

where  $U(\cdot)$  is the unit step function. Defining  $z \equiv \frac{y^2}{2}$ , we have

$$P(z) = \frac{1}{\sigma^2} \exp(-z) U(z). \quad (2.7)$$

The fading phenomena has been well explored in connection with electromagnetic communication links. Most of the effort has been directed toward a deep understanding of the fading phenomena and its aspects in frequency ranges used in radio communication. Relatively little information has been published in the literature describing and analyzing the fading phenomena and the character of the underwater acoustic communication channel.

### II.3 Channel character - experimental results

During 1989-1990, three experiments were conducted at sea. The objectives of the experiments were to measure the transmission characteristics of the acoustic channel at high frequency (10 to 20 kHz) and to explore the nature of fading and multipath in shallow water, midrange acoustic channel. The first two experiments were carried out on March 16, 1989 and on December 20, 1989 and were located at 32°40'N 117°35.6' W. The third experiment was conducted on May 22, 1990 and was located at 32°50'N 117°35'W.

During the three experiments the sea state was between zero and one and the wind speed was between 5 and 12 knots. The purpose of each experiment was to transmit a set of waveforms from a transducer deployed deep in the ocean from a ship and receive

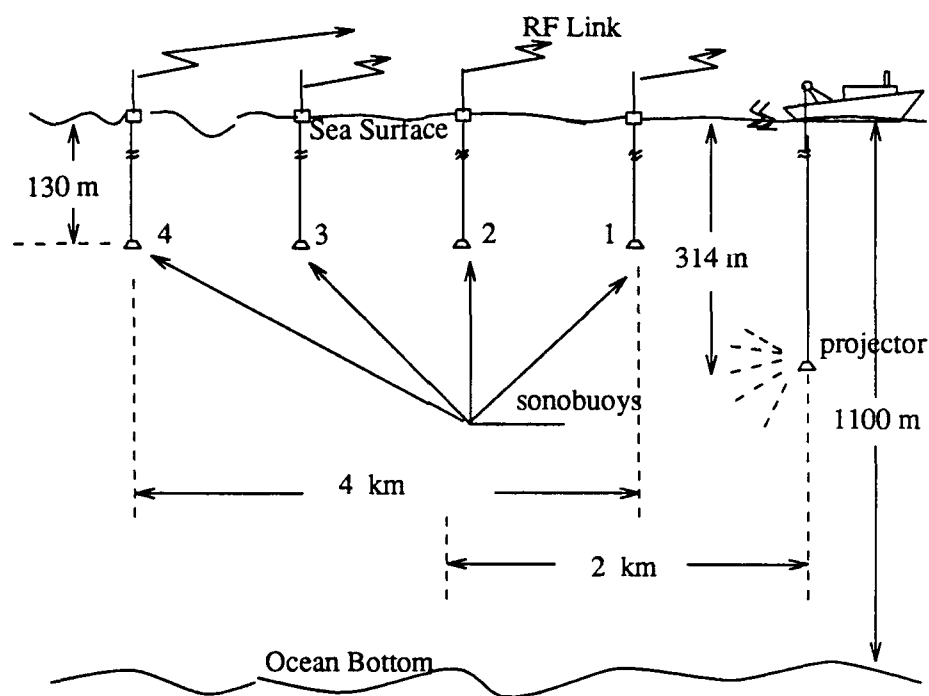


Figure 2.1 Experiment setup

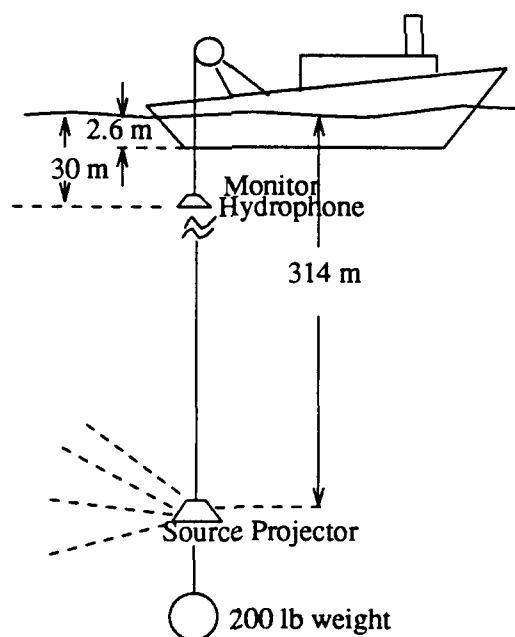
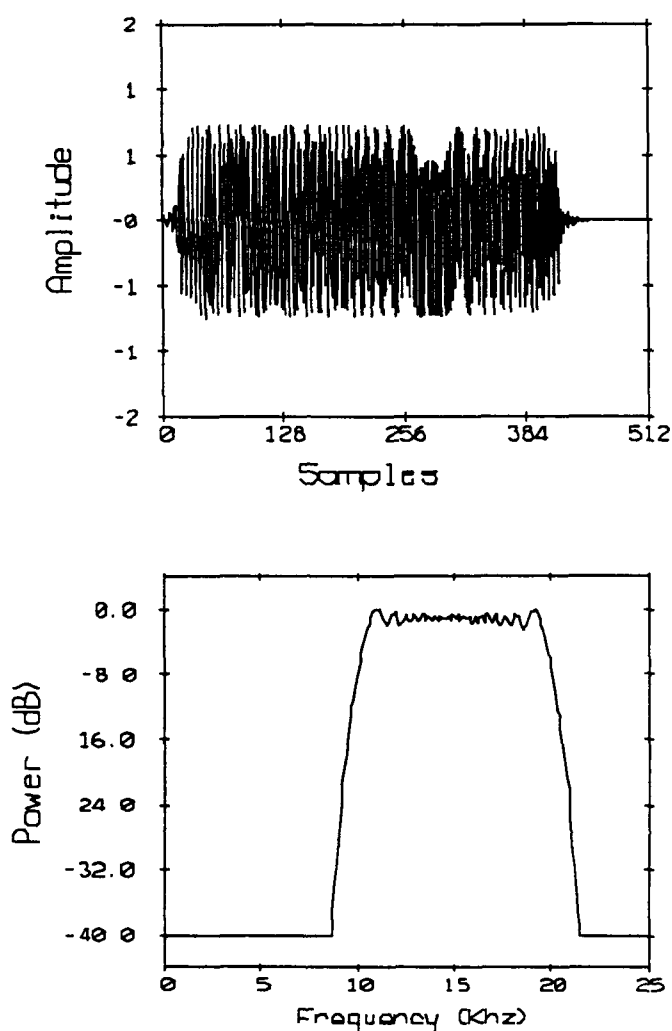


Figure 2.2 Projector and Monitor Hydrophone Location

the transmitted signal with four sonobuoys located 1 km apart and transmitting the received signal via an RF link back to the ship (see Figure 2.1 and 2.2). The transmitted and the received signals (from the sonobuoys) were recorded simultaneously. In addition, a monitor hydrophone was deployed close to the projector and provided a replica of the waveform which was transmitted through the water.

Among the many waveforms transmitted, two specific waveforms enabled us to measure the channel characteristics:

- (1) A set of nine tones equally spaced was transmitted for 2 minutes. This set of tones was retransmitted five times, where each time the space between the tones was changed (50, 100, 250, 500 and 1000 Hz apart). The fifth tone was always centered at 15 kHz.
- (2) A set of spread spectrum waveforms implemented by chirp signals was transmitted. Five different waveforms were transmitted, 1 msec chirp with time-bandwidth product of 10, 2 msec chirp with time bandwidth of 20, 4 msec chirp with time bandwidth of 40, 8 msec chirp with time bandwidth of 80, and 16 msec chirp with time bandwidth of 160. All these waveforms were designed such that they occupied a bandwidth of 10 kHz between 10 and 20 kHz. Figure 2.3 shows the 8 msec chirp and its power spectrum. Each waveform was transmitted every four seconds for 2 minutes.



**Figure 2.3** Time series and power spectrum of an 8 msec long chirp waveform.

The channel parameters measured were: (1) the channel multipath character, (2) the coherence function as a function of time. (indicates the nature of the time varying character of the acoustic channel), and (3) histograms of amplitude variation at each frequency component of the waveforms (enable us to measure the statistics of the fading and the correlation between two frequency components).

### II.3.1 The channel multipath characteristics

The waveforms that are received by the sonobouys are distorted replicas of the transmitted signal plus many other delayed replicas that result from the multipaths (see Figure 2.4). The multipath characteristics of the channel are calculated in two different ways. The first is based on inverse Fourier-transforming the ratio of the received and the transmitted chirp waveforms spectra. The second is by correlating the received and the transmitted waveforms and envelope-detecting the result. Typically, the channel multipath characteristics are characterized by the received signal from the direct path being much weaker than the signal received from the first multipath (caused by reflection from the sea surface) (see Figure 2.5). The other multipaths having larger delay are caused by reflection from the sea bottom or from multiple reflections (bottom and surface) and are much weaker than the first multipath.

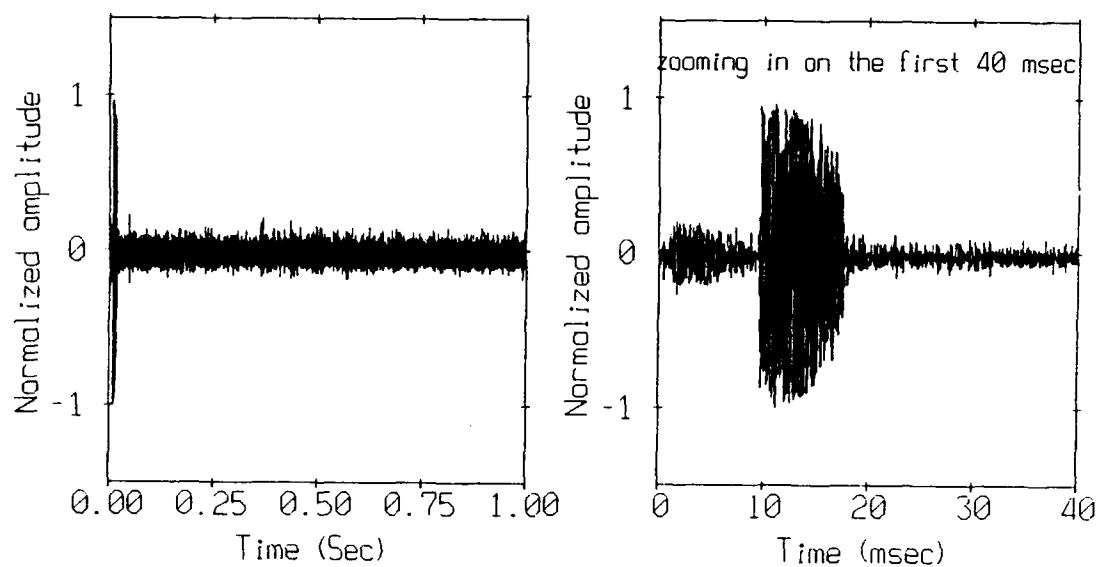


**Figure 2.4** Typical received signal

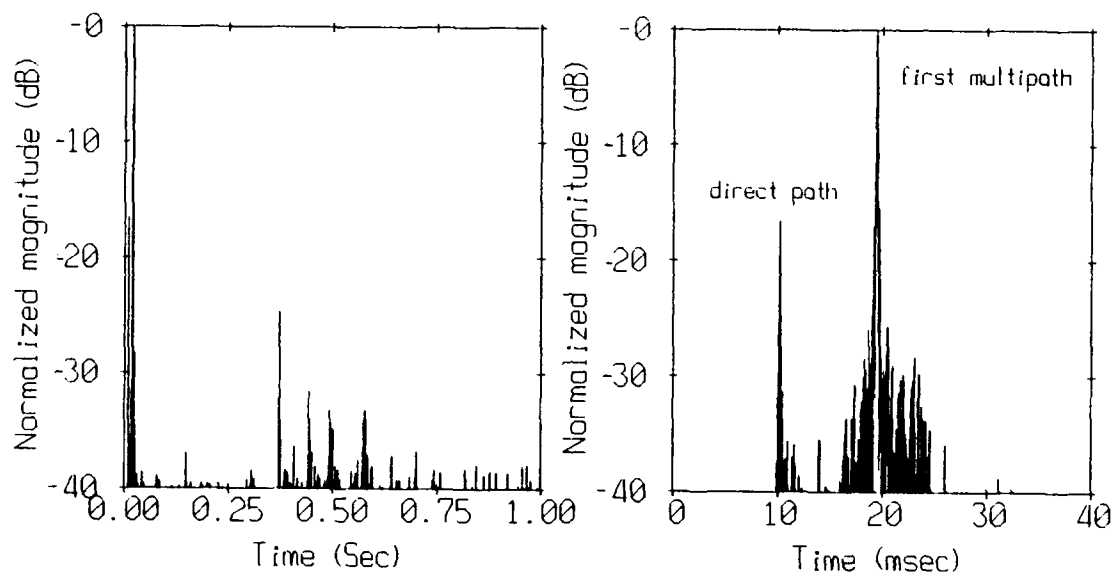


**Figure 2.5** Typical channel multipath character

The underwater acoustic channel is a time-varying channel and hence, the channel multipath character also varies with time. Figures 2.6 and 2.7 present the multipath character of the channel as calculated from twenty eight consecutive eight msec chirp signals transmitted every 4 seconds. The first 20 msec (the main path and two first multipaths) of each multipath character is shown in Figure 2.6. The channel multipath character in the time interval between 370 msec and 530 msec is shown in Figure 2.7. These two plots (which are typical examples of the three at-sea experiments) illustrate the time variation of the channel multipath character. Careful inspection of the first 20 msec (Figure 2.6) shows not only that the multipath intensity changes with time but that the multipaths die and rebuild during a long time of inspection. Another interesting property of the channel multipath character is that each multipath consists of a group of many close multipaths (see Figures 2.5 and 2.6) (micromultipath effect). This effect is more dominant, as the number of reflections (from bottom as well as from surface) become larger (see Figure 2.7).

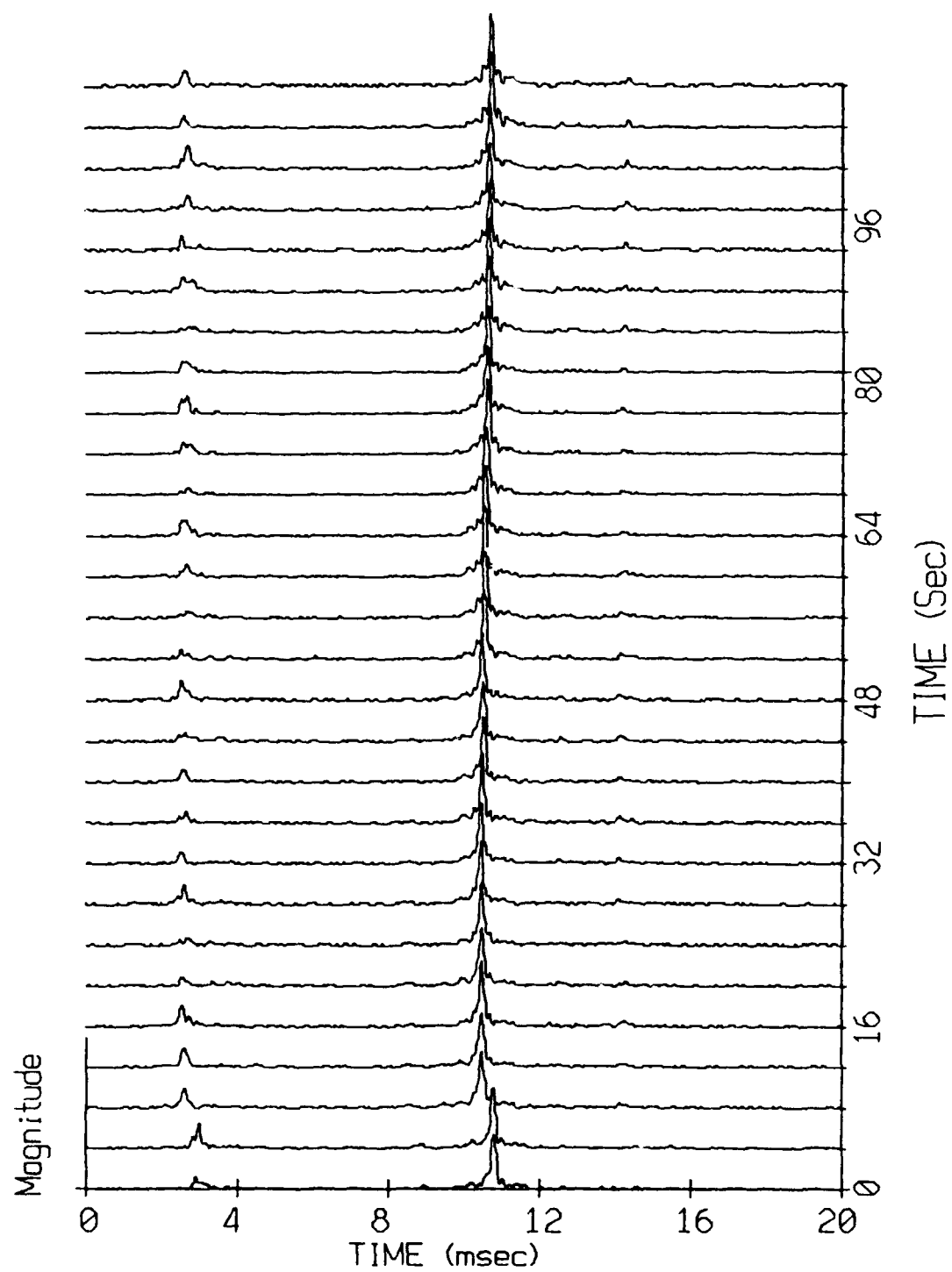


**Figure 2.6** Typical time variation of channel multipath character,  
(first 20 msec.)

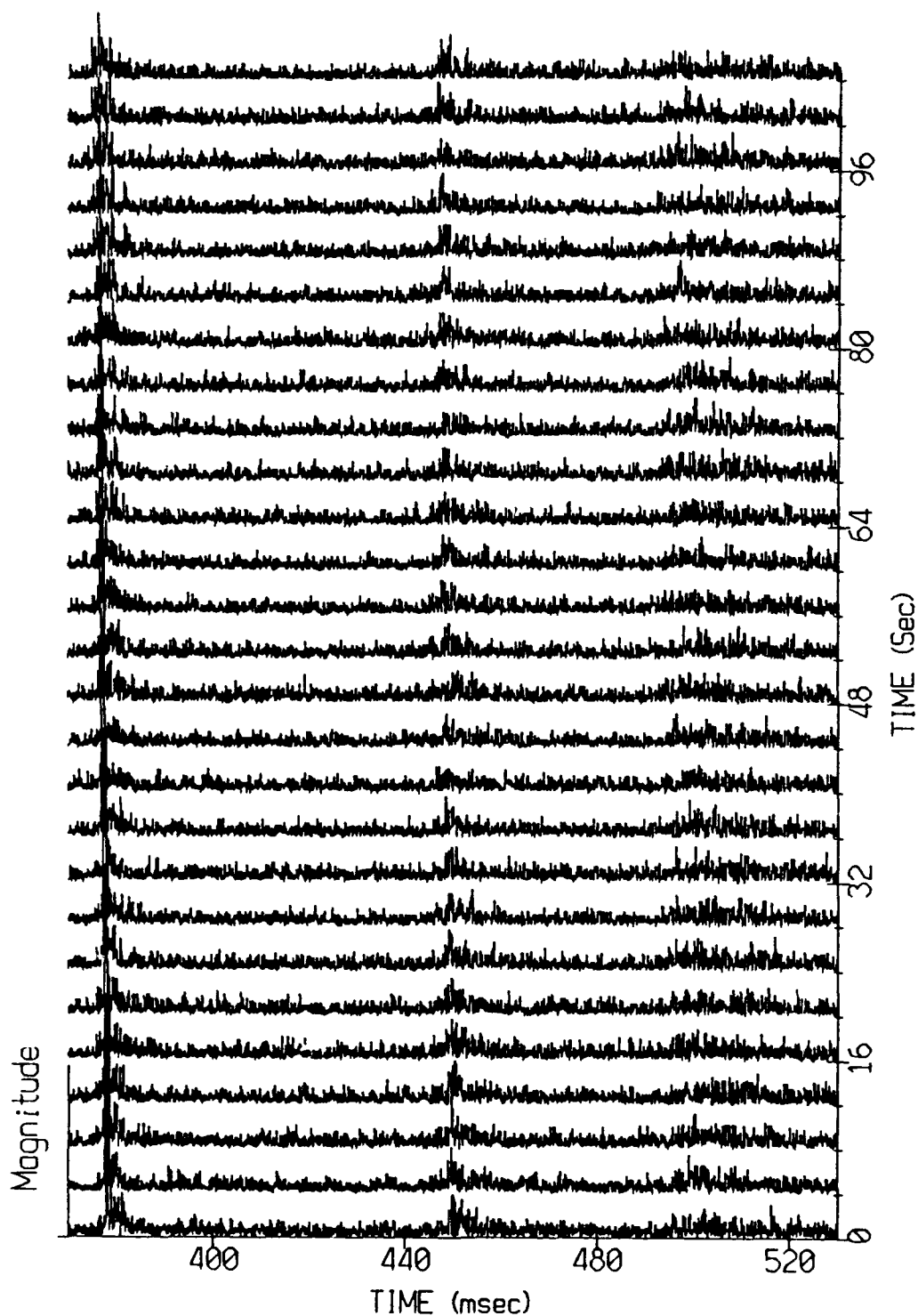


Figure 2.7 Typical time variation of channel multipath character,  
(time slice between 370 and 530 msec)

### II.3.2 Time variation properties of the channel

One of the characteristics of an underwater acoustic channel is its time varying property. The squared magnitude coherence (SMC) is a good measure of the correlation between the channel character in two different time intervals<sup>28</sup>. A spread spectrum waveform between 10 and 20 kHz (8 msec chirp) was transmitted every 4 seconds and the squared magnitude coherence function between the first received waveform and the rest of the waveforms was calculated (Figure 2.8). From the calculated SMC it is observed that for most frequency components, the channel properties are nearly time invariant and the coherence is very high (almost 1). An exception is in the frequency range between 13 and 16 kHz (normalized frequencies of 0.26 and 0.32), where the coherence becomes smaller as the time difference becomes larger. As a result, one can conclude that the rate of variation of the channel character is much lower than the bit rate (seconds compared with milliseconds) and that the channel can be assumed to be very slowly time-varying<sup>1</sup>. A different way to show the rate of variation of the channel character as the function of time is to look at the spectrum variation of the received signal as a function of time (see Figure 2.9). The spectrum has small variation in a time interval of some tens of seconds which show again that the channel is very slow time-varying.

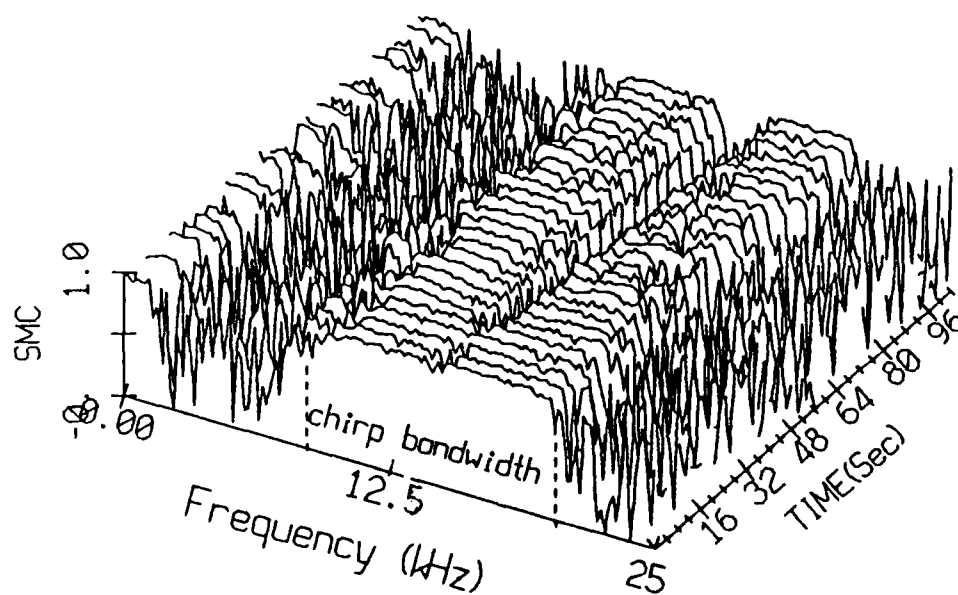


Figure 2.8 The square magnitude coherence function of the channel as a function of time.

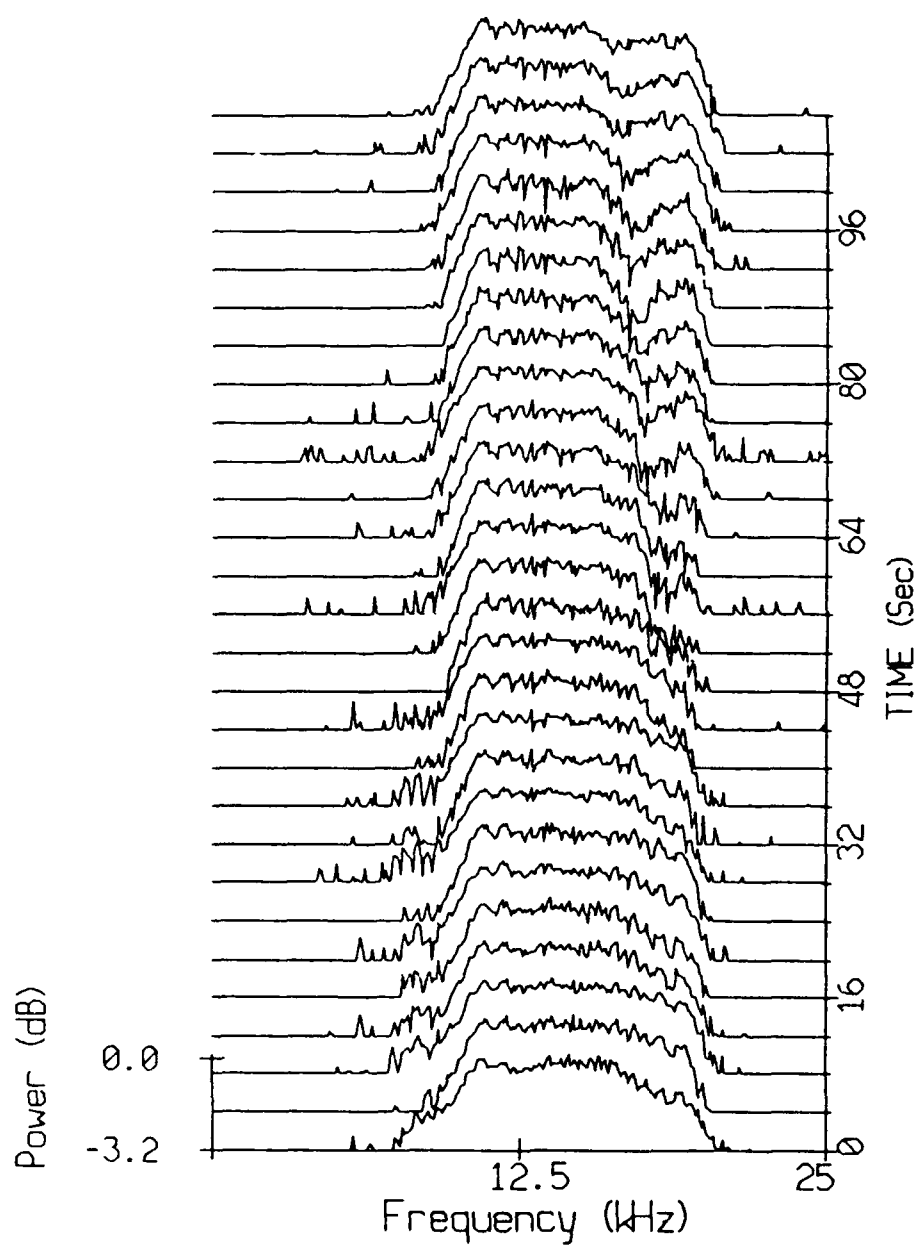


Figure 2.9 The spectra of 28 - 8 msec chirp signals received sequentially (one every 4 sec.)

### II.3.3 The frequency selectivity properties of the channel

Another characteristic feature of a communication channel is its frequency selectivity. This parameter was measured by transmitting a set of tones and calculating the correlation between the envelopes of the tones.

The envelope variation of each frequency component is presented in Figures 2.10 and 2.11. Figure 2.10 presents the envelope variation of each frequency component for tones separated 50 and 100 Hz apart and Figure 2.11 for 250 and 500 Hz apart. Figure 2.12 gives the envelope variation when the tones are separated 1000 Hz apart. The correlation coefficient of the envelope variation between the nine tone groups was calculated with respect to the center tone (15 kHz) (see Figure 2.13). The statistical distribution of the amplitude of each tone was calculated. Figures 2.14 and 2.15 present the histograms of the envelope of the tones when the tones are 250 Hz and 1000 Hz apart.

Inspection of the figures shows that the correlation of the fading phenomena between two frequencies is time dependent. The correlation between the same two frequencies obtains different values at different time intervals. As an example, the correlation between signals at 15 and 15.1 kHz is -0.039 in one case (tones 50 Hz apart) and 0.1111 in the second (tones 100 Hz apart). The correlation between two tones 500 Hz apart (15 and 15.5 kHz) is 0.15564 in one time interval and -0.0452 in other time interval. A second feature of the data is that not only the correlation function is time-varying, but the statistics of the envelope are also time-varying. Figure 2.16 gives the histogram of the envelope of the central tone (at 15 kHz) at five different time intervals of 65 seconds length and 120 seconds apart.

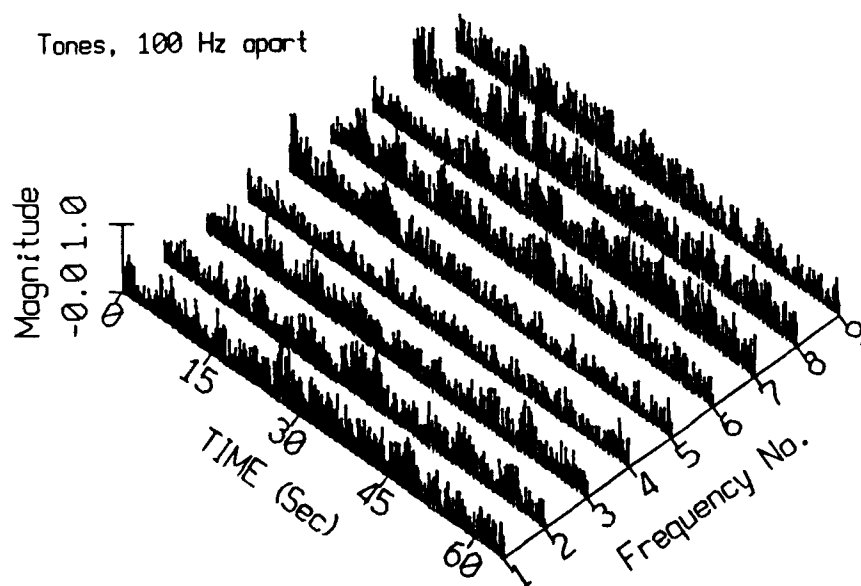
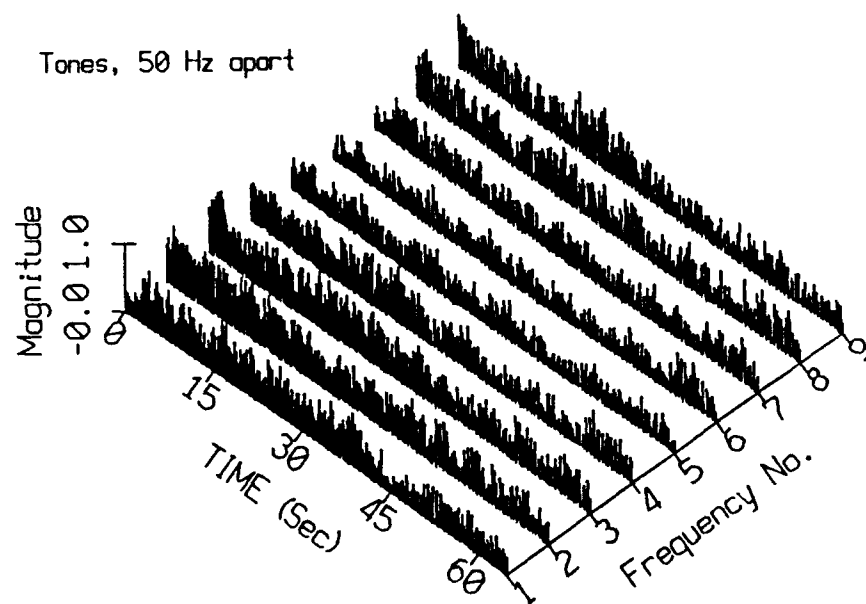


Figure 2.10 Amplitude variation of nine tones, 50 and 100 Hz apart

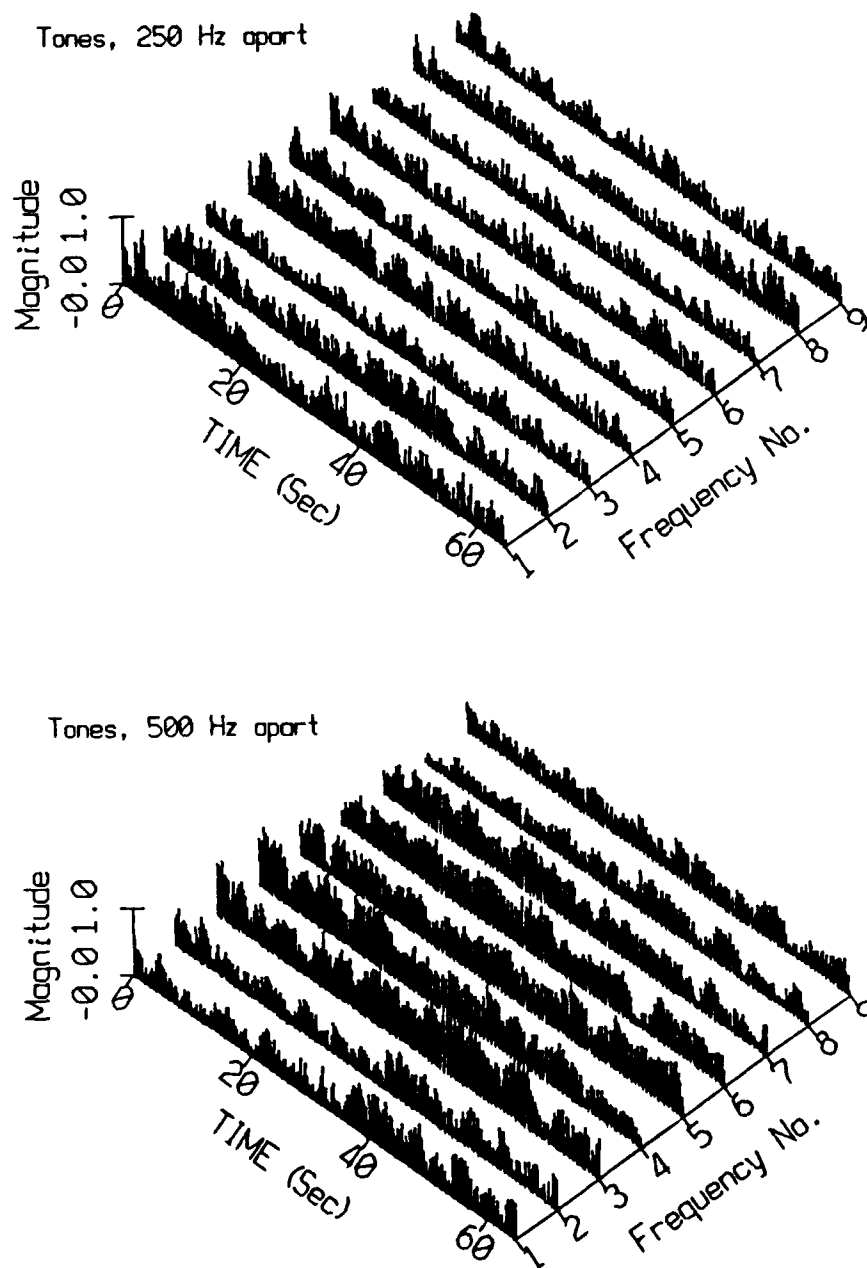


Figure 2.11 Amplitude variation of nine tones, 250 and 500 Hz apart

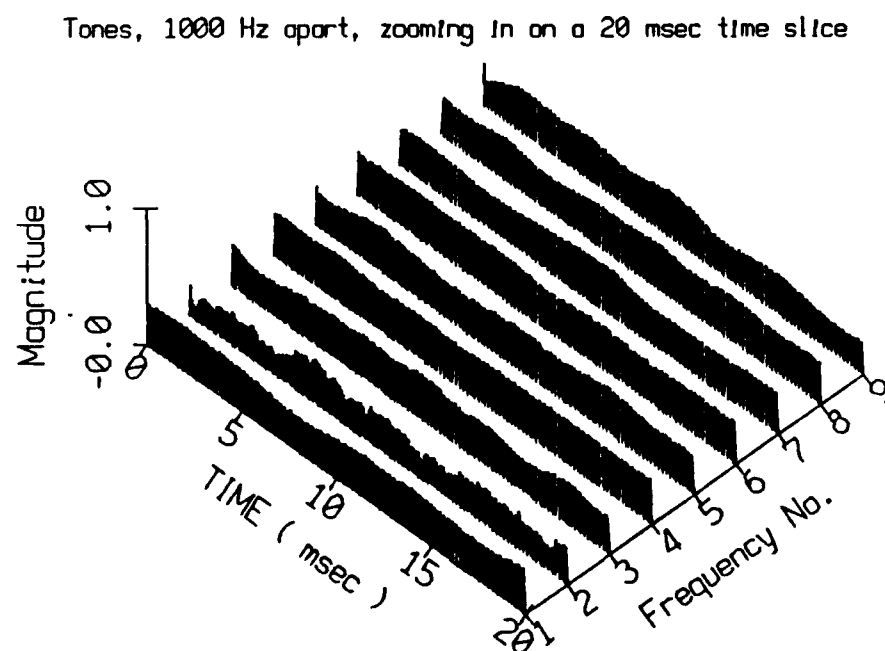
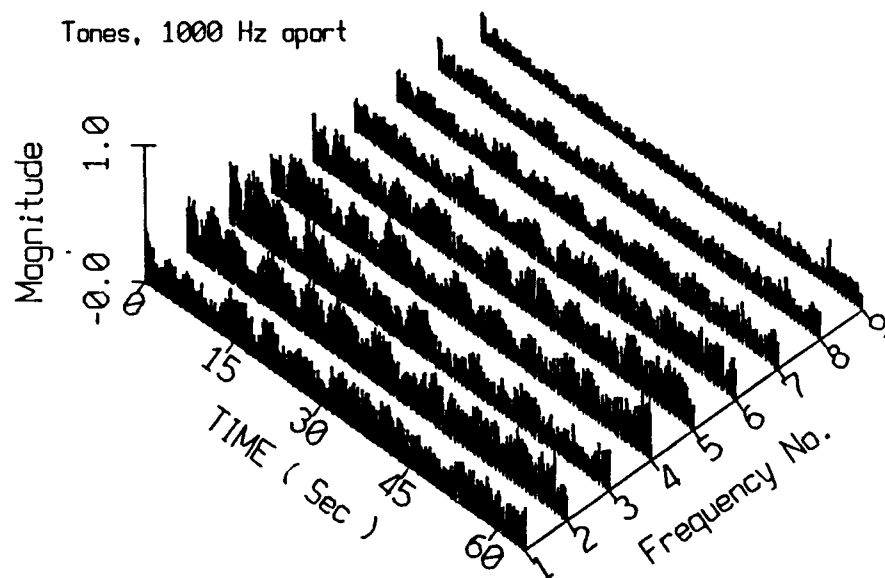


Figure 2.12 Amplitude variation of nine tones, 1kHz apart.

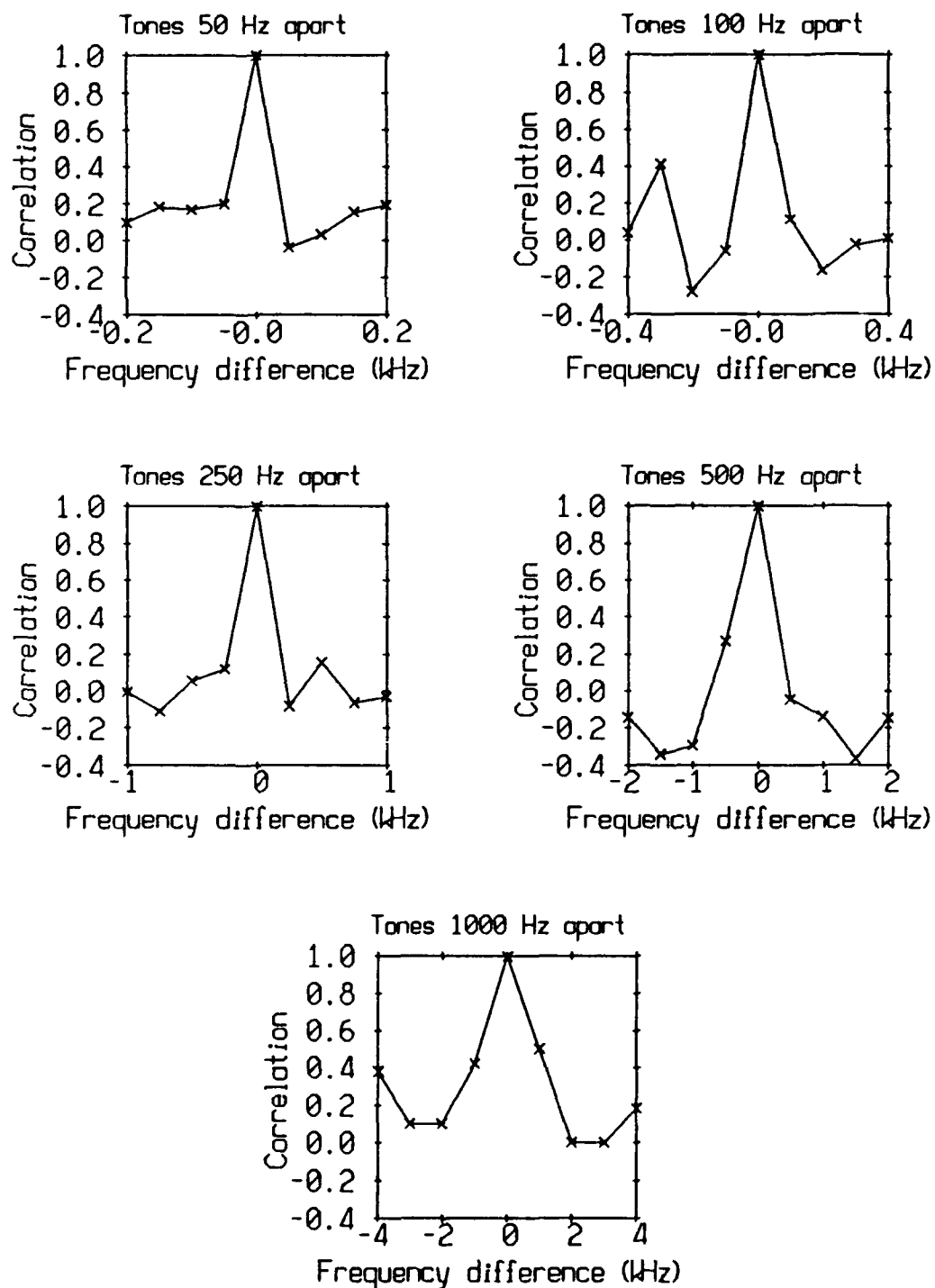


Figure 2.13 The correlation between the envelope of nine tones and the central tone for the five sets of tones.

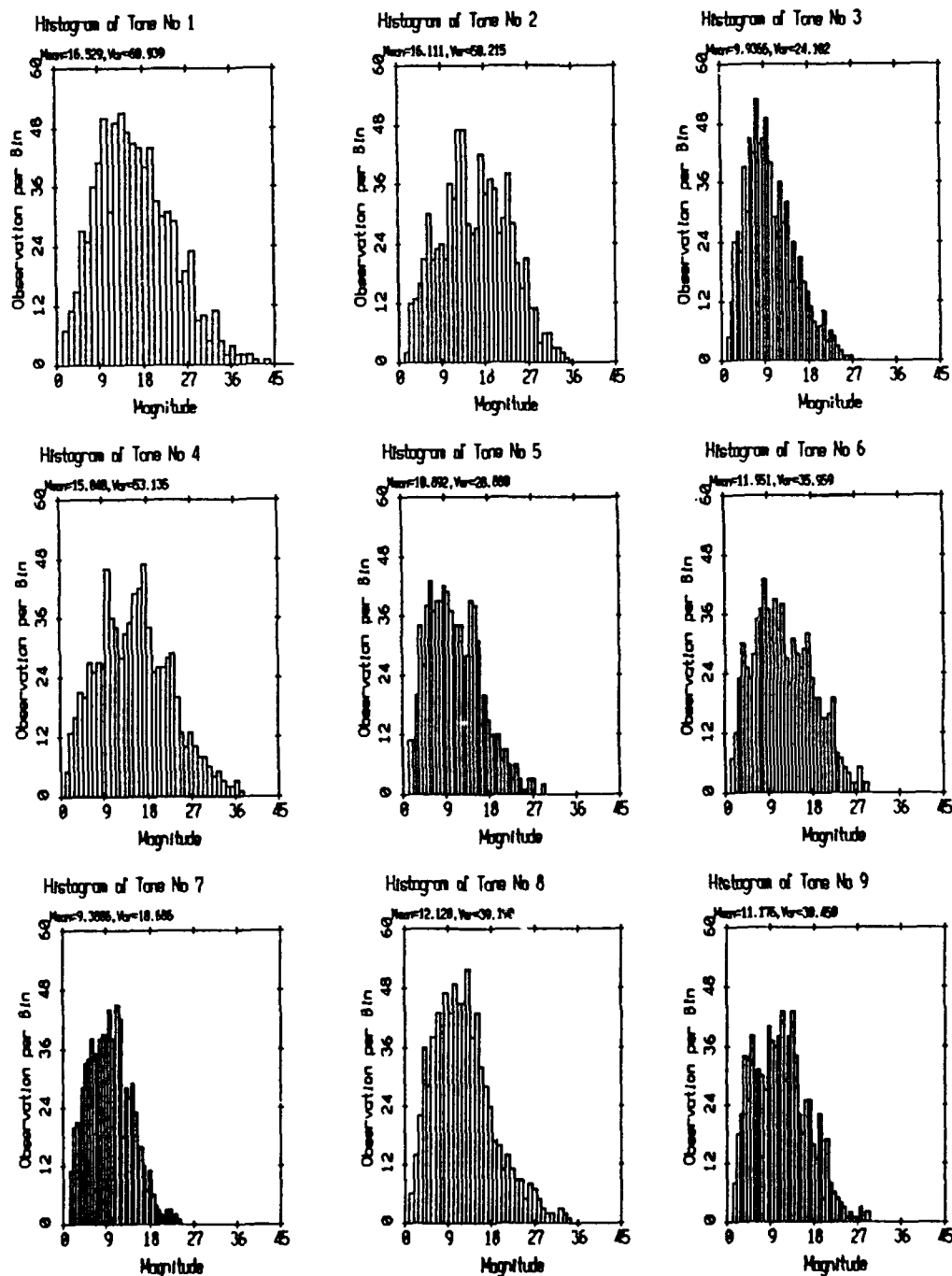


Figure 2.14 Histograms of the envelopes of the 250 Hz spaced tones.

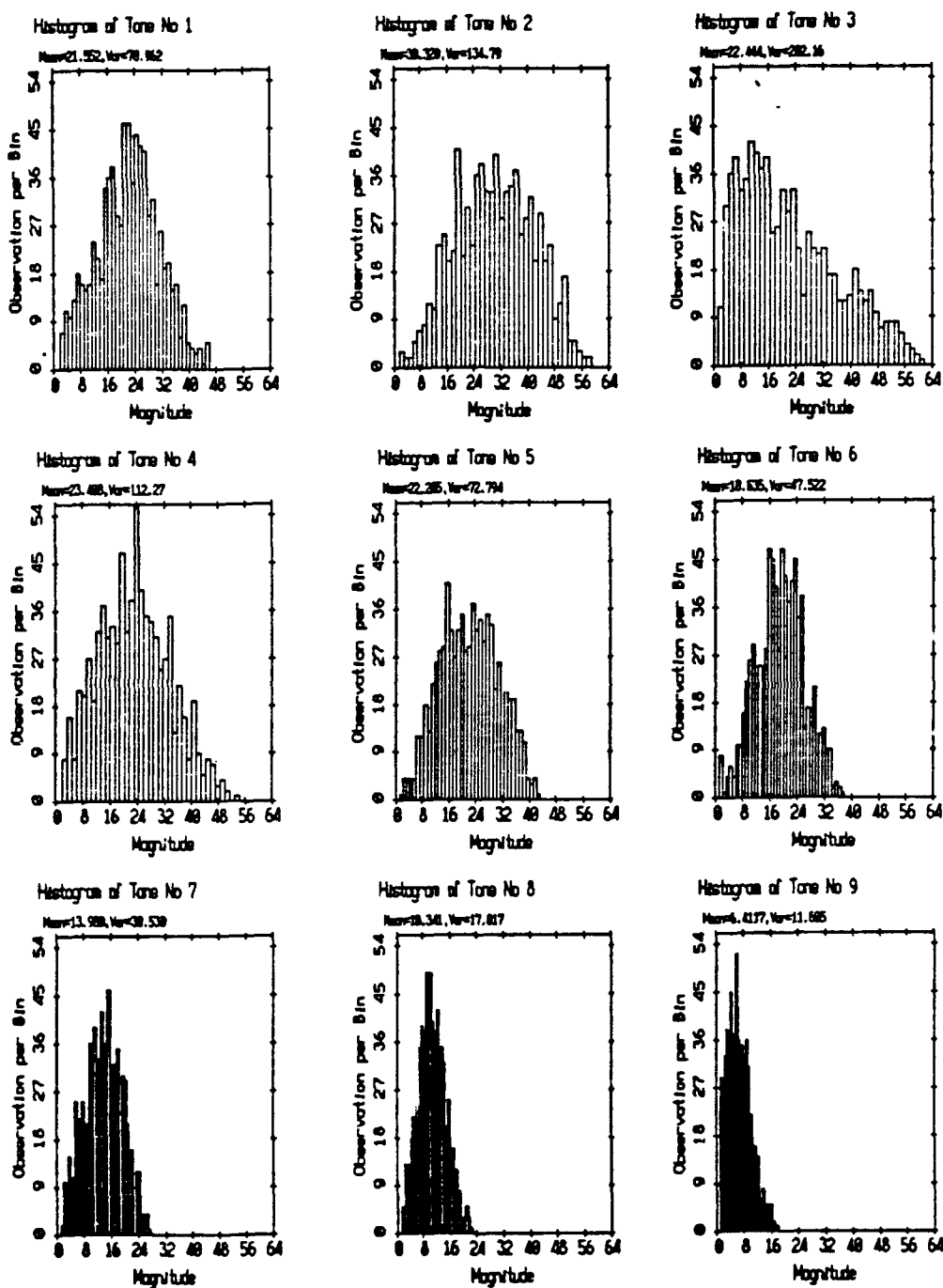


Figure 2.15 Histograms of the envelopes of the 1 kHz spaced tones

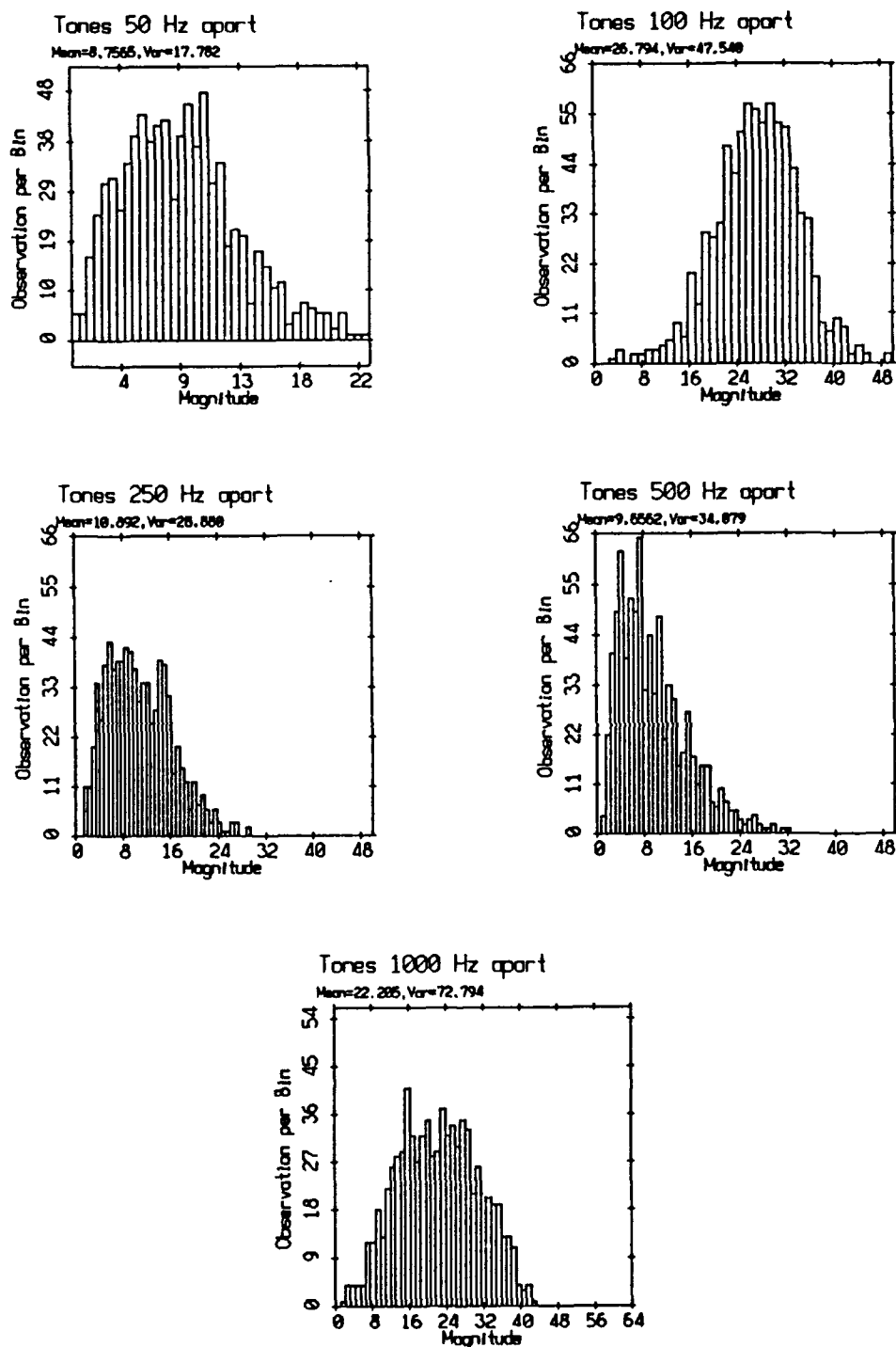


Figure 2.16 The histograms of the 15 kHz tone, at different time periods

From Figure 2.16, one can see that at each different time interval the statistics of the envelope change between a Rayleigh-like distribution and a Rayleigh-Rice like distribution<sup>86</sup>. The Rayleigh-like distribution exists when no specular multipath component exists, and the Rayleigh-Rice like distribution appears when a strong specular multipath component exists.

## II.4 Channel modeling

The analysis of the three at-sea experiments shows that the acoustic communication channel is a time-varying frequency selective channel, which suffers from strong multipath effects. A simplified model of this complicated channel is a sum of independent channels each having a different transfer function and a different delay depending on the delay caused by the multipath (see Figure 2.17). The channel is assumed to be a frequency selective Rayleigh fading channel with low correlation between two frequencies if they differ by 50-100 Hz.

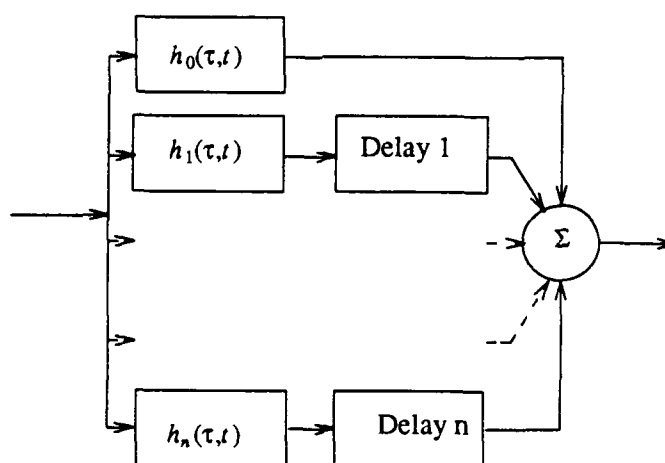


Figure 2.17 A simplified model of an underwater acoustic communication channel.

The equivalent lowpass multipath character of the channel can be described as

$$h_c(\tau, t) = h_0(\tau, t) + \sum_{i=1}^m h_i(\tau - TD_i, t) \quad (2.8)$$

where

$$h_i(\tau, t) = \begin{cases} f_i(\tau, t) & \tau \ll TD_i \\ 0 & \text{else} \end{cases}$$

$h_0(\tau, t)$  is the direct path and  $h_i(\tau, t)$ ,  $i = 1 \cdots n$  are the delayed (with delay of  $TD_i$ ) paths caused by the multipaths.

A more simplified model for the channel can be described as

$$h_c(\tau, t) = \alpha_0 \delta(\tau) + \sum_{i=1}^m \alpha_i \delta(\tau - TD_i). \quad (2.9)$$

As seen from Figures 2.4, 2.5 and 2.6, one of the multipath signal is much stronger than the direct path. This result was also verified experimentally and explained by Lord and Plemons (see their Figures).<sup>55</sup> For cases where an  $\alpha_i$  exists such that  $\alpha_i > \alpha_0$ , the transfer function of the channel is a non minimum phase transfer function.

A necessary condition for a function to be a minimum phase is that  $\sum_{i=1}^m |\alpha_i| < |\alpha_0|$ .

## III Modulation approach

### III.1 Introduction

The underwater acoustic communication channel has been described and modeled in Chapter 2. As fading is a dominant phenomena, when the modulation approach is selected, the ability to combat destructive fading must be considered. The stochastic nature of the channel destroys any phase coherence and therefore only incoherent modulation can be considered.

The simplest way to combat the fading channel is, to select signal parameters (symbol bandwidth, keying rate) that allow essentially distortionless reception of individual symbol waveforms. This is possible for unspread channels, by selecting a symbol waveform with roughly unity time-bandwidth product and for which the symbol duration  $T$  satisfies<sup>84</sup>

$$\frac{1}{\rho_H} \ll T \ll \frac{1}{B_D}$$

$\rho_H$  is defined in Chapter II.2 and  $B_D$  is the Doppler spread of the channel. For a keyed stream that does not satisfy the inequality above, other methods such as diversity, adaptive equalization, coding, and special waveforms and modulation must be used.

### III.2 Frequency diversity techniques for a selective fading channel

Almost all diversity techniques are based on the fact that errors occur when the channel is in a deep fade. Supplying the receiver with several replicas of the same information signal transmitted over independently fading channels will reduce

the probability that all the signals will fade simultaneously.

The main diversity methods are <sup>75,81,84</sup> : (1) space (spaced antenna) diversity, (2) angle (of arrival) diversity, (3) polarization diversity (not relevant in underwater acoustic communication), (4) frequency diversity and (5) time (signal-repetition (bit interleaving)) diversity.

A detailed analysis of several frequency diversity methods based on coherent and differential PSK and coherent and incoherent FSK modulation is given by Proakis <sup>75</sup> (Chapter 7 ) and by Stein<sup>81</sup>. Another frequency diversity method used successfully in radio communication fading channels is spread spectrum direct sequence modulation. However, the need for sequence acquisition and maintenance of synchronization while one of the terminals is in motion causes serious problems for this technique in an underwater communication system.

In this section, we will summarize the performance of the most common frequency diversity methods in the presence of frequency selective, very slowly time-varying Rayleigh fading.

### **III.2.1 The combining method**

Figures 3.1 and 3.2 give block diagrams of coherent and incoherent binary FSK receivers with combined L branches. The receivers are built from L duplicates of the same branch tuned to the L different carrier frequencies. Each branch is matched to the appropriate transmitted signal.

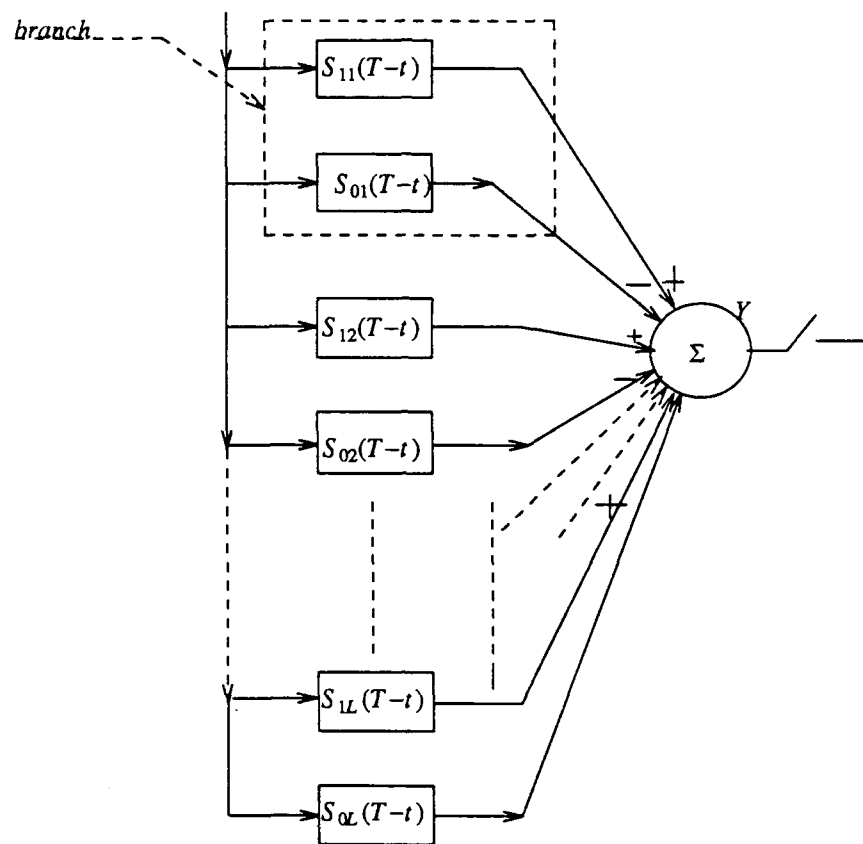


Figure 3.1 Coherent binary FSK receiver with  $L$  combined channels

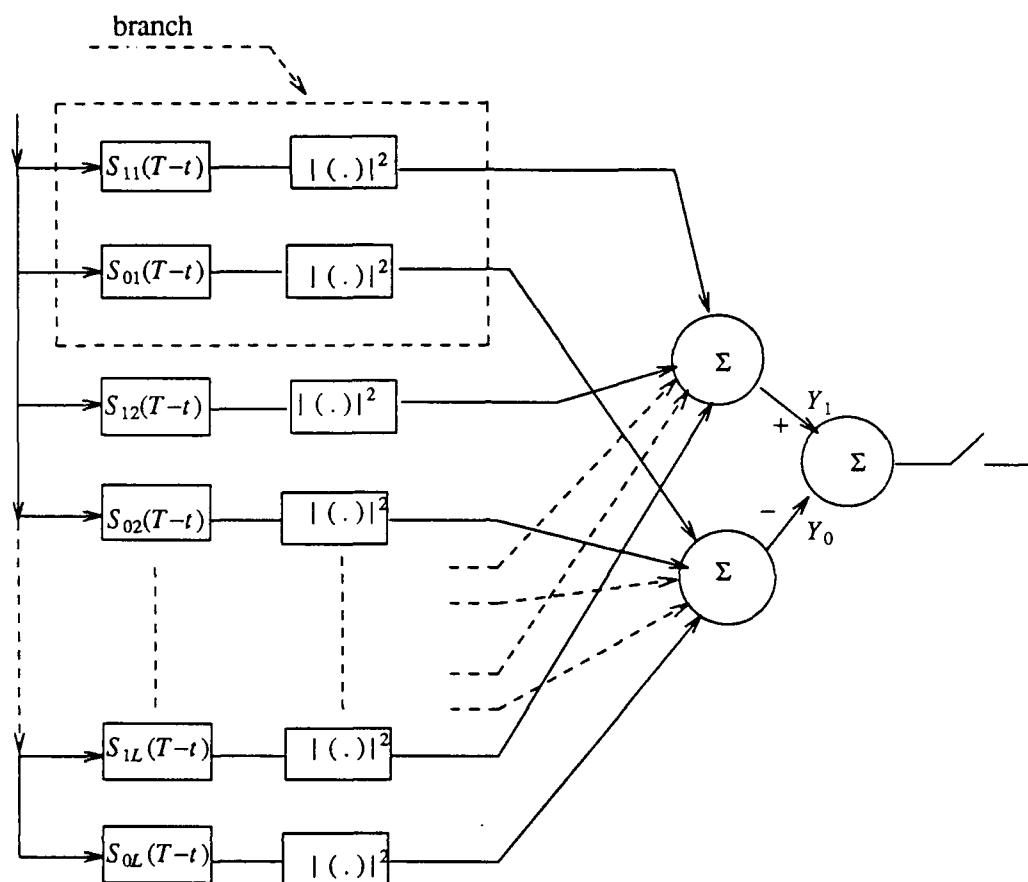


Figure 3.2 Incoherent binary FSK receiver with  $L$  combined channels

Figure 3.3 gives block diagram of a BPSK receiver with combined  $L$  branches

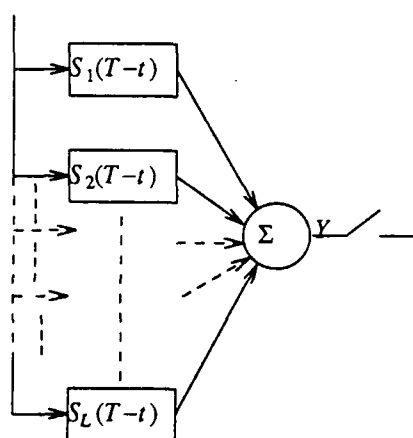


Figure 3.3 BPSK receiver with  $L$  combined channels

It is easy to show that when each branch independently fades, the optimal maximum likelihood decision rule is to sum the outputs of all the mark channels and all the space channels of the branch receivers and to compare them. Choosing the mark and the space at each branch such that they will fade together will significantly simplify the optimal receiver.

For a BPSK receiver with combined  $L$ -th order diversity and a very slowly time-varying frequency selective Rayleigh fading channel, the bit error probability is<sup>75</sup> [ p. 723 ]

$$P_e = \left\{ \frac{1-\mu}{2} \right\}^L \sum_{k=0}^{L-1} \binom{L-1+k}{k} \left\{ \frac{1+\mu}{2} \right\}^k \quad (3.1)$$

where  $\mu = \sqrt{\frac{\hat{\gamma}_c}{1+\hat{\gamma}_c}}$  and  $\hat{\gamma}_c$  is the average signal to noise ratio for all channels.

When a very slowly selective fading is assumed, the instantaneous signal to noise ratio at each branch remains constant for a long period of time relative to the message length. In such a case,  $\hat{\gamma}_c$  is considered as the average signal to noise ratio over all branches and since the transmitted power is divided among all  $L$  branches, we have:

$$\hat{\gamma}_c = \frac{1}{L} \sum_{l=1}^L \gamma_l = \frac{\hat{\gamma}_b}{L} \quad (3.2)$$

where  $\gamma_l$  denote the signal to noise ratio at the  $l$ th branch of the receiver.

Under the assumption that the mark and the space frequencies are close enough that they fade together and, again assuming a very slowly time-varying frequency selective Rayleigh fading, we find that the bit error probability is the same as (3.1) (BPSK) with  $\mu$  as follows:

(a) for the coherent case

$$\mu = \sqrt{\frac{\hat{\gamma}_c}{2 + \hat{\gamma}_c}} \quad (3.3)$$

and (b) for the incoherent case

$$\mu = \frac{\hat{\gamma}_c}{2 + \hat{\gamma}_c} \quad (3.4)$$

Figures 3.4 and 3.5 give the bit error probability for a binary incoherent FSK modulation and a binary coherent FSK with frequency diversity as a function of the number of diversity branches.

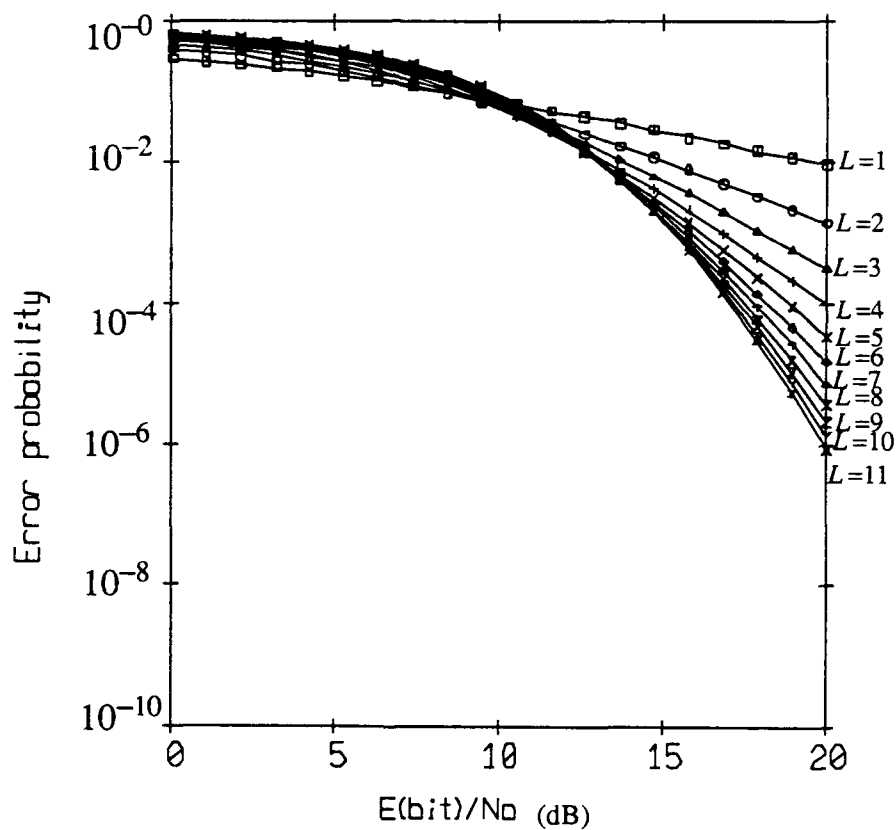


**Figure 3.4** Bit error probability of binary incoherent FSK with  $L$  order diversity as a function of SNR

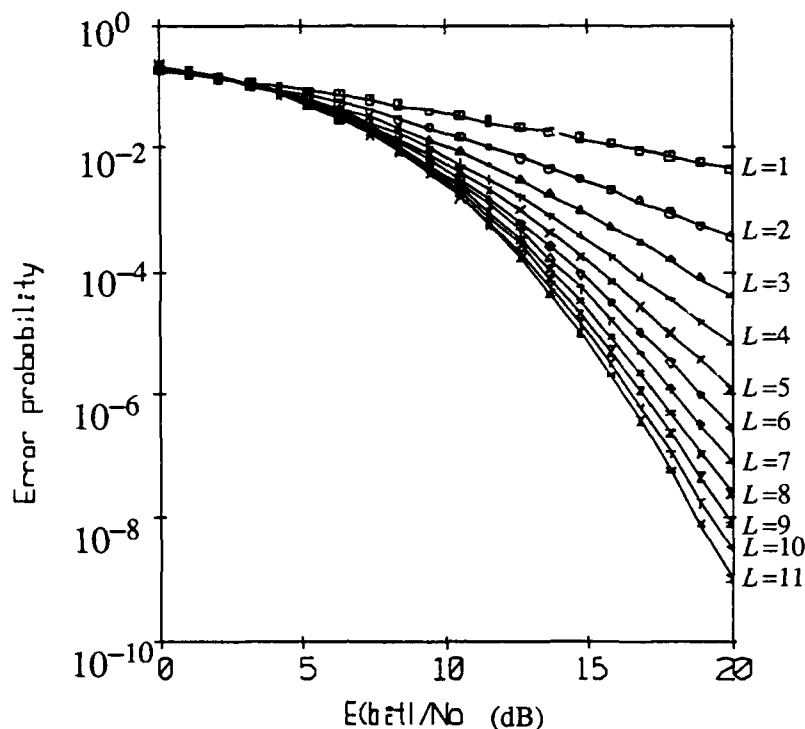


**Figure 3.5** Bit error probability of binary coherent FSK with  $L$  order diversity as a function of SNR.

### III.2.2. Switch diversity

Switch diversity is a method where only the branch having the largest signal to noise ratio <sup>72</sup> is used at any given instant for the decision rule.

For a Rayleigh fading channel,

$$P(\gamma_l) = \frac{1}{\hat{\gamma}_c} \exp\left\{-\frac{\gamma_l}{\hat{\gamma}_c}\right\} \quad (3.5)$$

If we define  $\gamma$  as the maximum from all  $\gamma_l$ , then for a switch diversity receiver with  $L$  branches,

$$P(\gamma) = \frac{L}{\hat{\gamma}_c} \exp\left(-\frac{\gamma}{\hat{\gamma}_c}\right) \left\{1 - \exp\left(-\frac{\gamma}{\hat{\gamma}_c}\right)\right\}^{L-1}, \quad (3.6)$$

and

$$P_e = \int_0^{\infty} p_{e/\gamma}(e) p_{\gamma}(\gamma) d\gamma. \quad (3.7)$$

For binary PSK with an L branch switch diversity receiver, the bit error probability is

$$P_e = \int_0^{\infty} \frac{L}{\hat{\gamma}_c} \exp\left(-\frac{\gamma}{\hat{\gamma}_c}\right) \left\{ 1 - \exp\left(-\frac{\gamma}{\hat{\gamma}_c}\right) \right\}^{L-1} \phi(-\sqrt{2\gamma}) d\gamma \quad (3.8)$$

where

$$\phi(x) = \frac{1}{\sqrt{2\pi}} \int_{-\infty}^x \exp(-\frac{1}{2}y^2) dy$$

and

$$P_e = \frac{L}{\sqrt{2\pi}\hat{\gamma}_c} \int_0^{\infty} \sum_{k=0}^{L-1} \left[ \begin{matrix} L-1 \\ k \end{matrix} \right] (-1)^k \exp\left(-\frac{\gamma k}{\hat{\gamma}_c}\right) \int_{-\infty}^{-\sqrt{2\gamma}} \exp(\frac{1}{2}y^2) dy d\gamma. \quad (3.9)$$

Changing the order of summation and integration, and integrating by parts, we obtain

$$P_e = \frac{L}{2} \sum_{k=0}^{L-1} k (-1)^k \left[ \begin{matrix} L-1 \\ k \end{matrix} \right] \left[ 1 - \sqrt{\frac{\hat{\gamma}_c}{k + \hat{\gamma}_c}} \right]. \quad (3.10)$$

For coherent binary FSK modulation, substituting  $\frac{1}{2}\gamma$  instead of  $\gamma$  in (3.8), will give us the following bit error

$$P_e = \frac{L}{2} \sum_{k=0}^{L-1} k (-1)^k \left[ \begin{matrix} L-1 \\ k \end{matrix} \right] \left[ 1 - \sqrt{\frac{\hat{\gamma}_c}{2k + \hat{\gamma}_c}} \right] \quad (3.11)$$

For incoherent FSK

$$\begin{aligned} P_e &= \frac{L}{2\hat{\gamma}_c} \int_0^{\infty} \exp\left(-\frac{\gamma}{\hat{\gamma}_c}\right) \left\{ 1 - \exp\left(-\frac{\gamma}{\hat{\gamma}_c}\right) \right\}^{L-1} \exp\left(-\frac{\gamma}{2}\right) d\gamma \\ &= \frac{L}{2\hat{\gamma}_c} \sum_{k=0}^{L-1} (-1)^k \left[ \begin{matrix} L-1 \\ k \end{matrix} \right] \left\{ \frac{2\hat{\gamma}_c}{2 + \hat{\gamma}_c + 2k} \right\}. \end{aligned} \quad (3.12)$$

### III.3 Special modulation techniques

#### III.3.1 Combined modulation and coding

Figure 3.6 shows a block diagram that describes the idea of combining coding and modulation<sup>71</sup>.

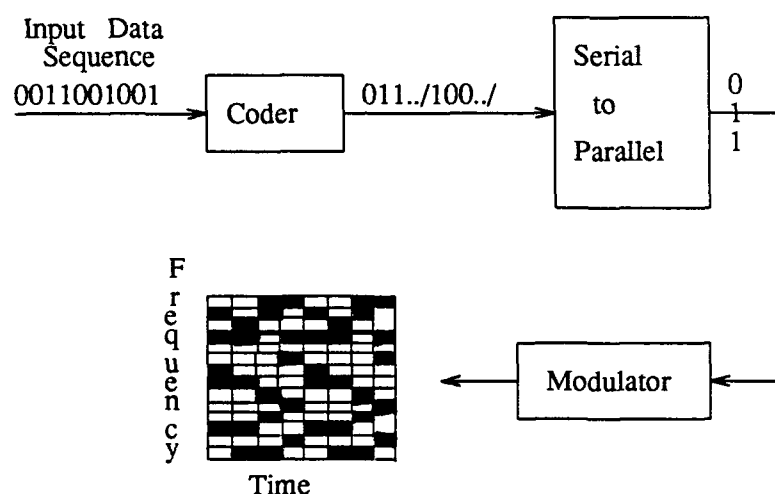


Figure 3.6 Combining coding and modulation - block diagram.

A stream of binary data bits is supplied to the encoder which encodes the information bits (most often to a  $(n,k)$  block code). The modulator accepts a block of  $n$  bits corresponding to a codeword and assigns each bit to a cell in the partitioned signal space. Waveforms are constructed by following the convention that a tone pulse is generated in a cell if a "one" is assigned to that cell and that no energy is transmitted in a cell to which a "zero" is assigned. This choice of basic cellular modulation is based on our assumed inability to detect received tones coherently. The waveform type that results for an ensemble of such signals is termed multitone on/off keying (MTOOK). An alternative mapping of the  $n$  bits into channel

waveforms can be accomplished by means of frequency shift keying. With FSK, each bit in a codeword is assigned two cells: one cell for a "one" and the other for a "zero".

The coded waveform technique has a major advantage over the regular frequency diversity methods because it combines coding gain and frequency diversity together. The obtained diversity order ( $L$ ) is  $\frac{d_{\min}}{2}$  where  $d_{\min}$  is the minimum Hamming distance of the code.

### III.3.2 Chirp as a frequency diversity technique

At least 25 years ago<sup>93</sup>, it already was recognized that a modulated chirp signal would be a simple and effective tool for combating the problem of fading, multipath, <sup>5,6,37</sup> impulse noise<sup>44,87</sup>, and cross-talk<sup>25</sup>. Furthermore, some successful experiments were carried out implementing chirp signals in underwater acoustic telemetry<sup>42</sup>. It is well known <sup>5,84</sup> that a communication system based on coherent signal detection is useless in a random fading environment. Thus, among all the modulation techniques based on chirps, only methods based on incoherent modulation are used. In a binary communication system, the mark and space are defined by two different signals. In a chirp modulation system, these two signals can occupy different frequency bands with the same or inverted slopes (frequency vs. time character), or can occupy the same frequency band but with inverted slopes. Berni & Gregg<sup>6</sup> found the optimal signal sets for the case where the two signals had opposite slopes and occupy partially overlapped frequency regions. Zaytsev & Zhuravlev<sup>96</sup> analyzed the performance of a FSK chirp modulation system where both signals (mark and space) occupied the same frequency bandwidth with opposite slopes.

Since a very slowly time-varying frequency selective Rayleigh fading channel has been assumed and the relative drift between the transmitter and the receiver is assumed to be very small, the difference between received phases in consecutive bits when coherent modulation is used is negligible. Therefore, DPSK chirp modulation /demodulation can be used. Figure 3.7 and Figure 3.8 show two applications of a binary DPSK receiver. Figure 3.7 is the most common and the most often used scheme.

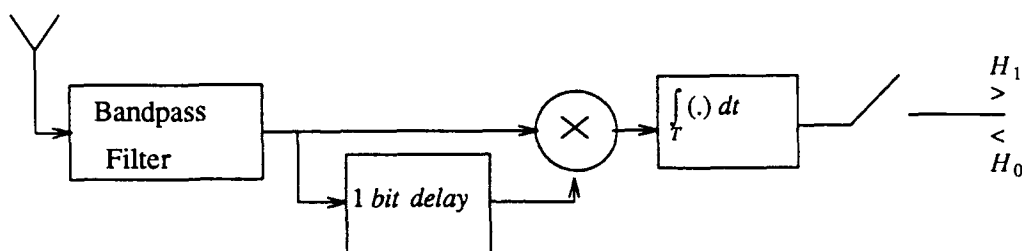


Figure 3.7 Suboptimum binary DPSK demodulator.

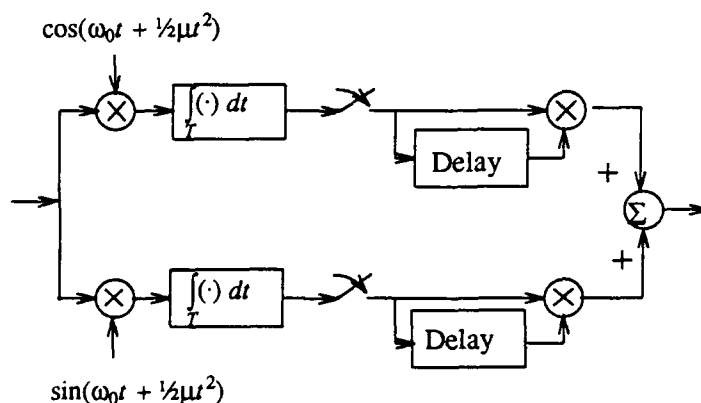


Figure 3.8 Optimum binary DPSK demodulator.

Although it has been shown that when the effect of the bandpass filter is taken into consideration, the demodulator shown in Figure 3.7 is not optimal. Due to its simplicity it is preferred over the configuration shown in Figure 3.8. J.H. Park<sup>69</sup> proved

that when the bandpass filter effect is considered, the demodulator shown in Figure 3.7 has worse performance (about 1 to 2 dB) than the optimum receiver. He also showed that the demodulator shown in Figure 3.8 is optimum. When the effect of the bandpass filter is neglected, both receivers give the same performance.

In Appendix A, we show that in the presence of a frequency selective Rayleigh fading channel with reasonable degree of diversity,  $K$ , the probability of error when chirp DPSK modulation is used turns out to be the same as regular DPSK modulation in the presence of AWGN. The bit error probability is inversely proportional to the exponent of the signal to noise ratio instead of being proportional to the inverse of the signal to noise ratio as in BPSK in the presence of Rayleigh fading. Binary DPSK chirp modulation as well as higher order DPSK can be used. Figure 3.9 shows the achieved bit error probability as a function of the signal to noise ratio<sup>54</sup> for 2,4,8,16 and 32-ary DPSK.

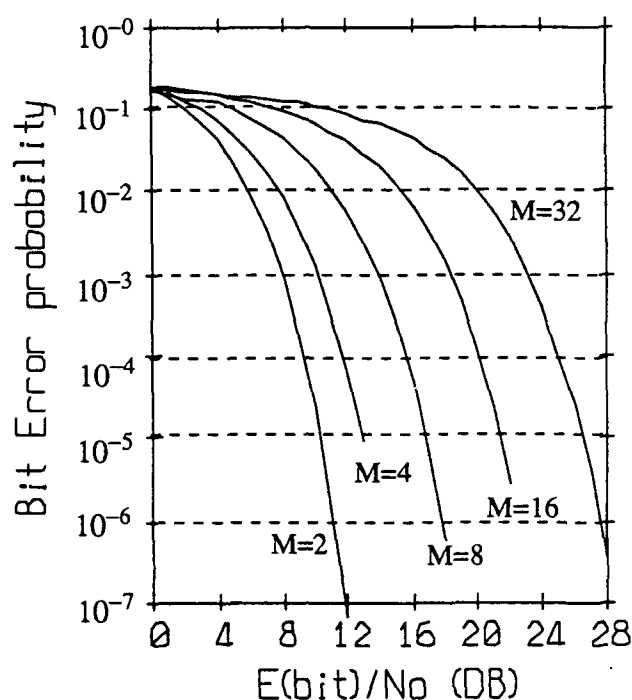
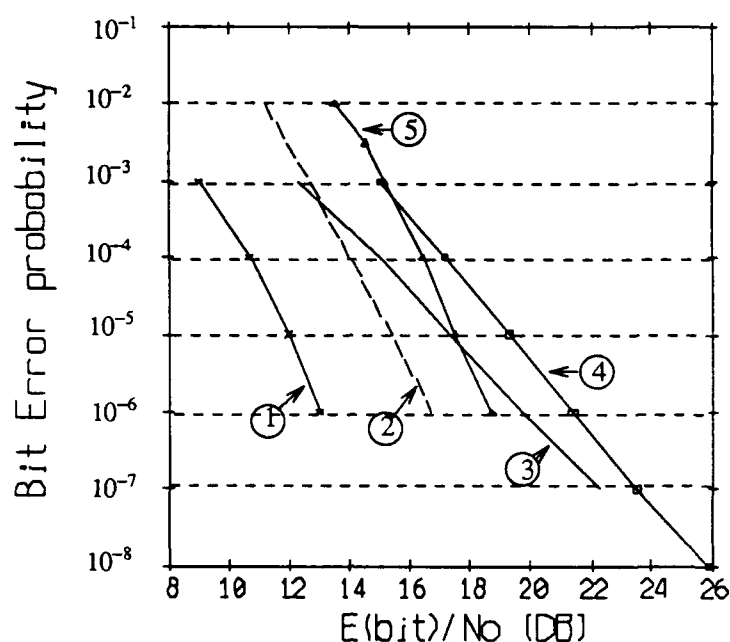


Figure 3.9 Bit error rate of 2,4,8,16 and 32-ary DPSK<sup>54</sup>

Let us define the bandwidth expansion of a modulation technique  $B_e$  as the time-bandwidth product per information bit. It is a measure of the efficiency of the modulation technique. As explained in Appendix A, when a chirp signal is used, a time bandwidth product greater than 10 is recommended in order to prevent significant intersymbol interference. When a 4-ary chirp DPSK is used, the bandwidth expansion of the system is 5 (for  $BT=10$ ). Figure 3.10 gives a comparison between different types of waveforms combined with coding with  $B_e = 4$  and a 4-ary chirp DPSK ( $B_e = 5$ ) the presense of Rayleigh frequency selective channel.



**Figure 3.10** Comparison of 4-ary chirp DPSK with various types of combined modulated and coded waveforms<sup>75</sup> (Chapter 7)

Curve 1 shows the probability of bit error for a 4-ary chirp DPSK modulation scheme. Curve 2 corresponds to a rate  $\frac{1}{2}$  binary convolutional code with constraint length 5 and with soft decision decoding. Curve 3 depicts the performance of a rate  $\frac{1}{2}$  dual -2 with block orthogonal [O(4,2)] inner code. Curve 4 corresponds to (20,5) combined Hadamard code and curve 5 corresponds to a (24,12) Golay code with soft decision decoding.

From Figure 3.10, one can conclude that a 4-ary chirp DPSK modulation is superior to the combined modulated and coded waveform with similar bandwidth expansion. Moreover, inspection of Figure A.10 (Appendix A) shows that the chirp DPSK also is superior to the BFSK and BPSK modulation methods even when a high order of frequency diversity is used.

### III.3.3 Unequal bit error rate method

Under given constraints, the main purpose of a communication system is, to transfer information between two points with as high a reliability as possible. In conventional communication, analog as well as digital, a lot of effort is directed toward methods of improving the reliability. In digital communication, sophisticated modulation schemes, channel equalization, and error correction are used to improve the system performance.

In conventional digital communication systems, all of the information symbols of a message are regarded equally significant and equal apriori symbol probability is assumed. In such cases, a common measure of the system performance is the achieved symbol (or bit) error rate at the receiver's output. However, in some cases, not all data are of equal value for the user. For example, an analog data which has been sampled by an A/D converter. Errors in the higher order bits (MSB) of numbers would be more costly than errors in the lower order bits. In such cases, when each bit has a different significance, the symbol (or the bit) error rate is not a good measure of the system performance any more and another measure has to be defined.

The following model of a digital communication system is considered. An analog signal is sampled and transmitted digitally via a noisy channel. The receiver, receives the digital data and reconstructs the analog data.

The sampled signal ( $V(n)$ ) at each sampling time can be described as

$$V(n) = \frac{1}{2^b} \sum_{i=0}^{b-1} C_{ni} 2^i \quad (3.13)$$

where  $C_{ni}$  is either one or zero.

Each sampled signal is uniquely described by its  $b$  bits  $C_{ni}$   $i=0,1,2,\dots,b-1$ , and the only data that is transmitted are the  $C$ 's. Each set of  $b$   $C_i$ 's that describes one

sample of the sampled signal is defined as a word (W). The receiver estimates the  $C_{ni}$ , and reconstructs the signal by

$$\hat{V}(n) = \frac{1}{2^b} \sum_{i=0}^{b-1} \hat{C}_{ni} 2^i, \quad (3.14)$$

where  $\hat{C}_{ni}$  is the estimated value of  $C_{ni}$ .

Instead of using the bit error rate as a performance measure, we define the mean square error (m.s.e) ( $\epsilon^2$ ) as a new measure of the system performance, where

$$\epsilon^2 \equiv E_n \left\{ [V(n) - \hat{V}(n)]^2 \right\} = \frac{1}{2^{2b}} E_n \left\{ \left[ \sum_{i=0}^{b-1} (C_{ni} - \hat{C}_{ni}) \right]^2 2^i \right\} \quad (3.15)$$

( $E[\cdot]$  denote expected value of  $[\cdot]$ ).

In Appendix C, we show that

$$\epsilon^2 = \frac{1}{2^{2b}} \sum_{i=0}^{b-1} p_i 2^{2i} \quad (3.16)$$

where  $p_i$  is the probability of incorrect detection of the  $i$ -th bit in the word (W). In the most general case, the bit error probability,  $p_i$ , at each bit may have different values. In a particular case, where all bits have the same bit error probability,  $p_i = p$  ;  $i = 0, 1, \dots, b-1$

$$\epsilon^2 = \frac{2^{2b} - 1}{3 \cdot 2^{2b}} p \quad (3.17)$$

Assume that for each word, W, a fixed amount of energy ( $E_w$ ) is allocated. An optimum way exists of assigning the energy between the bits which minimizes the m.s.e. For constant amplitude modulation schemes, the way of assigning different amounts of energy between the bits in the word is simply by having different bit duration for each bit. In communication systems which work at high bit rate, this method is impractical because of implementation difficulties. However, for systems with low bit rate (few hundreds of bits/sec) this method is practical.

In Appendix D, the optimal bit energy assignment is calculated for a DPSK

modulation under the constraints of constant word energy. Figure 3.11 shows the optimum normalized bit energy  $\bar{E}_{bi}$  ;  $i = 1, 2, \dots, b-1$  which gives the minimal M.S.E as a function of the signal-to-noise ratio for a 12 bit A/D converter and a binary DPSK modulation scheme. The normalized bit energy is defined as  $\bar{E}_{bi}$  = the  $i$ -th bit energy normalized by  $E'_b$  where  $E'_b$  is the total word energy ( $E_w$ ) divided by number of bits ( $b$ ).

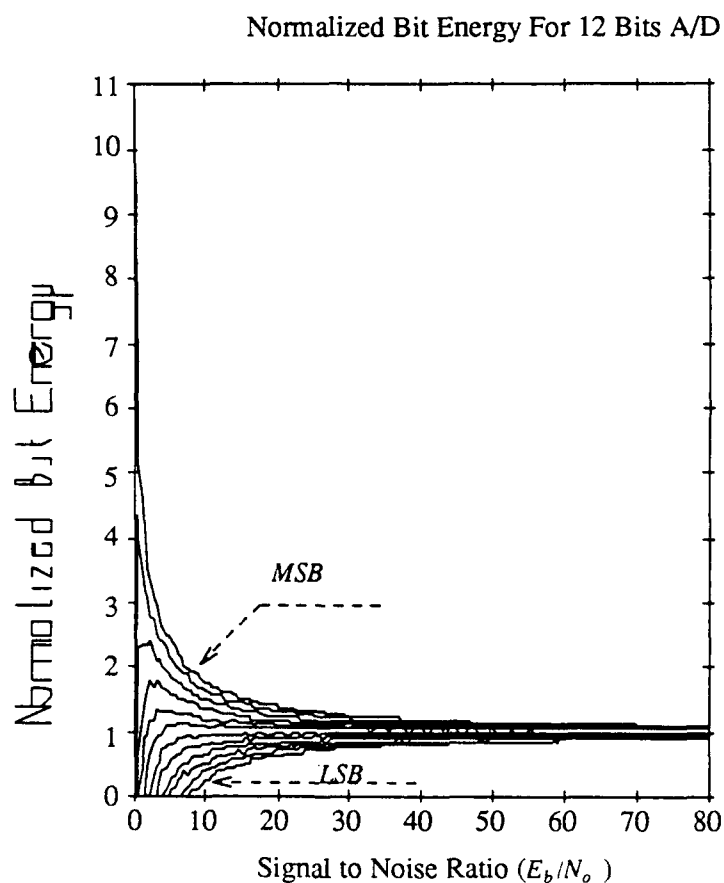


**Figure 3.11** Bit energy allocation that gives minimal M.S.E for a 12 bits A/D converter and BDPSK modulation

Figure 3.12 shows the ratio between the M.S.E when all bits have the same energy

and the case when energy is divided optimally.

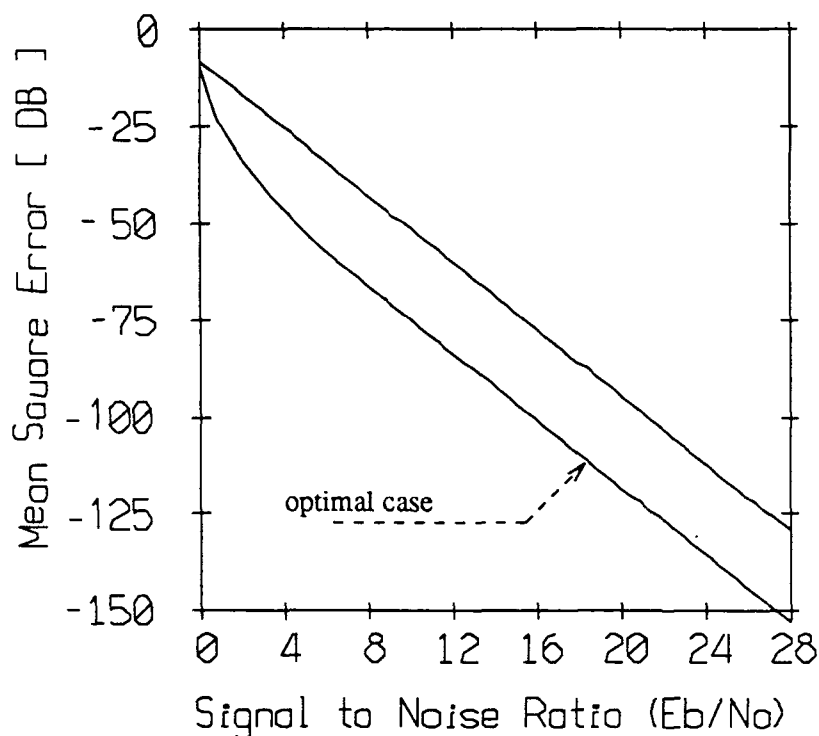


**Figure 3.12** Comparison of the M.S.E when equal bit energy is used and the optimal M.S.E, for 12 bit A/D converter.

Another interesting way to achieve unequal bit error probability is by using a modified error correction scheme. This class of error correction codes (ECC) family is known as UEP codes<sup>60</sup>. They have the property that a code can be designed to have different error correcting capability for different parts of the word.

In their pioneering work, Masnick and Wolf<sup>60</sup> have introduced the concept of unequal error protection codes. These codes have the property that some of the digits in a codeword will be decoded correctly if  $f_1$  errors occur, while others will be

decoded correctly only if  $f_2$  or fewer errors occur where  $f_1 > f_2$ . Boyarinov and Katsman<sup>8</sup> expanded the previous work and described a broad class of iterative and concatenated UEP codes.

### III.4 Do we need error correction?

Inherently, estimating an analog waveform from its digitized samples has an estimation error caused by the finite step size of the A/D converter.

This error usually is described as white noise and is known as quantization noise<sup>67</sup> [Chapter 9].

When digital data is modulated and transmitted through a non-ideal channel, errors occur in detecting the received signals. If the original signal is an analog signal which is digitized by an A/D converter, modulated and transmitted, the errors that occur during the detection process cause errors in the reconstructed analog signal. The error between the original and the reconstructed signals is a noise-like process and is defined as the detection error or the detection noise.

The variance of the A/D quantization error is<sup>67</sup>:

$$\sigma_q^2 = \frac{2^{-2b}}{12} \quad (3.18)$$

where  $b$  is the number of bits of the A/D converter. For the detection noise, the mean square error,  $\epsilon^2$ , (m.s.e) is given by (3.16) (or by (3.17) for equal bit error probability). If we keep the detection mean square error less than the quantization error, the contribution of the error caused by wrong decisions of the receiver will be negligible with respect to the quantization noise and no degradation of the system performance will occur. Let us require that

$$\frac{\sigma_q^2}{\epsilon^2} \geq 2 . \quad (3.19)$$

Substituting (3.17) and (3.18) into (3.19) leads to the requirement that

$$\frac{3 \cdot 2^{2b}}{12 \cdot 2^{2b} (2^{2b} - 1) p_e} \geq 2 , \quad (3.20)$$

or

$$p_e \leq \frac{1}{8 (2^{2b} - 1)} = 2^{-(2b+3)} .$$

For  $b = 8$ ,  $p_e$  has to be less than  $1.9 \times 10^{-6}$ . For  $b = 12$ ,  $p_e$  has to be less than  $2.9 \times 10^{-8}$ .

For optimal bit power management (III.3.3 and appendix C),  $p_e$  must be less than  $4 \times 10^{-5}$  for  $b = 8$ , and less than  $1.7 \times 10^{-6}$  for  $b = 12$

Let us now calculate the achieved bit error probability of a system with source level of  $170 \text{ dB}/1\mu\text{Pa}$ , where the distance between the receiver and the transmitter is  $5 \text{ km}$

Using the sonar equation<sup>85</sup>, the received signal level is

$$EL = SL - TL + DI \quad (3.21)$$

where the transmission loss,  $TL$ , is given by

$$TL \approx C_a \log(R) + \alpha R .$$

$C_a = 20$  for volume spreading and  $C_a = 10$  for cylindrical spreading. For transmitter and receiver located at a depth of few hundred meter, ocean depth of  $1 \text{ km}$ , and  $R = 5 \text{ km}$ ,  $C_a$  can be assumed to be 15. For  $\alpha = 1 \text{ dB}/\text{km}$ ,  $DI = 1$ ,  $R = 5 \text{ km}$  the received signal level is  $109 \text{ dB}/1\mu\text{Pa}$ . From Urick<sup>85</sup> [Figure 7.7, curve C], the sea noise level at  $10 \text{ kHz}$  is  $50 \text{ dB}/1\mu\text{Pa}/\sqrt{\text{Hz}}$ .

The received bit energy (for bit rate of  $1 \text{ kbit}/\text{sec}$ ) is

$$E_b = EL \cdot T = 109 - 30 = 79 \text{ [dB}/1\mu\text{Pa}]$$

and

$$\gamma_b = \frac{E_b}{N_0} = 29 \text{ dB}$$

which for binary DPSK gives a bit error rate much lower than  $2.9 \times 10^{-8}$ . In the worst case, when  $C_a = 20$ , the transmission loss is 91 dB which gives bit error probability of  $1.7 \times 10^{-6}$ . For bit a rate of 1 kbit/sec and an 8 bit A/D, the achieved bit error rate (even for the worst case of  $C_a = 20$  and no optimal power assignment) is on the order of the quantization noise. Therefore, no error correction (which reduces the effective bit rate) is required.

### III.5 Combined chirp DPSK and error correction

As we saw in III.4, no error correction is needed for the given scenario in order to achieve the desired system performance. However, if for any reason the signal to noise ratio decreases (reducing the transmitting power, higher ambient noise than is expected, making the distance between receiver and transmitter larger), error correction must be added to the system.

A necessary condition for chirp DPSK modulation is to keep the time-bandwidth product of the signal on the order of 10. Hence, in order to add an error correction capability in one hand, and not to reduce the information rate on the other hand, a higher order DPSK modulation must be used. In Appendix B we enclose curves of several common error correction techniques [Odenwalder<sup>66</sup>]. From these curves and from Figure 3.9, we can conclude that a significant coding gain can be achieved. As an example, using chirp QDPSK with code rate of  $\frac{1}{2}$  keeps the information rate and the time-bandwidth product the same as chirp BDPSK with the same symbol rate. However, if a bit error rate of  $10^{-6}$  is desired, a signal to noise ratio of 11.18 dB is required when BDPSK modulation is use, and approximately 8 dB is required when a QDPSK with extended (24,12) Golay code is used (from Figures

B.1 and 3.9). When a convolutional code with rate of  $\frac{1}{2}$  and constraint length of 7 is used even better performance can be achieved (Figure B.4 and 3.9) and a signal to noise ratio of approximately 6.5 dB is required to get the same performance as before.

If a higher information rate is required (for example, 2 kbit/sec instead of 1 kbit/sec), a 16-ary chirp QPSK with a rate  $\frac{1}{2}$  error correcting code can be used. When using the previous convolutional code, a signal to noise ratio of around 13 dB is required. Another way to achieve the same bit rate is just to choose a chirp QDPSK with the previous convolutional error correcting code but doubling the symbol rate. In this case, around 6.5 dB signal to noise ratio is required. The penalty that we pay is decreasing of the intersymbol interference and reducing the immunity to fading. This is due to the fact that the spectrum of the chirp signal is not flat any more and has higher side lobes on the other hand. Figure 3.13 shows the spectrum of a chirp signal with time-bandwidth product of 5.

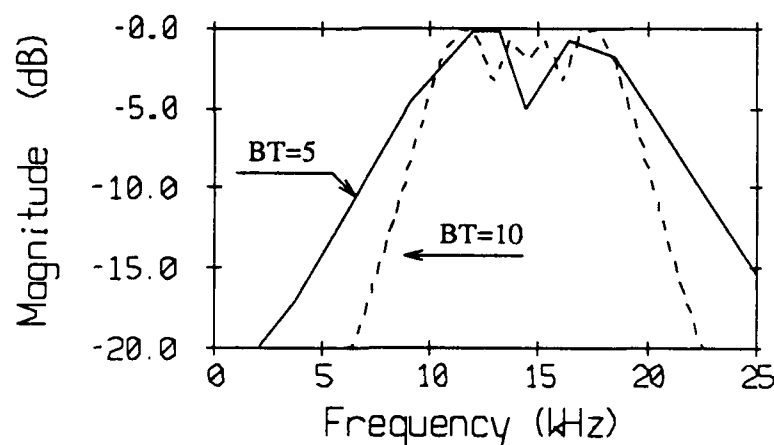


Figure 3.13: Spectra of chirp signals with time-bandwidth product of 5 and 10.

## IV Synchronization

### IV.1 Introduction

Power-efficient digital receivers generally require a digital clock synchronized to the received bit stream to control the integrate-and-dump detection filter or to control the timing of the output bit stream. The utility of any particular signaling waveform depends rather critically on the design of the synchronization system used to generate the receiver carrier phase, the fundamental clock and bit reference from the received signal. When coherent detection is used, perfect knowledge of the carrier frequency and phase is vital to the receiver in order to be able to detect the transmitted signal. For incoherent modulation schemes, only the knowledge of the carrier frequency is necessary to detect the transmitted signal.

DPSK modulation is semi coherent scheme. Perfect knowledge of the bit duration and precise bit synchronization are necessary at the receiver. Synchronization can be divided to three levels of hierarchy:

- (1) carrier recovery and phase synchronization.
- (2) timing recovery or symbol (bit) synchronization.
- (3) word or frame synchronization.

First, assuming that a carrier-type system is involved, there is a problem of carrier and phase synchronization concerning the generation of a reference carrier with a phase closely matching that of the data signal. This reference carrier is used at the receiver to perform a coherent demodulation operation. Next comes the problem of synchronizing the receiver clock with the baseband data-symbol sequence. This

commonly is called symbol (or bit) synchronization. Depending on the type of system under consideration, the problem of word, or frame synchronization will be encountered further down in the hierarchy.

Basically, there are two approaches to providing synchronization. Either a separate channel is allocated for sending the synchronization signal or the synchronization information appears on the same channel as the data and is derived from the data bearing signal itself. As discussed here, bit synchronization is restricted to self-synchronization techniques that extract the clock time directly from the noisy received signal.

When a coherent modulation approach is used, precise knowledge of the phase and the carrier waveform is necessary. For an incoherent approach, scheme the phase of the signal is not information bearing and only a rough knowledge of the carrier waveform must be known. Both approaches need good bit synchronization in order to achieve the maximum performance of the system.

For DPSK modulation scheme, the information bearing signal is the phase difference between two adjacent symbols. As the signal reference is always the previous pulse, no need of carrier or phase recovery exists. But, as the information bearing signal is the phase difference between two adjacent signal, very accurate bit synchronization is required. By bit synchronization, we mean time of arrival and bit duration estimation.

The purpose of timing recovery in DPSK systems is to recover a clock at the symbol rate or a multiple of the symbol rate from the modulated waveform. This clock is required to adjust the delay in the receiver (Figures 3.7 and 3.8) and to sample the received signal at the correct time instants.

Practical timing recovery circuits cannot perfectly duplicate the clock used

at the remote transmitter. The most basic requirement is that the average frequency of the derived timing waveform must be exactly equal to the average frequency of the transmitted signal. Although the average frequency of the derived timing must be exact, the timing signal usually has phase or timing jitter. In DPSK modulation this timing jitter is a fundamental impairment and dramatically reduces the receiver performance. It is necessary to know not only how often to sample the data bearing signal and the exact bit duration but also where to sample it. The choice of sampling instant is called the timing phase.

For conventional modulation approaches (the carrier waveform is a fixed frequency signal), the frequency recovery (which enables the estimation of bit duration) and the time of arrival techniques are thoroughly analyzed and well covered and documented in the literature. Simon & Lindsey<sup>54</sup> (Chapter. 9), Holmes<sup>45</sup>, Ziemer & Peterson<sup>97</sup> (Chapter. 6), Lee & Messerschmitt<sup>52</sup> (Part IV) and Franks<sup>34</sup> described and analyze the most common methods of timing, carrier, and bit synchronization.

Although a lot of effort is directed toward producing stable synthesizers and clocks, In most communication systems, a long term instability always exists and a frequency and clock shift between the transmitter and the receiver occurs. Carrier and clock recovery techniques which synchronize the carrier frequency and the clocks of the transmitter and the receiver, are developed and analyzed in several references<sup>7,34,52,82</sup>. In most communication systems, the bit duration is directly derived from the carrier frequency and synchronization to the carrier frequency enables the synchronization of the bit duration.

Since the carrier recovery block is not necessarily needed for DPSK demodulation and all the common methods of carrier recovery are not applicable when the carrier is a chirp signal, a different scheme of bit synchronization is proposed here. This method is based on the fact that the envelope of the matched filter output is a

periodic function with a period equal to the bit duration

In this chapter, we will present methods for bit synchronization and time of arrival estimation for a chirp DPSK modulation scheme. Moreover, we will show that the bit synchronizer is not sensitive to the fading and the multipath phenomena which are dominant in underwater acoustic communication.

#### IV.2 The optimum bit synchronizer

In the following we present a method to find the bit duration and the timing phase for chirp DPSK modulation. The received signal  $z(t)$  [Figure 4.1] is characterized by:

$$z(t) = y(t, \varepsilon) + n(t) = \sum_{i=0}^{\infty} a_i \bar{y}(t, \varepsilon) + n(t) \quad (4.1)$$

where  $a_i$  takes on the values  $+A$  or  $-A$  with probability  $\frac{1}{2}$ ,  $R_{a_i} = A^2 \delta(i - j)$ , and  $\bar{y}(t)$  is a time limited signal between  $[-\frac{T}{2} \leq t \leq \frac{T}{2}]$ , which depends on the modulation scheme used.

Wintz & Luecke<sup>94</sup> and Lindsey & Simon<sup>54</sup> showed that for known bit duration  $T$  and for a time interval of  $K \cdot T$  seconds long, the maximum a posteriori (MAP) estimator of  $\varepsilon$  is the  $\varepsilon$  which maximizes

$$\Lambda(z, \varepsilon) = \sum_{i=0}^K \ln \cosh \left[ \frac{2}{N_0} \int_{T_i(\varepsilon)} z(t) \bar{y}(t - iT - \varepsilon) dt \right] \quad (4.2)$$

The  $\ln(\cosh(\cdot))$  nonlinearity is approximately a square law device for small arguments and has approximately a magnitude function for large arguments, that is,

$$\ln \cosh(x) \approx \begin{cases} \frac{|x|}{2} & |x| \gg 1 \\ \frac{x^2}{2} & |x| \ll 1 \end{cases} \quad (4.3)$$

Using the approximation in (4.3), a suboptimum bit synchronizer configuration, which can easily be implemented is given in Figure 4.1.

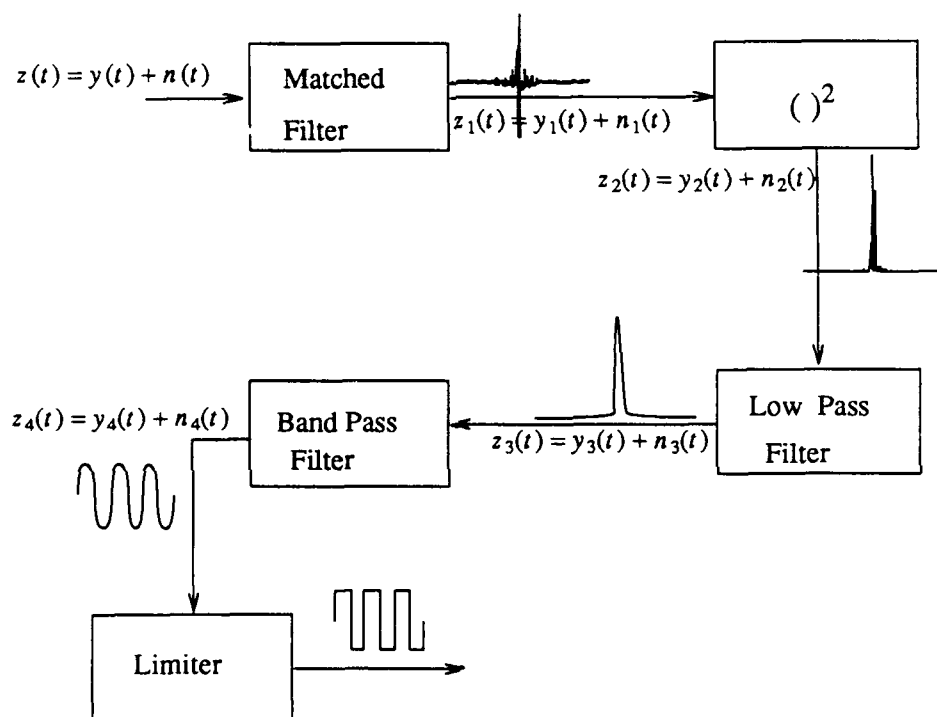


**Figure 4.1** Bit synchronization - block diagram of a suboptimum scheme.

The noisy input bit stream,  $z(t)$ , is first fed to a filter matched to the input wave shape ( $y(t)$ ), then squared and fed to the bandpass filter. The bandpass filter output is approximately a sine wave whose positive-going zero crossings estimate the data transition times. The bandpass filter bandwidth determines the synchronizer memory and the variance of the timing jitter. A limiter and an antibouncing circuit is used to provide a rectangular shaped periodic signal which drives the timing circuits

(Figure 4.1).

The output of the matched filter,  $z_1(t)$ , is

$$z_1(t) = y_1(t, \epsilon) + n_1(t) \quad (4.4)$$

where

$$y_1(t, \epsilon) = \sum_{i=0}^{\infty} a_i \tilde{y}_1(t - iT - \epsilon) \quad (4.5)$$

and

$$\tilde{y}_1(t) = \tilde{y}(t) * h(t)$$

$$n_1(t) = n(t) * h(t) .$$

$h(t)$  is the impulse response of the matched filter. After squaring and low pass filtering, (the lowpass cutoff frequency  $\omega_0 < \omega_{LP} < 2\omega_0$ ), we get

$$z_3(t, \epsilon) = y_3(t, \epsilon) + n_3(t) , \quad (4.6)$$

where

$$y_3(t, \epsilon) = A^2 \sum_{i=0}^{\infty} \tilde{y}_3(t - iT - \epsilon) + DC \text{ term}$$

and  $n_3(t)$  is a zero mean random process.  $y_3(t, \epsilon)$  also can be written as

$$y_3(t, \epsilon) = A^2 \tilde{y}_3(t) * \sum_{i=0}^{\infty} \delta(t - iT - \epsilon) + DC \text{ term} .$$

The power spectrum of  $y_3(t)$  is

$$Y_3(\omega) = A^2 \exp(-j\omega\epsilon) \tilde{Y}_3(\omega) \times \omega_T \sum_{i=0}^{\infty} \delta(\omega - i\omega_T) + DC \text{ term} \quad (4.7)$$

where  $\omega_T = \frac{2\pi}{T}$

Since the spectrum of  $Y_3(\omega)$  consists only of discrete frequencies which are multiples of the bit rate, bandpass filtering  $Y_3(\omega)$  with a narrow filter centered at one of the discrete frequencies gives the timing phase and the bit rate or any multiple of the bit frequency. If the bandpass filter is centered around  $\omega_T$ , then

$$y_4(t) = A_T \cos(\omega_T t + \phi) \quad (4.8)$$

where

$$A_T = \omega_T A^2 \bar{Y}_3(\omega_T)$$

and  $\bar{Y}_3(\omega)$  is the Fourier transform of  $\bar{y}_3(t)$ .

#### IV.2.1 System performance

Two metrics generally are used to measure the performance of a bit synchronizer, the rms jitter or timing misalignment and the mean of the absolute value of the jitter. In this chapter, we will calculate the rms jitter of the proposed scheme. No general expression of timing misalignment exists and different results exist for any bit synchronization implementation.

Wintz & Luecke<sup>94</sup> developed results for a RC lowpass filter with 3-dB bandwidth  $B = \frac{1}{T}$  followed by a square-law detector used to synchronize a NRZ PAM modulation scheme. The clock component is recovered with a phase locked loop or a bandpass filter with an equivalent bandpass memory of  $KT$  ( $KT$  is the observation time). The expected magnitude of error for a raised-cosine input wave form is approximately equal to

$$\frac{1}{T} E[|\varepsilon|] \approx \frac{0.33}{\sqrt{K} \gamma_b} \quad ; \quad \gamma_b > 5, K \geq 18$$

L. E. Franks<sup>34</sup>, Meyers & Franks<sup>61</sup>, Holmes<sup>45</sup> and Chiu & Lee<sup>20</sup> also have analyzed different types of bit synchronizers and presented their performance.

The signal component at the matched filter output is  $y_1(t) = y(t) * h(t)$  and the noise component  $n_1(t)$  is:  $n_1(t) = n(t) * h(t)$  where  $h(t)$  is the matched filter impulse response and is equal to:  $h(t) = \bar{y}^*(-t)$ . The  $(\cdot)^*$  denotes the complex conjugate of  $(\cdot)$ . Without losing generality,  $\varepsilon$  can be assumed to be zero. Then for  $y(t)$  a narrow band

process, the match filter output,  $(z_1(t))$  can be written in quadrature form as

$$z_1(t) = \left[ \sum_{i=0}^{\infty} a_i g(t - iT) + n_c(t) \right] \cos(\omega_0 t) - n_s(t) \sin(\omega_0 t) , \quad (4.9)$$

where  $g(t)$  is the lowpass equivalent match filter output to the input  $\bar{y}(t)$ .

The lowpass filter output,  $z_3(t)$ , is then

$$z_3(t) = \frac{1}{2} \left[ \sum_{i=0}^{\infty} a_i g(t - iT) + n_c(t) \right]^2 + \frac{1}{2} [n_s(t)]^2 \quad (4.10)$$

$z_3(t)$  is a nonstationary noncentral chi-squared random process with two degrees of freedom and probability density function,  $p_{z_3}(z_3, t)$ , equal to

$$p_{z_3}(z_3, t) = \frac{1}{2\sigma_{n_1}^2} \exp \left[ -\frac{[(\bar{y}_3(t))^2 + z_3]^2}{2\sigma_{n_1}^2} \right] I_0 \left[ \sqrt{z_3(t)} \frac{(\bar{y}_3(t))^2}{\sigma_{n_1}^2} \right] U(z_3) \quad (4.11)$$

and  $\overline{(\cdot)} = (\cdot)$  modulo T. The autocorrelation  $R_{z_3}(t, t-\tau)$  of  $z_3(t)$  is:

$$R_{z_3}(t, t-\tau) = E [z_3(t) z_3(t-\tau)] \quad (4.12)$$

$$= \frac{A^4}{4} g^2(\bar{t}) g^2(\bar{t}-\tau) + \frac{A^2 \sigma_{n_1}^2}{4} \left\{ 2g^2(\bar{t}-\tau) + 2g^2(\bar{t}) \right\} + A^2 R_{n_1}(\tau) g(\bar{t}) g(\bar{t}-\tau) + \sigma_{n_1}^4 + 2R_{n_1}^2(\tau) .$$

Define

$$n_3(t) = z_3(t) - y_3(t)$$

where

$$y_3(t) = E [z_3(t)] = \frac{1}{2} A^2 g^2(\bar{t}) + \sigma_{n_1}^2 . \quad (4.13)$$

For  $n(t)$ , a AWGN process with two sided spectral density  $\frac{N_0}{2}$  and  $A$  as defined in (4.1),  $n_3(t)$  is a zero mean random process with autocorrelation  $R_{n_3}(t, \tau)$  given by

$$R_{n_3}(t, \tau) = E [n_3(t) n_3(t-\tau)] = A^2 \frac{N_0}{2} g(\tau) g(\bar{t}) g(\bar{t}-\tau) + \left[ \frac{N_0}{2} g(\tau) \right]^2 . \quad (4.14)$$

For a large signal to noise ratio,  $n_3(t)$  is well approximated by a non stationary zero mean Gaussian random process with autocorrelation function as in (4.14),

and

$$\sigma_{n_s}^2(t) = A^2 g^2(\bar{t}) \sigma_{n_1}^2 + \sigma_{n_1}^4 \quad (4.15)$$

$n_4(t)$  is also a zero mean Gaussian random process with autocorrelation function is equal to

$$R_{n_s}(t, \tau) = R_{n_1}(t, \tau) * h_{BP}(t) * h_{BP}^*(-t)$$

where  $h_{BP}(t)$  is the impulse response of the bandpass filter.

The estimated timing phase,  $\hat{\epsilon}$ , is the instant when  $z_4(t)$  crosses the zero axis (Figure 4.2).

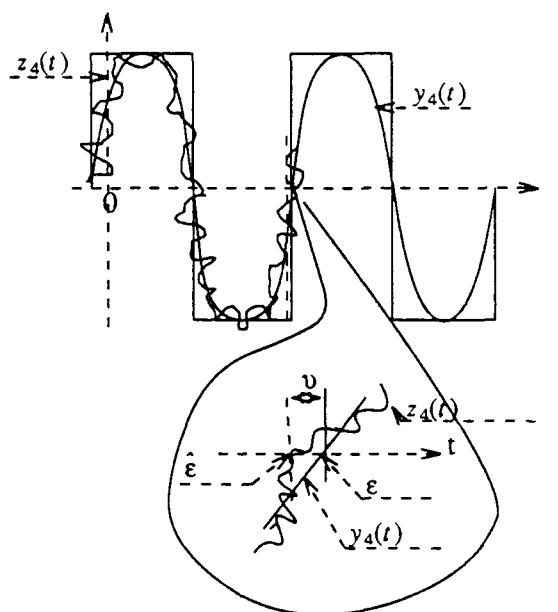


Figure 4.2 Bit synchronizer - estimation error.

Define  $v$  as the error between the true  $\epsilon$  and the estimator ( $\hat{\epsilon}$ ). Without loss of generality, assume that  $\epsilon = 0$ . The variance of the bit synchronizer error is then:

$$\sigma_v^2 = \int_{-\frac{T}{2}}^{\frac{T}{2}} v^2 P(v) dv$$

Assuming that the autocorrelation function of  $n_a(t)$  is differentiable and using the analysis of the well-known level crossing problem (Papoulis<sup>68</sup> Chapter 11-4) we get (assuming an antibouncing circuit exists in the limiter block)

$$\sigma_v^2 = \frac{1}{\pi} \int_{-\frac{T}{2}}^{\frac{T}{2}} v^2 \left[ \frac{-R''_{n_a}(0,0)}{R_{n_a}(0,0)} \right]^{\frac{1}{2}} \exp \left[ -\frac{[A_T \sin(\omega_T v)]^2}{2 R_{n_a}(0,0)} \right] dv \quad (4.16)$$

$$= \frac{1}{\pi} \int_{-\frac{T}{2}}^{\frac{T}{2}} v^2 \left[ \frac{\int_{-\infty}^{\infty} \omega^2 S_{n_a}(0,\omega) d\omega}{\int_{-\infty}^{\infty} S_{n_a}(0,\omega) d\omega} \right]^{\frac{1}{2}} \exp \left[ -\frac{[A_T \sin(\omega_T v)]^2}{2 \int_{-\infty}^{\infty} S_{n_a}(0,\omega) \frac{d\omega}{2\pi}} \right] dv,$$

where

$$R''_{n_a}(0,0) = \frac{\partial^2}{\partial \tau^2} R_{n_a}(t,\tau) \Big|_{t=0,\tau=0}.$$

For an ideal bandpass filter with  $B_{B.P}$  bandwidth and a channel free from multipath, substituting (4.8) and (4.15) in (4.16) we get

$$\sigma_v^2 = \frac{1}{\pi} \left[ \frac{\int_{-\infty}^{\infty} \omega^2 S_{n_a}(0,\omega) d\omega}{\int_{-\infty}^{\infty} S_{n_a}(0,\omega) d\omega} \right]^{\frac{1}{2}} \quad (4.17)$$

$$\times \int_{-\frac{T}{2}}^{\frac{T}{2}} v^2 \exp \left[ -\frac{\omega_T^2 \gamma_b^2 S_g^2(\omega_T) \sin^2(\omega_T v)}{8 \pi^2 \left[ \frac{2 \gamma_b}{T} g(0) + 1 \right] \int_{-\frac{B_{B.P}}{2}}^{\frac{B_{B.P}}{2}} S_{g^2}(\omega) d\omega} \right] dv$$

where  $S_{g^2}(\omega)$  is the Fourier transform of  $g^2(t)$ , and  $\gamma_b$  is defined as  $\frac{A^2 T}{2 N_0}$ . The value

of  $\left[ \frac{\int_{-\infty}^{\infty} \omega^2 S_{n_a}(0,\omega) d\omega}{\int_{-\infty}^{\infty} S_{n_a}(0,\omega) d\omega} \right]^{\frac{1}{2}}$  is known as the r.m.s. bandwidth of the process  $n_a(t)$  and

denoted by  $\left[ \overline{\omega^2} \right]^{\frac{1}{2}}$  (Helstrom<sup>41</sup> pp 474).

Since the bandpass filter is relatively narrowband, we can assume that in the relevant bandwidth  $S_g(\omega)$  is constant and is equal to  $S_g(\omega_T)$ . In this case,

$$\int_{-\frac{B_{BP}}{2}}^{\frac{B_{BP}}{2}} S_g(\omega) d\omega \approx B_{BP} S_g(\omega_T) \quad (4.18)$$

and for ideal bandpass filter

$$\left[ \frac{\int_{-\infty}^{\infty} \omega^2 S_{n_s}(0, \omega) d\omega}{\int_{-\infty}^{\infty} S_{n_s}(0, \omega) d\omega} \right]^{\frac{1}{2}} = \sqrt{\frac{T}{3}} \frac{B_{BP}^2}{4}$$

For a chirp input signal defined as:

$$\bar{y}(t) = \text{Re} [ \exp j (\omega_0 t + \frac{1}{2} \mu t^2) ] \quad -\frac{T}{2} \leq t \leq \frac{T}{2} \quad (4.19)$$

The matched filter impulse response  $h(t)$  is

$$h(t) = \text{Re} [ \exp j (\omega_0 t - \frac{1}{2} \mu t^2) ] \quad -\frac{T}{2} \leq t \leq \frac{T}{2} \quad (4.20)$$

The signal component,  $\bar{y}_1(t)$ , at the matched filter output is

$$\bar{y}_1(t) = \cos(\omega_0 t) g(t) \quad (4.21)$$

where

$$g(t) = \frac{2}{\mu |t|} \sin\left(\frac{1}{2} [\mu T |t| - t^2]\right) \quad ; \quad -T \leq t \leq T$$

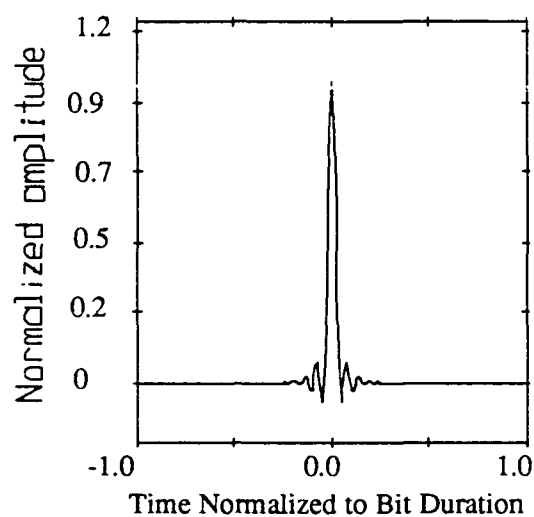


Figure 4.3 The equivalent lowpass matched filter output -  $g(t)$

Using "  $K$  " as defined by Wintz & Luecke <sup>94</sup>,  $B_{B,P}$  can be approximated as

$$\frac{\omega_T}{K}.$$

After some simple substitutions we get

$$\sigma_v^2 = \frac{1}{\pi} \left[ \overline{\omega^2} \right]^{\frac{1}{2}} \int_{-\frac{T}{2}}^{\frac{T}{2}} v^2 \exp \left[ -\frac{K \omega_T^3 \gamma_b^2 S_g(\omega_T) \sin^2(\omega_T v)}{8 \pi^2 [2\gamma_b + 1]} \right] dv. \quad (4.22)$$

Figure. 4.4 gives the normalized error standard deviation  $\frac{\sigma_v}{T}$  as a function of the signal to noise ratio for different values of  $K$  when the chirp signal has a time-bandwidth product of  $20\pi$  and bit rate ( $\frac{1}{T}$ ) of 1 kbits/sec

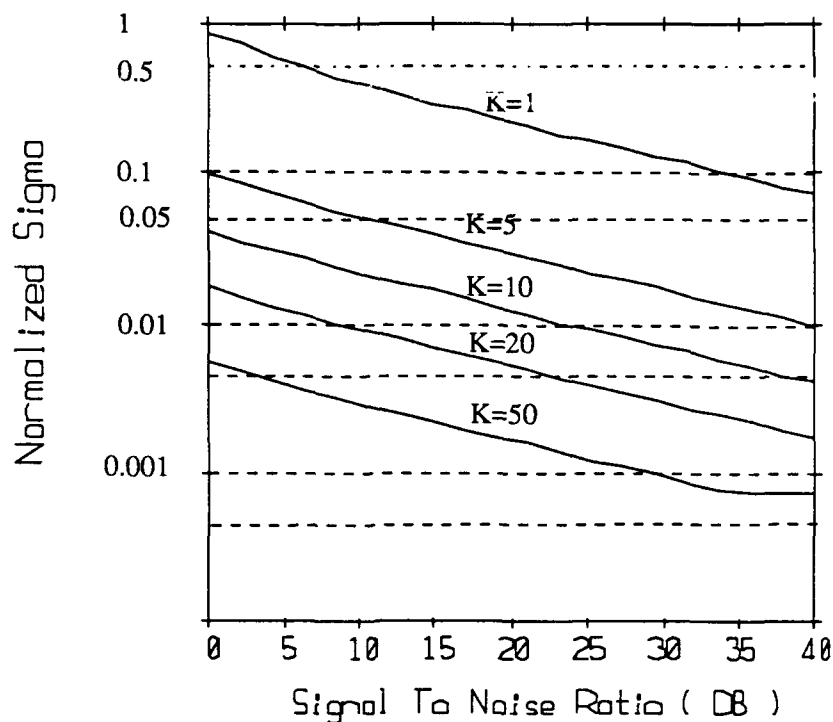


Figure 4.4 The normalized error standard deviation as a function of the signal to noise ratio for different values of K.

#### IV.III Bit synchronization using time of arrival estimation method

In the ocean acoustic channel, there are two major obstacles towards the successful use of the bit synchronizer scheme presented above. The frequent non-specular multipath implies noise in addition to the ambient noise, and the presence of specular multipath does not guarantee tracking of the principal timing phase. In the presense of multipath, the signal component at the matched filter output is

$$y_1(t, \epsilon) = y_d(t, \epsilon) + y_{ms}(t, \epsilon) + y_{nr}(t, \epsilon) , \quad (4.23)$$

where  $y_d(t, \epsilon)$  is the direct path component and is equal to

$$y_d(t, \epsilon) = \sum_{i=0}^{\infty} a_i \bar{y}_1(t - iT - \epsilon)$$

$y_{ms}(t, \epsilon)$  is the specular multipath contribution and is given by

$$y_{ms}(t, \epsilon) = \sum_{i=0}^{\infty} b_i \bar{y}_1(t - iT - \epsilon - \zeta)$$

where  $\zeta$  is the time delay between the direct and the indirect paths. For a stationary or a very slowly moving receiver and/or transmitter, the time delay  $\zeta$  is a slowly varying function with a time varying mean and a small variance.

The nonspecular multipath contribution  $y_{ns}(t, \epsilon)$  is

$$y_{ns}(t, \epsilon) = \sum_{i=0}^{\infty} c_i \bar{y}_1(t - iT - \epsilon + \theta_i)$$

where  $\theta_i$  is uniformly distributed between 0 and  $2\pi$ . For this case, the output of the square law device (Figure 4.1) is

$$\begin{aligned} y_3(t) = & [A^2 \bar{y}_3(t - \epsilon) + k^2 \bar{y}_3(t - \zeta)] * \sum_{i=0}^{\infty} \delta(t - iT) + C^2 \bar{y}_3(t) * \sum_{i=0}^{\infty} \delta(t - iT + \theta_i) \quad (4.24) \\ & + 2 \sum_{i=0}^{\infty} \left[ a_i \bar{y}_3(t - iT - \epsilon) b_i \bar{y}_3(t - iT - \zeta) \cos(\alpha - \epsilon) + a_i \bar{y}_3(t - iT - \epsilon) c_i \bar{y}_3(t - iT - \theta_i) \cos(\epsilon - \theta_i) \right. \\ & \left. + b_i \bar{y}_3(t - iT - \zeta) c_i \bar{y}_3(t - iT - \theta_i) \cos(\zeta - \theta_i) \right] \end{aligned}$$

where  $\alpha$  is the phase difference between the direct and the indirect paths,  $A = |a_i|$  and  $B = |b_i| = kA$  for all  $i$ . The first term in (4.24) is a periodic function with period  $T$ . The second and the third terms are noise-like signals. In the frequency domain

$$Y_3(\omega) = A^2 \left[ \exp(-j\omega\epsilon) + k^2 \exp(-j\omega\alpha) \right] \bar{Y}_3(\omega) \times \omega_T \sum_{i=0}^{\infty} \delta(\omega - i\omega_T) + NOISE$$

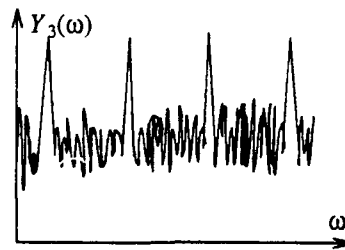


Figure 4.5 Bit synchronization - spectrum of the low pass filter output

It can be seen that multipath is a destructive phenomenon for the bit synchronization concept described above. It increases the overall noise level and prevents good bit synchronization. The estimated timing phase  $\hat{\epsilon}$  falls somewhere between the real  $\epsilon$  and  $\alpha$  which is far away from  $\epsilon$ .

Modification of single pulse time of arrival estimation is an alternative bit synchronization concept which enables us to synchronize to the timing phase even in the presence of specular multipath. As before, assume that the bit duration  $T$  is perfectly known. In such a case it is easy to prove [ Helstrom<sup>41</sup> page 376 ] that the maximum likelihood estimate  $\hat{\epsilon}$  of  $\epsilon$  is the time at which the rectified output of the matched filter is maximum. The output will have many peaks and the highest of them identifies the time  $\epsilon$ . Figure 4.6 shows a block diagram of the system for the multiple case.

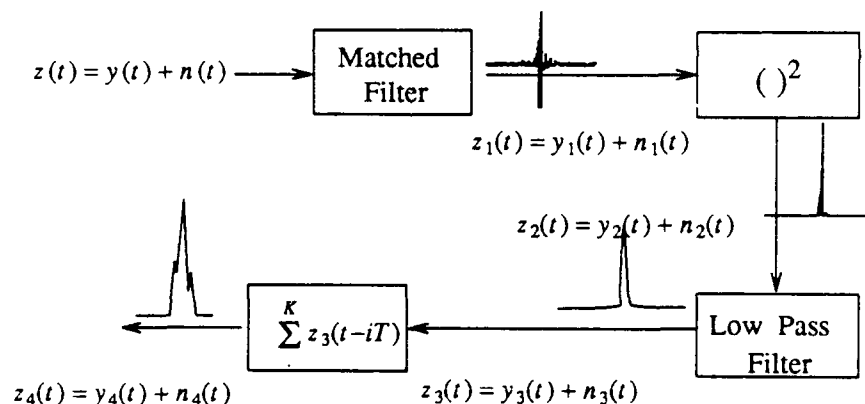


Figure 4.6 Bit synchronization - autocorrelation implementation

The synchronizer output,  $z_4(t, \epsilon)$ , is

$$z_4(t, \epsilon) = \frac{1}{K} \sum_0^K z_3(t - iT) \quad (4.25)$$

In the presence of multipath, the signal component at the synchronizer output is

$$y_4(t) = \frac{1}{K} \left[ \sum_{i=0}^K A^2 \bar{y}_3(t-\epsilon) + B^2 \bar{y}_3(t-\zeta) + C_i^2 \bar{y}_3(t-\theta_i) + \text{cross terms} \right] \quad (4.26)$$

The third term in (4.26) is due to the nonspecular multipath phenomenon and is completely random in phase and amplitude. The fourth term is also a random process. For  $\theta_i$  uniformly distributed between  $-\pi$  and  $\pi$ , these two terms have a zero mean and for  $K$  large enough, they vanish.

For a single pulse, the variance of the estimator  $\hat{\epsilon}$  is<sup>41</sup>

$$\text{Var } \hat{\epsilon} \approx \left[ 2 \gamma_b \beta^2 \right]^{-1} \quad (4.27)$$

and for multiple pulses,

$$\text{Var } \hat{\epsilon} \approx \left[ 2 K \gamma_b \beta^2 \right]^{-1}$$

where

$$\beta^2 = \frac{\int_{-\infty}^{+\infty} \left[ \frac{d}{dt} \bar{y}(t) \right]^2 dt}{\int_{-\infty}^{+\infty} [\bar{y}(t)]^2 dt}$$

or, according to Parseval's theorem

$$\beta^2 = \frac{\int_{-\infty}^{+\infty} [\omega^2 | \bar{Y}(\omega) |^2] d\omega}{\int_{-\infty}^{+\infty} [ | \bar{Y}(\omega) |^2] d\omega}$$

For incoherent detection (which is our case)  $\bar{y}(t)$ , is substituted by  $g(t)$ .

The signal  $z_4(t) = \frac{1}{K} \sum_{p=0}^{K-1} z_3(t - pT)$  and explicitly,

$$\begin{aligned} z_4(t) = & \frac{1}{2} A^2 g^2(t) + \frac{1}{2} (k A)^2 \overline{g(t-\zeta)} + \frac{1}{2K} \sum_{p=0}^{K-1} n_c^2(t-pT) + \frac{1}{2K} \sum_{p=0}^{K-1} n_s^2(t-pT) \\ & + \frac{1}{K} \sum_{p=0}^{K-1} \sum_{i=0}^{\infty} a_{i-p} b_{i-p} g[t-(i+p)T] g[t-(i+p)T-\zeta] \cos \alpha_{i-p} \end{aligned} \quad (4.28)$$

$$\begin{aligned}
& + \frac{1}{K} \sum_p n_c(t-pT) \sum_i a_{i-p} g[t-(i+p)T] \\
& + \frac{1}{K} \sum_p n_c(t-pT) \sum_i b_{i-p} g[t-(i+p)T-\zeta] \cos \alpha_{i-p} \\
& + \frac{1}{K} \sum_p n_s(t-pT) \sum_i b_{i-p} g[t-(i+p)T-\zeta] \sin \alpha_{i-p}
\end{aligned}$$

For  $y_4(t)$  defined as  $y_4(t) = E[z_4(t)]$  and  $n_4(t)$  defined as  $n_4(t) = z_4(t) - y_4(t)$  we get

$$y_4(t) = \frac{1}{2} A^2 g^2(\bar{T}) + \frac{1}{2} k^2 A^2 g^2(\bar{T}-\bar{\zeta}) + k A^2 g(\bar{T}) g(\bar{T}-\bar{\zeta}) E[\cos \alpha] + \sigma_{n_1}^2 \quad (4.29)$$

and

$$R_{n_4}(t, t-\tau) = E[n_4(t) n_4(t-\tau)] = \quad (4.30)$$

$$\begin{aligned}
& = \frac{1}{K} \sum_p \sum_q R_{n_1}((q-p)T+\tau) + \frac{A^2}{K} \sum_p \sum_q R_{n_1}((q-p)T+\tau) \left[ \Gamma_{\bar{\tau}+\bar{\zeta}} k g(\bar{T}) g(\bar{T}-(\bar{\tau}+\bar{\zeta})) E[\cos \alpha_p] \right. \\
& \quad + \Gamma_{\bar{\tau}-\bar{\zeta}} k g(\bar{T}-\bar{\zeta}) g(\bar{T}-\bar{\zeta}+(\bar{\zeta}-\bar{\tau})) E[\cos \alpha_p] + k^2 g(\bar{T}-\bar{\zeta}) g(\bar{T}-\bar{\zeta}-\bar{\tau}) E[\cos \alpha_p \cos \alpha_q] \\
& \quad + k^2 g(\bar{T}-\bar{\zeta}) g(\bar{T}-\bar{\zeta}-\bar{\tau}) E[\sin \alpha_p \sin \alpha_q] + k^2 g(\bar{T}) g(\bar{T}-\bar{\tau}) \left. \right] + \sigma_{n_1}^2 k A^2 g(\bar{T}) g(\bar{T}-\bar{\zeta}) E[\cos \alpha_p] \\
& \quad + k^2 A^4 g(\bar{T}) g(\bar{T}-\bar{\zeta}) g(\bar{T}-\bar{\zeta}+\bar{\zeta}-\bar{\tau}) g(\bar{T}-\bar{\zeta}-\bar{\tau}) \left[ E[\cos \alpha] \right]^2 - \sigma_{n_1}^4
\end{aligned}$$

where  $\Gamma_{(\cdot)} = p - \#$  of bits in  $(\cdot)$ .

For  $R_{n_1} = \frac{N_0}{2} g(\tau)$ , (4.30) becomes:

$$R_{n_4}(t, t-\tau) = \quad (4.31)$$

$$\begin{aligned}
& \frac{1}{K} \left[ \frac{N_0}{2} g(\bar{\tau}) \right]^2 + A^2 \frac{N_0}{2} g(\bar{\tau}) \left[ g(\bar{T}) g(\bar{T}-\bar{\tau}) + \frac{\Gamma_{(\bar{\tau}-\bar{\zeta})}}{K} k g(\bar{T}) g(\bar{T}-(\bar{\tau}+\bar{\zeta})) E[\cos \alpha] \right. \\
& \quad + \frac{\Gamma_{(\bar{\tau}+\bar{\zeta})}}{K} k g(\bar{T}-\bar{\zeta}) g(\bar{T}-\bar{\zeta}+(\bar{\zeta}-\bar{\tau})) E[\cos \alpha] + k^2 g(\bar{T}-\bar{\zeta}) g(\bar{T}-\bar{\zeta}-\bar{\tau})
\end{aligned}$$

$$\begin{aligned}
& + k^2 g(\bar{t}-\bar{\zeta}) g(\bar{t}-\bar{\zeta}-\tau) \Big] \\
& - \left[ \frac{N_0}{2} g(0) \right]^2 + \frac{N_0}{2} g(0) k A^2 g(\bar{T}) g(\bar{T}-\bar{\zeta}) E[\cos \alpha] \\
& + k^2 A^4 g(\bar{T}) g(\bar{T}-\bar{\zeta}) g(\bar{t}-\bar{\zeta}+\bar{\zeta}-\tau) g(\bar{t}-\bar{\zeta}-\tau) \left[ E[\cos \alpha] \right]^2
\end{aligned}$$

Two cases are analysed. In the first, the phase  $\alpha$  varies very slowly and assumed to be constant for a time period of  $K T$  bits. For this case,

$$y_4(t) = \frac{1}{2} A^2 g^2(\bar{T}) + \frac{1}{2} k^2 A^2 g^2(\bar{t}-\bar{\zeta}) + k A^2 g(\bar{T}) g(\bar{T}-\bar{\zeta}) \cos \alpha + \frac{N_0}{2} g(0) \quad (4.32)$$

and

$$R_{n_s}(t, t-\tau) = \quad (4.33)$$

$$\begin{aligned}
& \frac{1}{K} \left[ \frac{N_0}{2} g(\bar{\tau}) \right]^2 + A^2 \frac{N_0}{2} g(\bar{\tau}) \left[ g(\bar{T}) g(\bar{T}-\tau) + \frac{\Gamma(\bar{\tau}-\bar{\zeta})}{K} k g(\bar{T}) g(\bar{T}-(\bar{\tau}+\bar{\zeta})) \cos \alpha \right. \\
& \left. + \frac{\Gamma(\bar{\tau}+\bar{\zeta})}{K} k g(\bar{t}-\bar{\zeta}) g(\bar{t}-\bar{\zeta}+(\bar{\tau}-\bar{\zeta})) \cos \alpha + k^2 g(\bar{t}-\bar{\zeta}) g(\bar{t}-\bar{\zeta}-\tau) \right] \\
& + k^2 A^4 g(\bar{T}) g(\bar{T}-\bar{\zeta}) g(\bar{t}-\bar{\zeta}+\bar{\zeta}-\tau) g(\bar{t}-\bar{\zeta}-\tau) \left[ \cos \alpha \right]^2
\end{aligned}$$

In the second case, the phase  $\alpha$  varies very rapidly and is assumed to be uniformly distributed between  $[-\pi - \pi]$ . Then:

$$y_4(t) = \frac{1}{2} A^2 g^2(\bar{T}) + \frac{1}{2} k^2 A^2 g^2(\bar{t}-\bar{\zeta}) + \frac{N_0}{2} g(0) \quad (4.34)$$

and

$$R_{n_s}(t, t-\tau) = \frac{1}{K} \left[ \frac{N_0}{2} g(\bar{\tau}) \right]^2 + A^2 \frac{N_0}{2} g(\bar{\tau}) \left[ g(\bar{T}) g(\bar{T}-\tau) + k^2 g(\bar{t}-\bar{\zeta}) g(\bar{t}-\bar{\zeta}-\tau) \right] \quad (4.35)$$

In the presense of specular multipath, the performance of the estimator is not only governed by the additive noise, but also by the probability of locking onto the indirect path instead of the direct one. Let us define the case when the synchronizer is

locked to the peak at  $\epsilon$  as State 1, and when it is locked on the peak at  $\zeta$  as State 2. The locking probabilities state diagram is depicted in Figure 4.7

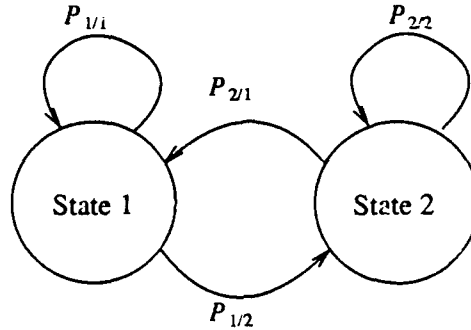


Figure 4.7 Error state diagram.

If the bit synchronizer is in State 1, it will not change its state in the next observation if the peak at  $\epsilon$  is higher than at  $\zeta$ . The probability for this event,  $P_{1/1}$ , is

$$P_{1/1}/\alpha = \int_{x=-\infty}^{+\infty} \int_{q=-\infty}^x P_{z_d(0), z_d(\zeta)}[z_d(0)=x, z_d(\zeta)=q] dq dx \quad (4.36)$$

For large signal to noise ratio and large  $K$ ,  $P_{z_d(0), z_d(\zeta)}$  can be assumed as normal and then

$$P_{1/1}/\alpha = \left[ 2\pi \sigma_{n_d(0)} \sigma_{n_d(\zeta)} \sqrt{1-\rho^2} \right]^{-1} \quad (4.37)$$

$$\times \int_{x=-\infty}^{+\infty} \int_{q=-\infty}^{x+\Delta y} \exp \left[ -\frac{\sigma_{n_d(\zeta)}^2 x^2 - 2\rho \sigma_{n_d(0)} \sigma_{n_d(\zeta)} x q + \sigma_{n_d(0)}^2 q^2}{2 [\sigma_{n_d(0)} \sigma_{n_d(\zeta)}]^2 (1-\rho^2)} \right] dq dx$$

where  $\Delta y \equiv y_d(0) - y_d(\zeta)$  and

$$\rho^2 \equiv \frac{R_{n_d}(0, \zeta)}{\sigma_{n_d(0)} \sigma_{n_d(\zeta)}}$$

After some simple algebraic manipulation, we get

$$P_{1/1} = \left[ 2\pi \sigma_{n_d(0)}^2 \right]^{-\frac{1}{2}} \int_{x=-\infty}^{+\infty} \exp \left[ -\frac{x^2}{2 \sigma_{n_d(0)}^2} \right] \phi \left[ \frac{\Delta y [\sigma_{n_d(0)} - \rho \sigma_{n_d(\zeta)}]}{\sigma_{n_d(0)} \sigma_{n_d(\zeta)} \sqrt{1-\rho^2}} \right] dx \quad (4.38)$$

Assume the synchronizer was initially locked onto the direct path (State 1).

If a decision is made every  $T_s$  seconds, ( $T_s = K T$  where  $K$  is the number of bit averaged), the mean time of being locked on State 1 is

$$T_{lock1} = T_s P_{1/2} \frac{P_{1/1}}{(1-P_{1/1})^2} . \quad (4.39)$$

The mean time of being locked onto state 2, if initially locked on State 1 is

$$T_{lock2} = T_s P_{2/1} P_{1/2} \frac{1}{(1-P_{2/2})^2} \quad (4.40)$$

Since  $P_{1/2} = 1 - P_{1/1}$ , and  $P_{2/1} = 1 - P_{2/2}$  we get that

$$T_{lock1} = \frac{P_{1/1} T_s}{1 - P_{1/1}} \quad (4.41)$$

$$T_{lock2} = \frac{T_s P_{1/2}}{1 - P_{2/2}}$$

and

$$\Lambda \equiv \frac{T_{lock1}}{T_{lock2}} = \frac{P_{1/1}(1-P_{2/2})}{(1-P_{1/1})^2} . \quad (4.42)$$

Figures 4.8-4.10 shows the dependence of  $\log \Lambda$  on the signal to noise ratio ( $\gamma_b$ ) for  $K = 100$  and for several values of  $k$  and  $\alpha$ , for the case when  $\alpha$  varies very fast.

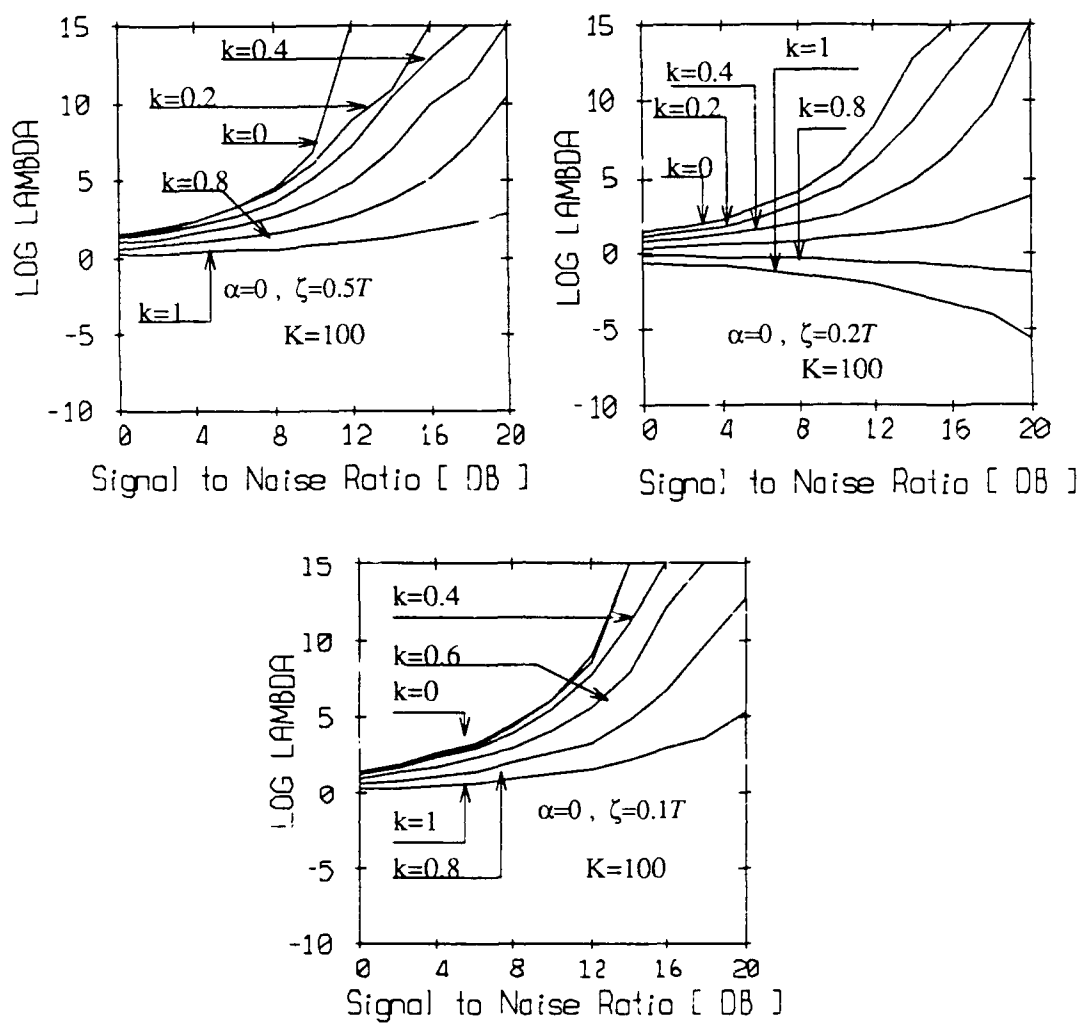


Figure 4.8  $\Lambda$  as a function of signal-to-noise ratio for various values of  $k$ ,  $\zeta$ , and for  $\alpha=0$ .

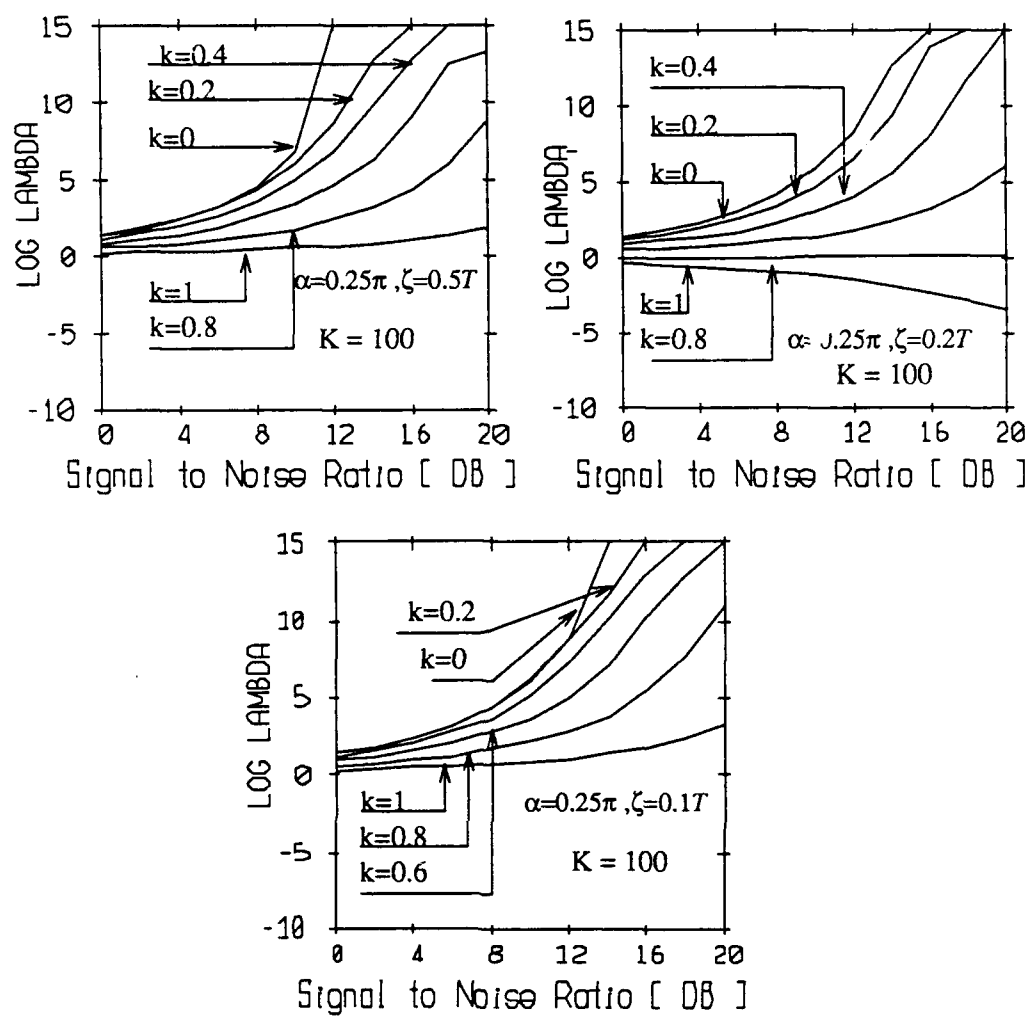


Figure 4.9  $\Lambda$  as a function of signal-to-noise ratio for various values of  $k$ ,  $\zeta$ , and for  $\alpha = 0.25\pi$ .

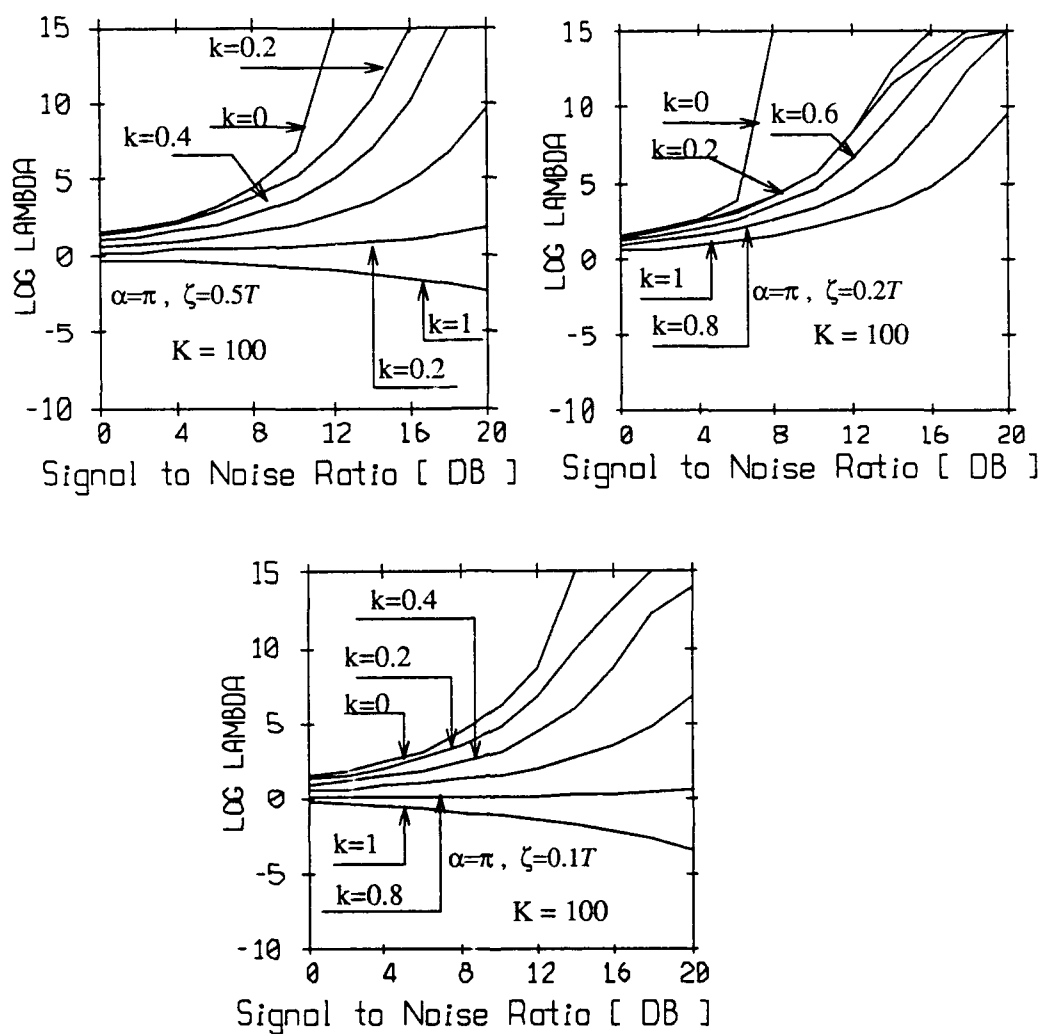


Figure 4.10  $\Lambda$  as a function of signal-to-noise ratio for various values of  $k$ ,  $\zeta$ , and for  $\alpha = \pi$ .

Figure 4.11 shows the dependence of  $\log \Lambda$  on the signal-to-noise ratio ( $\gamma_b$ ), for  $K = 100$  and for several values of  $k$  for the case where  $\alpha$  changes very rapidly.

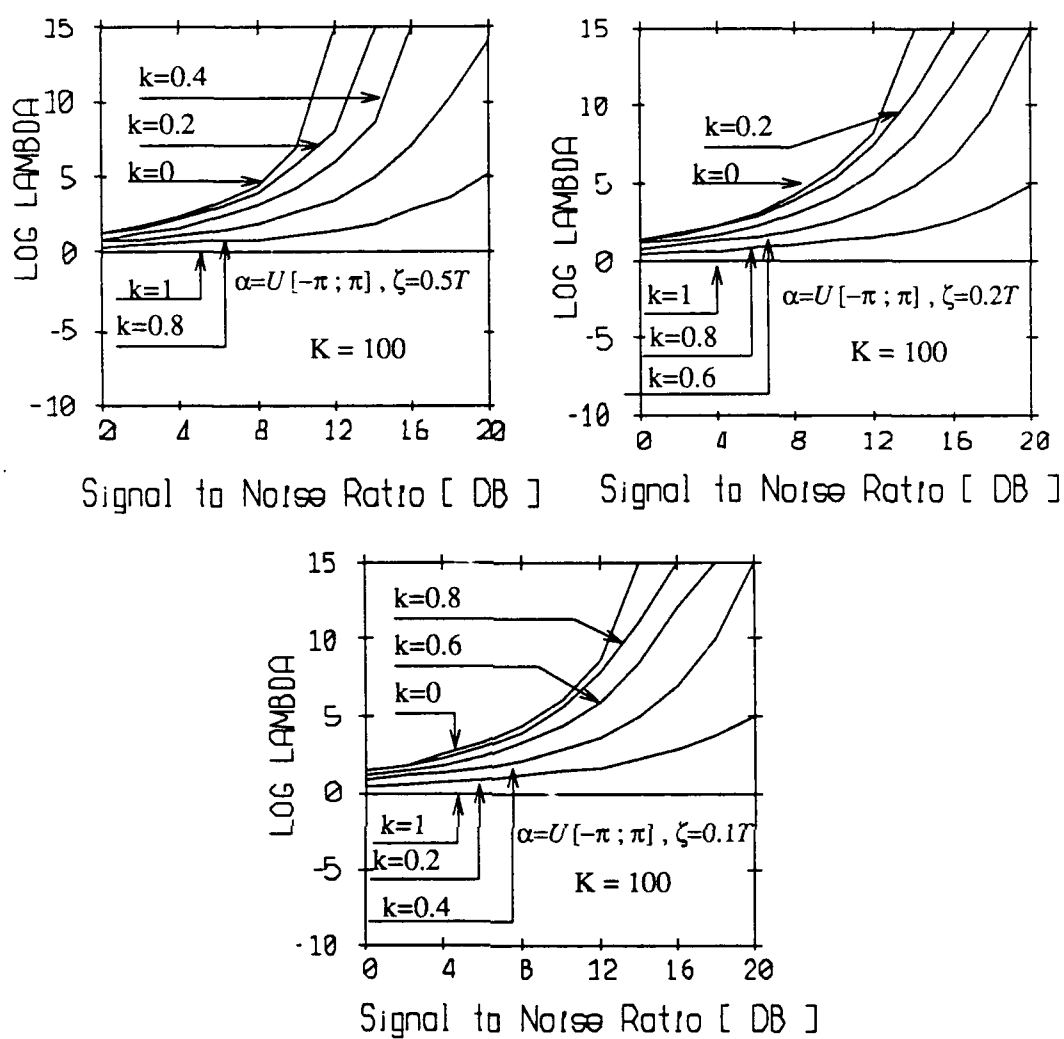


Figure 4.11  $\Lambda$  as a function of signal-to-noise Ratio for various values of  $k, \zeta$  and for  $\alpha$  changing very rapidly.

## V Equalization

### V.1 Introduction

The most severe problem in underwater acoustic communication is intersymbol interference (ISI). The major causes of the intersymbol interference are: a) channel multipath and b) shape of the modulated data. A careful inspection of the character of the underwater communication channel shows that two kinds of ISI exist - that due to "macro" multipaths and that due to the "micro" multipaths. Delayed replicas of the original signal (caused by reflection from the ocean surface and bottom, which can be on the order of several thousand of bits) are scrambled at the receiver with the signal received from the direct path and are disastrous to the receiver. The "micro" multipaths result in spreading the signal in addition to producing ISI from some of the adjacent symbols.

Even though multipath seriously degrades the receiver performance, it is known that, the theoretical channel capacity of a wide band link is not seriously reduced<sup>46</sup>. This theoretical result explains why so much effort is directed toward solving the channel equalization problem. However, this result applies only when exact knowledge of the channel parameters is exist which is a condition that hardly ever is met in practice. Therefore, adaptive receiver structures are required in order to suppress interference arising from unknown and/or changing multipath channels. Considerable research has been performed investigating performance criteria for optimizing the equalizer parameters. Since the most meaningful performance measure for a digital communication system is the average probability of error, it is desirable to choose the filter parameters to minimize this performance index. However, the probability of error is a highly nonlinear function of the equalizer parameters.

Consequently, the probability of error as a performance index for optimizing the equalizer parameters is impractical.

Two criteria have found widespread use in optimizing equalizer parameters. One is the peak distortion criterion and the other is the least-mean-square error criterion. The peak distortion criterion is defined as the worst-case intersymbol interference at the output of the equalizer. The minimization of this performance index is called the peak distortion criterion. The least-mean-square error (LMS) criterion is defined as minimizing the mean-square value of error between the equalizer output and the desired signal. The LMS equalizer minimizes the signal to distortion ratio at its output within the constraints of the equalizer time span and the delay through the equalizer.

In general, the equalizer is a recursive filter with poles as well as zeros. A filter with poles has two serious disadvantages compared with an all-zero filter: (1) it becomes unstable if the poles move outside the unit circle (during the adaptive process, or because of round off errors) and (2) its performance surface generally is non-quadratic and may have local minima<sup>92</sup>. For these reasons, recursive adaptive filters are found only in a limited number of applications. These disadvantages and the fact that any transfer function can be expressed as an all-zero transfer function with an infinite number of zeros are the reasons why most equalizers are implemented as transversal filters (where filters with an infinite number of zeros are approximated by filters with a finite number of zeros). Both RF as well as undersea channels are time varying. Therefore, adaptive equalizer structures are required in order to suppress interference arising from unknown and/or changing multipaths.

Much work has been done in the field of equalizer performance and implementation both as fixed as well as adaptive equalizers. The paper by Qureshi<sup>76</sup> and books by Proakis<sup>75</sup> (Chap. 6) and Lee and Messerschmitt<sup>52</sup> (Chap.8) provide a good

review of the equalization literature. The books by Haykin<sup>39</sup> and Widrow<sup>92</sup> provide good review of adaptive filtering concepts.

However, none of the existing equalizer configurations can be implemented directly for an underwater acoustic channel. Two characteristics of the underwater acoustic channel makes the existing equalizer structures impractical: (1) the very long multipath on the order of some thousands of bits and (2) the non-minimal phase character of the channel. These two basic characteristics of the underwater acoustic channel makes it completely different from a conventional radio link. The reason why the delay of the multipath is so large is due to the speed of sound in the ocean being relatively small. The nonminimal phase characteristics of the channel is due to the multipath from the sea surface is often being much stronger than the direct path.

When a zero forcing criterion is used, the transfer function of the equalizer is given by<sup>75</sup>

$$H_e(z,t) = \frac{1}{H_c(z,t)} \quad (5.1)$$

where  $H_c(z,t)$  is the  $z$  transform of the channel impulse response. When the LMS criterion is used, the transfer function of the equalizer satisfies<sup>75</sup>

$$H_e(z,t) = \frac{1}{H_c(z,t) + N_0} \quad (5.2)$$

In both cases, the transfer function of the equalizer is proportional to the inverse of the transfer function of the channel. Due to the large delay of the multipath arrivals, the transfer function of the channel has many zeros and, as a result, the transfer function of the equalizer has many poles. As mentioned previously, the equalizer must be implemented as an all zero transfer function due to stability problems. Implementing the equalizer as an all zero transfer function requires a number of taps which is much larger than the maximal delay of the channel. When a short multipath exists, this condition is reasonable, but when the delay is very long as in the case of the underwater

channel, such an implementation is not acceptable. Furthermore, a more serious problem is the non-minimal phase property of the channel since a stable inverse of a non-minimal phase transfer function does not exist.

## V.2 An LMS equalizer for underwater acoustic channel

Following (2.9) the  $z$  transform of the channel impulse response is:

$$H_c(z, t) = \alpha_0 + \sum_{i=1}^m \alpha_i z^{-D_i} \quad (5.3)$$

where  $D_i$  is the number of samples at  $TD_i$ . Without loss of generality, it can be assumed that the largest  $\alpha$  is  $\alpha_k$ ,  $k \neq 0$ . In this case, (5.3) can be written as :

$$H_c(z, t) = \alpha_k z^{-D_k} H'_c(z, t) \quad (5.4)$$

where

$$H'_c(z, t) = \sum_{i=k}^{m-k} \alpha'_i z^{-D'_i}$$

$\alpha'_i = \frac{\alpha_i}{\alpha_k}$  and  $D'_i = D_i - D_k$ . Furthermore we can assume that  $\alpha_k = 1$ . In this case, the strongest path is considered to be the main path and obviously,  $H'_c(z, t)$  is a noncausal filter. Instead of writing  $H'_c(z, t)$  as a summation, it can be written as a product:

$$H'_c(z) = H_0 \prod_{i=0}^N (z_i - z^{-1}) = H_0 \prod_{i=0}^L (z'_i - z^{-1}) \prod_{i=0}^{N-L} (z_i^O - z^{-1}) \equiv H_c(z)^c H_c^{\pi}(z) \quad (5.5)$$

$z'_i$  are the zeros of  $H'_c(z)$  which are inside the unit circle and  $z_i^O$  are the zeros which are outside the unit circle. The index  $t$  has been omitted for convenience but it is clear that the transfer function is time dependent. For high signal to noise ratio, the transfer function of the equalizer reduces to be the inverse of the channel transfer function no matter what optimization criterion is used:

$$H_e(z) \approx \frac{1}{H_c'(z)} = H_e^c(z) H_e^{nc}(z). \quad (5.6)$$

$H_e^c(z)$  and  $H_e^{nc}(z)$  are the causal and the noncausal parts of  $H_e(z)$ , respectively,

where

$$H_e^c(z) = \frac{1}{H_c^c(z)} \quad (5.7)$$

and

$$H_e^{nc}(z) = \frac{1}{H_c^{nc}(z)} \quad (5.8)$$

$H_e^{nc}(z)$  is a noncausal filter and cannot be implemented practically. Rewriting (5.8) as

$$H_e^{nc}(z) = \sum_{n=-\infty}^{-1} \beta^n z^{-n} = z^\Delta \beta^{-\Delta} \sum_{n=-\infty}^{\Delta-1} \beta^n z^{-n} \quad (5.9)$$

and approximating the infinite sum by a finite sum of  $\Delta$  terms, delaying by  $z^{-\Delta}$  and substituting into (5.6) leads to

$$H_e(z) \approx \frac{1}{\prod_{i=0}^L (z_i^L - z^{-1})} \sum_{n=0}^{\Delta-1} \beta^n z^{-n} \quad (5.10)$$

$H_e(z)$ , as appears in (5.10) is a stable causal filter and can be implemented.

Due to the problems of instability and convergence, it is preferable to implement a filter (especially if it is adaptive) by a FIR filter. Any IIR filter can be approximated by a transversal filter with a finite number of taps. A rule of thumb says that the required number of taps is 5 to 10 times the number of poles in the IIR filter. When the number of poles is relatively small, such implementation is acceptable. On the other hand, when the number of poles is very large (typically a few thousand in the underwater communication channel), implementing a transversal filter with the number of taps 5 to 10 times larger is not practical.

An alternative method to directly inverting the channel transfer function must be found. Since almost perfect knowledge of the original data exists at the output of the decision device, we are able to build the equalizer as a modified

combination of a feed forward equalizer and a version of a decision feedback equalizer<sup>52,75</sup> (DFE). The idea behind this configuration is to use the strongest path as the reference rather than just the first arrival. The received signal  $y(n)$  is sent to the feed-forward filter  $\hat{h}_e^{nc}(n)$  (Figure 5.1) which filters out the noncausal part of the input. The output  $x(n)$  is the causal part of  $y(n)$ . Now, the data stream taken from the output of the decision device  $\hat{d}(n)$  is sent to the feedback filter  $\hat{h}_e^c(n)$  which approximates the causal part of the channel. Subtracting this output  $u(n)$  from  $x(n)$  will leave us with the strongest path signal. The architecture in Figure 5.1 looks like more like an echo canceller than a classic equalizer. The strongest signal is almost always the main path or the first multipath. Thus, the noncausal filter in (5.8) has relatively few poles and can be realized as a transversal filter (the summation part in (5.10)).

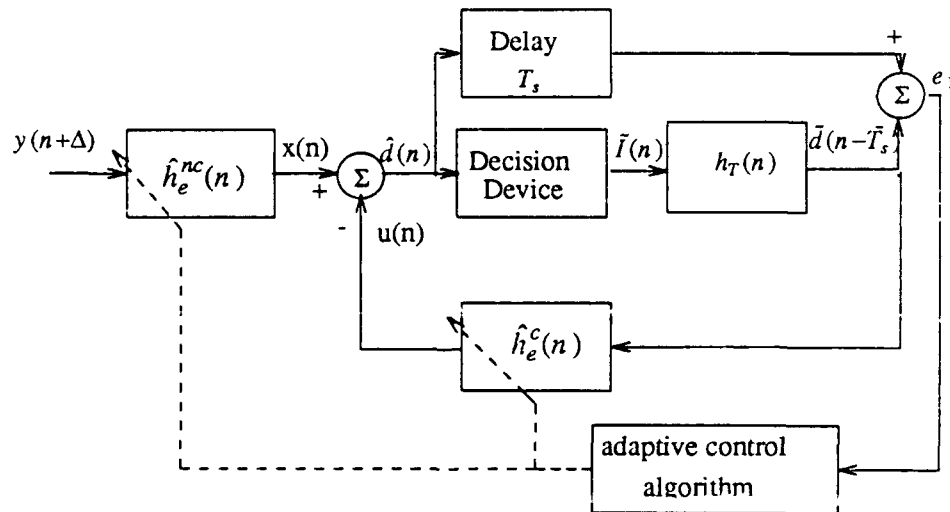


Figure 5.1 A block diagram of an underwater channel equalizer.

If  $d(n)$  is the signal transmitted by the transmitter, the received signal  $y'(n)$  is

$$y'(n) = d(n) * h_c(n) \quad (5.11)$$

where  $h_c(n)$  is the impulse response of the channel. Defining  $y(n) = y'(n + D_k)$ , taking the z transform, and substituting (5.5)

$$Y(z) = D(z) H_c(z) = D(z) H_c^e(z) H_c^{nc}(z) \quad (5.12)$$

From Figure 5.1:

$$X(z) = Y(z) \hat{H}_e^{nc}(z)$$

where  $\hat{(\cdot)}$  denotes the estimator of  $(\cdot)$ . If  $\hat{H}_e^{nc}(z) = \frac{1}{H_c^{nc}(z)}$ , we get that:

$$X(z) = D(z) H_c^e(z).$$

On the other hand, the output of the decision device is  $\tilde{I}(n)$  where:

$$I(n) = \sum_{i=-\infty}^n \tilde{d}_i \delta(n-i) \quad (5.13)$$

and  $\tilde{d}_i$  is the detected signal and takes on the values +1 or -1. For all practical purposes, it can be assumed that  $\tilde{d}_i = d_i$  for all  $i$ .  $I(n)$  is sent to the filter  $h_T(n)$  which generates the signal  $\tilde{d}(n)$ .  $\tilde{d}(n)$  is the detected version of the original transmitted signal, and in high signal to noise ratio,  $\tilde{d}(n) \approx d(n)$ . The sequence  $\tilde{d}(n)$  is fed into  $\hat{h}_e^e(n)$ , which is the feedback part of the equalizer where:

$$\hat{h}_e^e(n) = \begin{cases} h_c^e(n) & n \geq 1 \\ 0 & \text{else} \end{cases} \quad (5.14)$$

The z transform of the output of  $\hat{h}_e^e(n)$   $U(z)$  is:

$$\begin{aligned} U(z) &= D(z) \hat{H}_e^e(z) = D(z) [H_c^e(z) - h_c^e(0)] \\ &= X(z) - h_c^e(0) D(z) \end{aligned} \quad (5.15)$$

where  $D(z)$  is the z transform of  $d(n)$ . The z transform of the output of the equalizer  $\hat{D}(z)$  is:

$$\begin{aligned} \hat{D}(z) &= X(z) - U(z) \\ &= D(z) h_c^e(0) \end{aligned} \quad (5.16)$$

Note that if  $h_c^e(0) \approx 1$ , then  $\hat{d}(n) \approx d(n)$

### V.2.1 Calculation of filter weights

In developing the filter weight calculation method, it is convenient to use matrix notation. The composition of the  $M_c \times 1$  tap-weight vector of  $\hat{h}_e^c(n)$  is defined as  $\underline{w}_c$ :

$$\underline{w}_c^T = [w_1^c, w_2^c, \dots, w_{M_c}^c]$$

The tap-weight vector of  $\hat{h}_e^c(n)$  is defined as  $\underline{w}_{nc}$ :

$$\underline{w}_{nc}^T = [w_1^{nc}, w_2^{nc}, \dots, w_{M_{nc}}^{nc}]$$

The superscript  $T$  signifies transposition. The  $M_c \times 1$  output vector at time  $n$  is defined as  $\underline{d}(n)$ :

$$\underline{d}^T(n) = [d(n), d(n-1), \dots, d(n-M_c+1)]$$

and the  $M_{nc} \times 1$  input vector at time  $n$  is defined as  $\underline{y}(n)$ :

$$\underline{y}^T(n) = [y(n), y(n-1), \dots, y(n-M_{nc}+1)]$$

Define the estimation error  $e(n)$  as:

$$e(n) \equiv \hat{d}(n) - \bar{d}(n) \quad (5.17)$$

where  $\hat{d}(n)$  is the detected value and  $\bar{d}(n)$  is the estimated value of  $d(n)$  at the input to the decision device. The mean squared error is:

$$J = E(|e(n)|^2) \quad (5.18)$$

where  $E(\cdot)$  is the expected value of  $(\cdot)$ . Writing (5.18) explicitly one gets:

$$J = E \left[ [ \underline{w}_{nc}^H \underline{y}(n) - \underline{w}_c^H \underline{d}(n) - \bar{d}(n) ] [ \underline{y}^H(n) \underline{w}_{nc} - \underline{d}^H(n) \underline{w}_c - \bar{d}^*(n) ] \right] \quad (5.19)$$

After some simple algebraic manipulations we get:

$$J = \underline{w}_{nc}^H R_y \underline{w}_{nc} - \underline{w}_c^H R_{dy} \underline{w}_{nc} - \underline{w}_{nc}^H R_{dy}^H \underline{w}_c \quad (5.20)$$

$$- \underline{p}_{dy} \underline{w}_{nc} - \underline{w}_{nc}^H \underline{p}_{dy}^H + \underline{w}_c^H \underline{R}_d \underline{w}_c + \underline{p}_d \underline{w}_c + \underline{w}_c^H \underline{p}_d^H + \sigma^2$$

where the superscript  $H$  signifies Hermitian transposition and

$$\begin{aligned} \underline{R}_y &\equiv E[\underline{y}(n) \underline{y}^H(n)], \\ \underline{R}_{dy} &\equiv E[\underline{\tilde{d}}(n) \underline{y}^H(n+\Delta)], \\ \underline{R}_d &\equiv E[\underline{\tilde{d}}(n) \underline{\tilde{d}}^H(n)], \\ \underline{p}_d &\equiv E[\underline{\tilde{d}}(n) \underline{\tilde{d}}^H(n)], \\ \underline{p}_{dy} &\equiv E[\underline{\tilde{d}}(n) \underline{\tilde{y}}^H(n+\Delta)] \end{aligned} \quad (5.21)$$

Rearranging (5.20) leads to the familiar form:

$$J = \underline{W}^H \underline{R} \underline{W} - \underline{P}^H \underline{W} + \sigma^2 \quad (5.22)$$

where

$$\underline{W}^T \equiv [\underline{w}_{nc}^T, \underline{w}_c^T]$$

$$\underline{P}^T \equiv [\underline{p}_{dy}^T, -\underline{p}_d^T]$$

$$\underline{R} \equiv \begin{bmatrix} \underline{R}_y & -\underline{R}_{dy}^H \\ -\underline{R}_{dy} & \underline{R}_d \end{bmatrix}$$

Minimizing the mean square error leads to the well known Wiener-Hopf equation:

$$\underline{W}_o = \underline{R}^{-1} \underline{P} \quad (5.23)$$

When the tap-weight vector equals its optimum value  $\underline{W}_o$ , the mean square error attains its minimum value  $J_{\min}$  which is equal to

$$J_{\min} = \sigma^2 - \underline{P}^H \underline{R}^{-1} \underline{P} \quad (5.24)$$

One approach to solving (5.23) is by using direct matrix inversion techniques. Although, this procedure is quite straightforward, it can present serious computational difficulties (especially when the filter contains a large number of tap weights and the input data rate is high as is in our situation). An alternative procedure is to use the method of the steepest descent<sup>63</sup> which leads to the following

recursive relation:

$$W(n+1) = W(n) + \mu [P - R W(n)], \quad n = 0, 1, 2, \dots, \quad (5.25)$$

The parameter  $\mu$  controls the size of the incremental correction applied to the tap-weight vector as processed from one iteration cycle to the next.

Usually, the values of  $R$  and  $P$  are unknown and have to be estimated. The most common way of estimating  $R$  and  $P$  is to use instantaneous estimates that are based on sample values of the tap-input vector and desired response as defined by:

$$\tilde{R}(n) \equiv \begin{bmatrix} \underline{\tilde{y}}(n) \underline{\tilde{y}}^H(n) & -\underline{y}(n+\Delta) \underline{\tilde{d}}^H(n) \\ -\underline{\tilde{d}}(n) \underline{y}^H(n+\Delta) & \underline{\tilde{d}}(n) \underline{\tilde{d}}^H(n) \end{bmatrix} \quad (5.26)$$

and

$$\tilde{P}^T(n) = [\underline{\tilde{d}}(n) \underline{y}^H(n), \underline{\tilde{d}}(n) \underline{\tilde{d}}^H(n)] \quad (5.27)$$

Substituting (5.26) and (5.27) in (5.25) will lead to the well known LMS adaptive algorithm proposed by Widrow and Hoff<sup>91</sup>.

### V.3 Error propagation

In the decision-feedback equalizer (DFE), the equalizer depends on results produced by the decision device in the receiver. When no error exists in detecting the transmitted data, the DFE always has an advantage (and often a substantial advantage) over purely linear equalization<sup>31</sup>. However, when perfect detection of the transmitted signal does not occur, the presence of error propagation due to the effect of past decision errors raises the question of whether error propagation is catastrophic and if not, over what interval does the effect last on the average.

Following the definitions of Figure 5.1,

$$\hat{d}(n) = x(n) - u(n) \quad (5.28)$$

where

$$x(n) = d(n) * h_c^e(n) + n_c(n) = I(n) * h_T(n) * h_c^e(n) + n_c(n) \quad (5.29)$$

$n_c(n)$  is the ambient noise passed through the filter  $h_c^{nc}(n)$ , and:

$$u(n) = \tilde{d}(n - N_s) * \hat{h}_c^e(n) = \tilde{I}(n - N_s) * h_T(n) * \hat{h}_c^e(n) \quad (5.30)$$

Using the channel model defined by (2.9), substituting in (5.13) and (5.14), and using the assumption that  $\frac{TD_i}{T_s}$  is an integer number of bits for all  $i$ , one obtains:

$$\hat{d}(n) = d_n h_T(n) + \sum_{i=0}^{m-k} \alpha_i (\tilde{d}_{n-TD_i} - d_{n-TD_i}) h_T(n) \quad (5.31)$$

The assumption that  $\frac{TD_i}{T_s}$  equals an integer number of bits for all  $i$  corresponds to the case that maximal damage occurs from a wrong decision. The DFE equalizer is applicable only in systems which have relatively small errors at the decision device output. Therefore, one can assume that only one error in the  $m - k$  relevant bits occurs. The worst case is when an error exists in the  $d_i$  which corresponds to the  $\alpha$  of the largest absolute value. Without loss of generality the error can be assumed the  $n - 1^{th}$  bit.

Eight different cases can occur as indicated in Table 5.1.

Case No.	$d_n$	$d_{n-1}$	$\hat{d}_{n-1}$
1	1	1	1
2	1	-1	1
3	1	-1	-1
4	1	1	-1
5	-1	1	1
6	-1	-1	1
7	-1	-1	-1
8	-1	1	-1

**Table 5.1:** Possible combinations of present, previous, and detected bits.

For symmetry reasons, Cases 1-4 are the same as Cases 5-8.

For Cases 1 and 3 :

$$\hat{d}(n) = d(n) + n_c$$

and the corresponding bit error probability is

$$P_{e1} = P_{e3} = f\left(\frac{E_b}{N_0}\right)$$

where the function  $f(\cdot)$  depends on the modulation/demodulation scheme is used.

For Case 2:

$$\hat{d}(n) = d(n) + 2\alpha_1 d(n) + n_c$$

and

$$P_{e2} = f\left[(1 + 2\alpha_1)^2 \frac{E_b}{N_0}\right]$$

and for Case 4:

$$\hat{d}(n) = d(n) - 2\alpha_1 d(n) + n_c$$

with

$$P_{e4} = f \left[ (1 - 2\alpha_1)^2 \frac{E_b}{N_0} \right]$$

Again, due to symmetry, the same results are accepted for  $\alpha$  positive or  $\alpha$  negative.

Without loss of generality, let us assume that  $\alpha > 0$ .

The relation between making an error or correct decision, depending on the previous decision is a two state Markoff process as depicted in Figure 5.2.

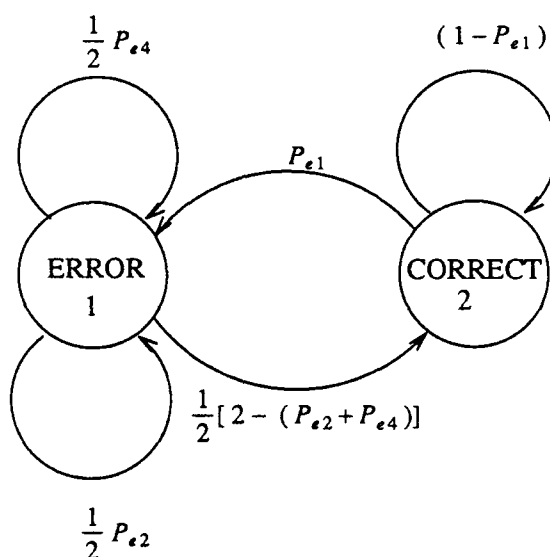


**Figure 5.2** The relationship between the decision of the present and the previous bits

Given that the previous bit was detected incorrectly, then the present bit will be detected incorrectly with probability  $P_{e2}$  for the events described as Cases 2 and 8 in Table 5.1. The present bit will be detected incorrectly with probability  $P_{e4}$  for the events described as Cases 4 and 6 in Table 5.1.

The average time between an error decision and the next correct decision  $\bar{T}_{ep}$  is:

$$\begin{aligned}\bar{T}_{ep} &= \frac{1}{2} [2 - (P_{e2} + P_{e4})] \sum_{n=1}^{\infty} n \left[ \frac{1}{2} (P_{e2} + P_{e4}) \right]^{n-1} \\ &= \frac{1}{1 - \frac{1}{2} (P_{e2} + P_{e4})}\end{aligned}\quad (5.32)$$

In the worst case,  $P_{e4} = 1$  and:

$$\bar{T}_{ep} = \frac{1}{\frac{1}{2} - \frac{1}{2} P_{e2}} \quad (5.33)$$

Since  $\bar{T}_{ep}$  is a finite number, the error propagation is of finite duration. Moreover, since  $P_{e2}$  is a very small number, the average error propagation is no more than two bits. Hence, under condition of low bit error rate, the degradation of system performance due to the error propagation is negligible.

#### V.4 Numerical example

Assume a channel with the following impulse response:

$$h_c(n) = d(n) - 2.6d(n-1) + 1.25d(n-2) - 0.1d(n-3) \quad (5.34)$$

and transfer function  $H_c(z)$

$$H_c(z) = 1 - 2.6z^{-1} + 1.25z^{-2} - 0.1z^{-3} = (1 - 2z^{-1})(1 - 0.5z^{-1})(1 - 0.1z^{-1}) \quad (5.35)$$

$H_c(z)$  has three zeros, two of them are inside the unit circle and one ( $z = 2$ ) is outside the unit circle, which causes  $H_c(z)$  to be a non-minimum phase transfer function.

Following the definitions in (5.7) and (5.8), we obtain:

$$\begin{aligned}H_e^c(z) &= \frac{1}{H_c^c(z)} = \frac{1}{(1 - 0.5z^{-1})(1 - 0.1z^{-1})} \\ H_e^{\infty}(z) &= \frac{1}{H_c^{\infty}(z)} = \frac{1}{(1 - 2z^{-1})} = \sum_{n=-\infty}^{-1} [2z^{-1}]^n\end{aligned}\quad (5.36)$$

Choosing  $\Delta = 5$  and following (5.9) and (5.10):

$$H_e(z) = \frac{1}{(1 - 0.5z^{-1})(1 - 0.1z^{-1})} 2^{-5} z^5 \sum_{n=0}^4 [2z^{-1}]^n \quad (5.37)$$

From (5.8) and (5.14) we obtain:

$$\hat{H}_e^{nc}(z) = 2^{-5} \sum_{n=0}^4 [2z^{-1}]^n \quad (5.38)$$

and

$$\hat{H}_e^c(z) = -0.6 + 0.05z^{-1} \quad (5.39)$$

A computer simulation was run to illustrate the performance of the method. A long sequence of +1 or -1 randomly selected was sent to a block with transfer function as in (5.34) which simulated the under water acoustic channel. The output  $y(n)$  of this block was sent to a block which simulated the receiver as in Figure 5.1 and the weights of the two filters were calculated. In order to illustrate the performance of the method, a single pulse was transmitted and analyzed in the receiver with the filter weights that had been calculated before. The example of the single pulse shows how the equalizer cancels all the multipaths except the strongest one. Figures 5.3 - 5.6 provide simulation results where a single impulse was transmitted by the transmitter, passed through a channel with the impulse response in (5.34) and processed by the receiver in Figure 5.1. In each figure, the weights of the filters were calculated in a different way. Figure 5.3 corresponds to filter weights calculated directly from (5.38) and (5.39).

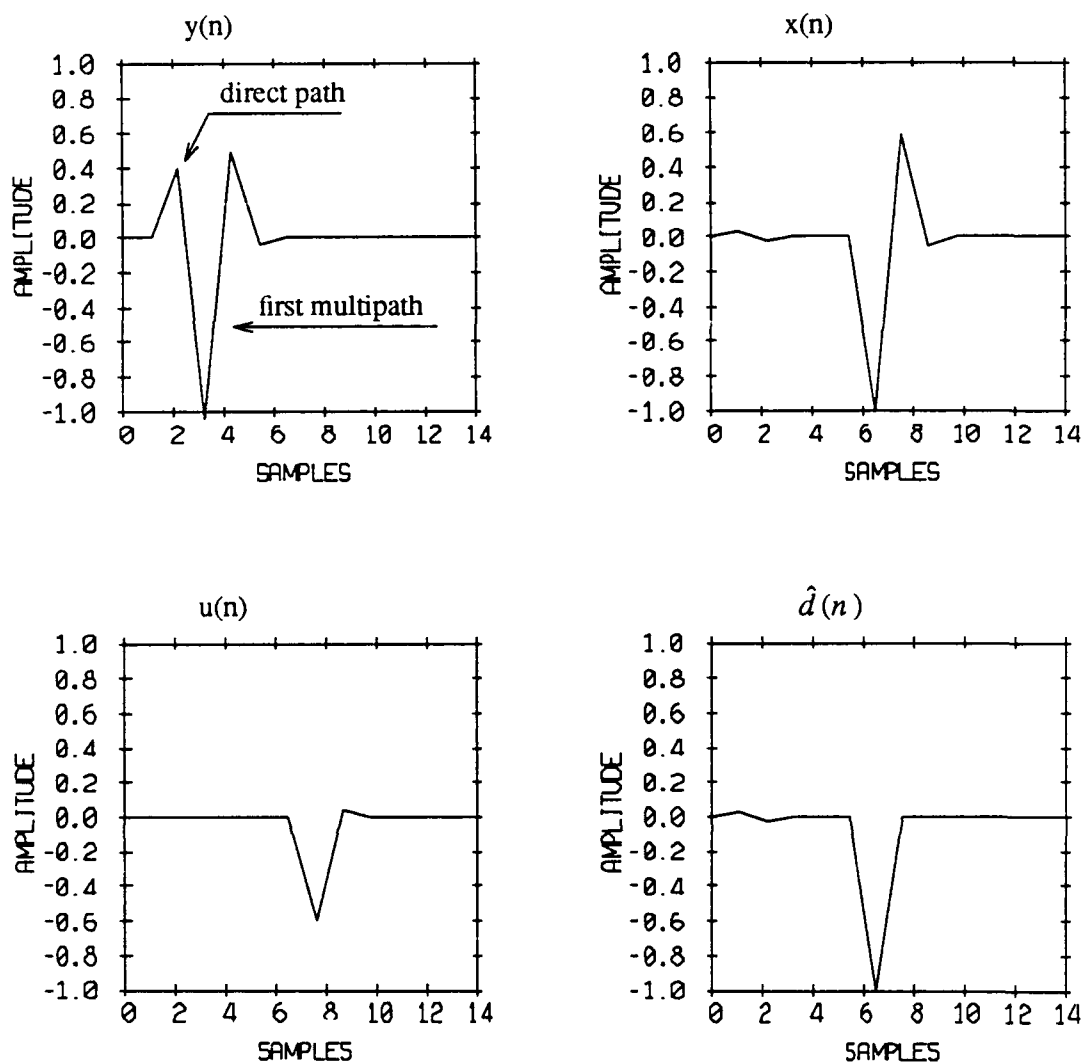


Figure 5.3 Equalizer weights calculated directly from (5.38) and (5.39)

$y(n)$  is the distorted signal received by the receiver,  $x(n)$  is the output of the forward filter  $\hat{h}_d^w(n)$ ,  $u(n)$  is the output of the feedback filter  $\hat{h}_e^c(n)$ , and  $\hat{d}(n)$  is the equalized signal. Figure 5.4 shows the results for the case where the filter weights were calculated using the Wiener-Hopf equation. In both cases, the channel was considered noiseless. Figure 5.5 and Figure 5.6 show the results when the LMS algorithm was used. In Figure 5.5, the channel was assumed to be noiseless and in Figure 5.6, a

noisy channel (AWGN) was considered where  $\frac{E_b}{N_0} = 10$  dB.

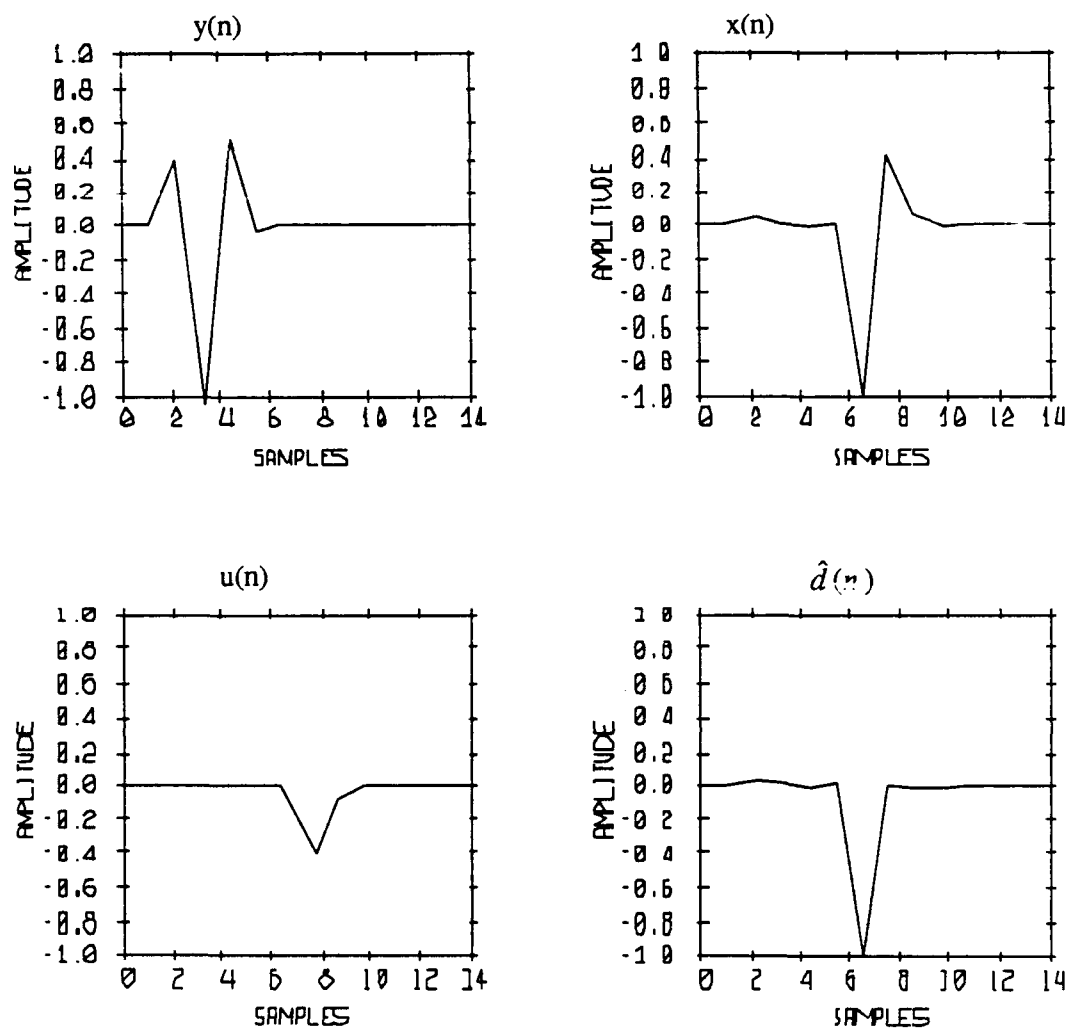


Figure 5.4 Equalizer weights calculated using the Wiener-Hopf LMS algorithm in noiseless channel.

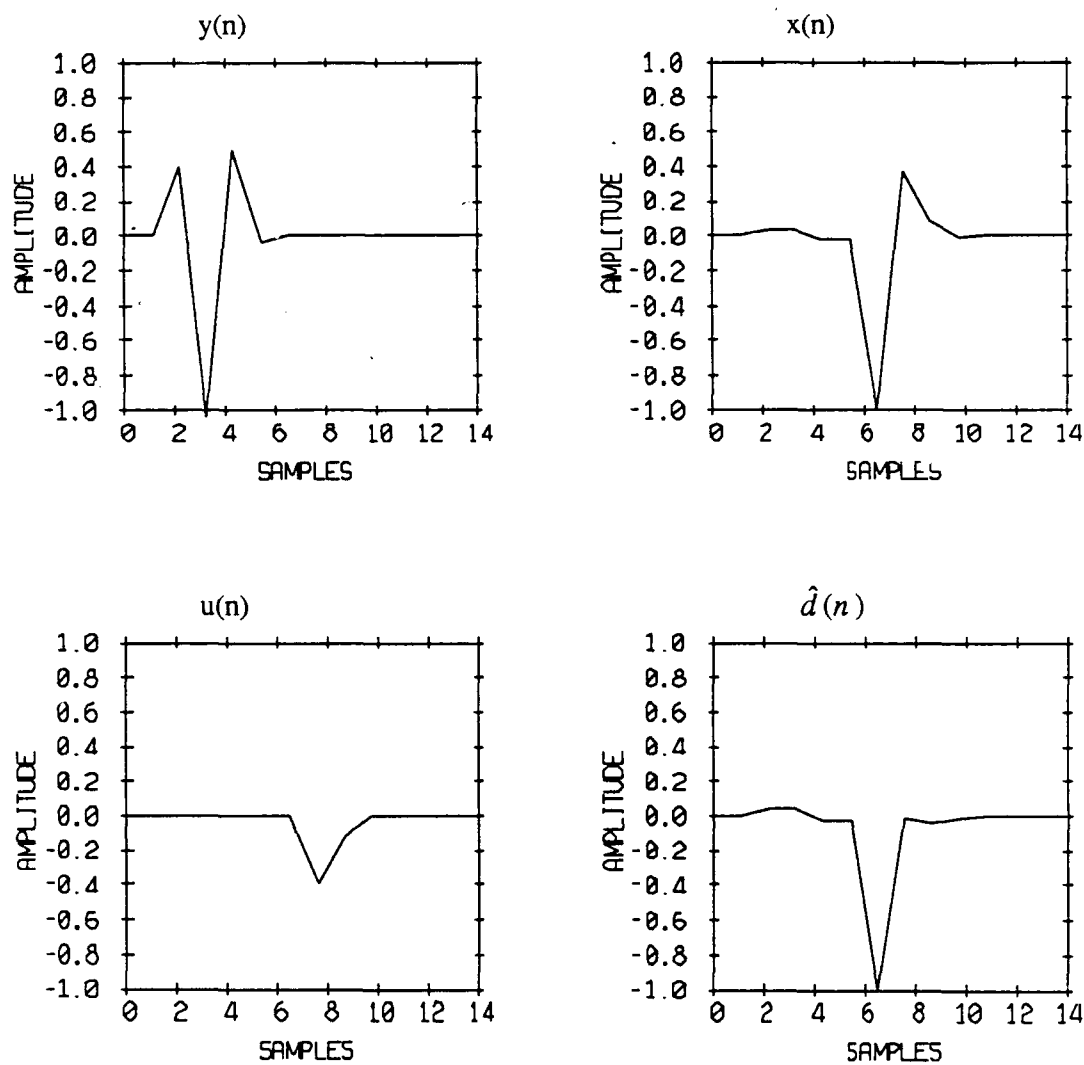


Figure 5.5 Equalizer weights calculated using the LMS algorithm (500 iterations) (no noise).

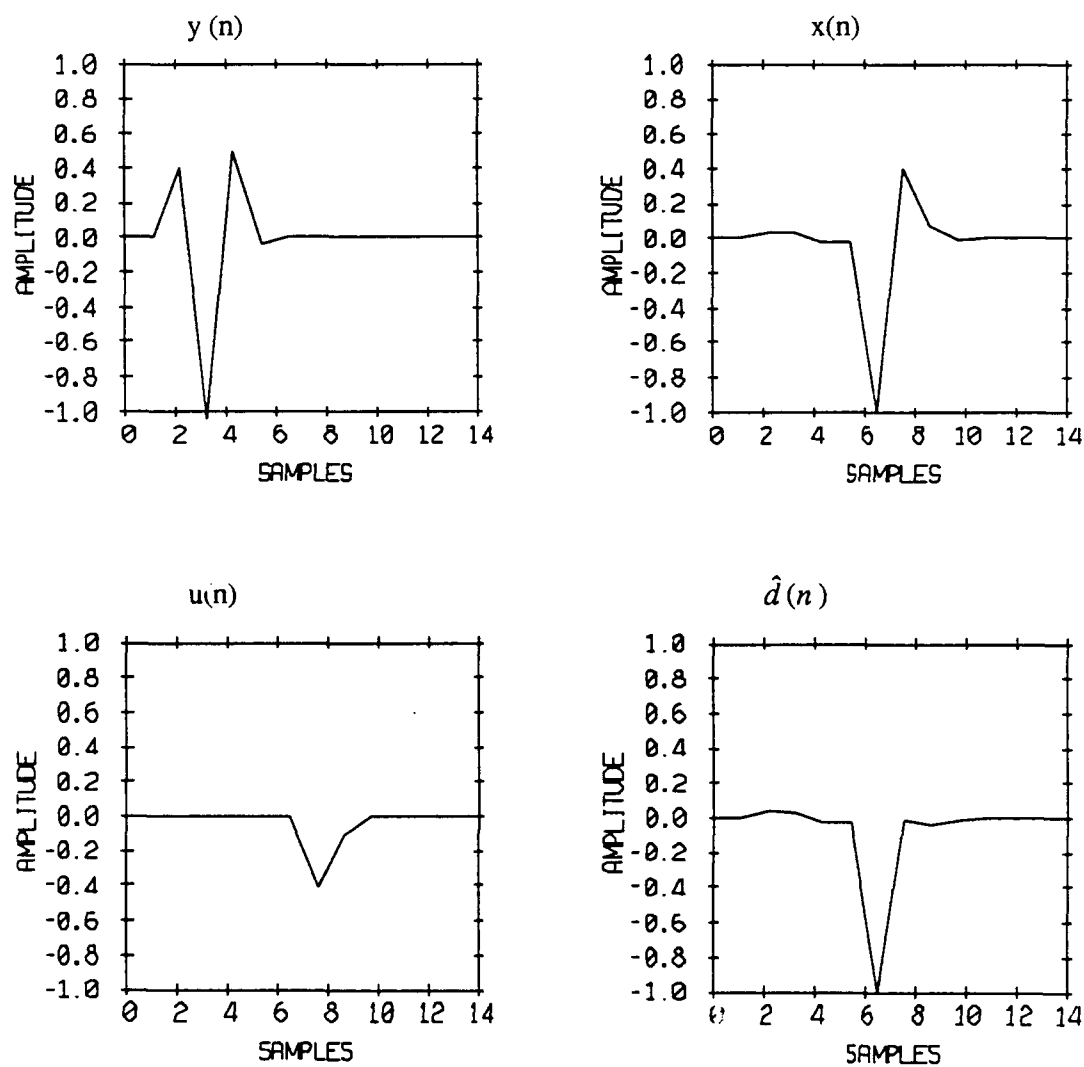


Figure 5.6 Equalizer weights calculated using the LMS algorithm (500 iterations) ( $\frac{E_b}{N_0} = 10\text{dB}$ ).

## VI Examples and Discussion of Results

A new technique to combat destructive channel fading for underwater acoustic communication has been proposed. This technique combines both chirp and differential phase shift keying (DPSK) modulation. Chirp DPSK modulation is an efficient modulation scheme in the presence of a slowly time-varying, frequency selective fading channel.

Ignoring the fading problem and neglecting its destructive effects causes a communication link which behaves nicely in a non-fading environment to be useless under fading conditions. The bit error probability which is proportional to the inverse exponent of the signal-to-noise ratio in a non-fading environment, becomes inversely proportional to the signal-to-noise ratio itself under fading conditions. Thus, dramatic degradation in system performance occurs. As an example, achieving a bit error probability of  $10^{-6}$  in binary coherent PSK with no fading requires a signal-to-noise ratio of approximately 10.5 dB. In the presence of a Rayleigh fading channel, achieving the same bit error probability requires 54 dB of signal-to-noise ratio. Using frequency diversity methods improves the performance of the communication link. The more parallel branches that are used, the better the system performance. The random nature of the fading phenomena makes a coherent modulation scheme useless since the channel itself destroys the coherence of the transmitted signal.

In the presence of slowly time-varying (relative to the bit rate), frequency selective fading, the chirp DPSK modulation is a good anti-fading modulation scheme. Chirp modulation is very attractive as an anti-fading modulation scheme due to its spectral properties. For large time-bandwidth products ( $BT_c$ ), the power spectrum has almost a rectangular shape, (i.e. a flat spectrum in the relevant bandwidth and almost zero outside of it). The flatness of the spectrum is similar to using a large

number of parallel diversity branches. The equivalent number of branches is on the order of the number of degrees of freedom ( $K$ ) of the channel. The maximum number of equivalent diversity branches is achieved without increasing the problem of cross-talk. Another advantage of chirp DPSK modulation is the simplicity of the receiver realization which is equivalent to a single channel DPSK receiver.

When dealing with frequency diversity techniques, the available number of diversity branches depends on the ratio between the available bandwidth  $B$  and the bit rate  $R_c$  (the bit rate is the inverse of the bit length  $T_c$ ). Assuming the information bandwidth is approximately  $R_c$ , then in order to prevent strong cross-talk between adjacent channels, the number of diversity channels is bounded above by  $L < \frac{B}{R_c}$ . On the other hand, the number of degrees of freedom ( $K$ ) in the chirp DPSK modulation technique depends only on the nature of the channel (i.e. on the ratio between the available bandwidth  $B$  and the frequency selectivity  $\rho_H$  where  $K = \frac{B}{\rho_H}$ ). The chirp modulation technique can be considered plausible only for cases when the time-bandwidth product ( $BT_c$ ) is greater than or equal to 10. Under this condition, the assumption of a flat spectrum and constant phase of the chirp signal across the relevant bandwidth holds. The spectrum and the phase of a chirp signal with  $BT = 10$  is shown in Figure 6.1.

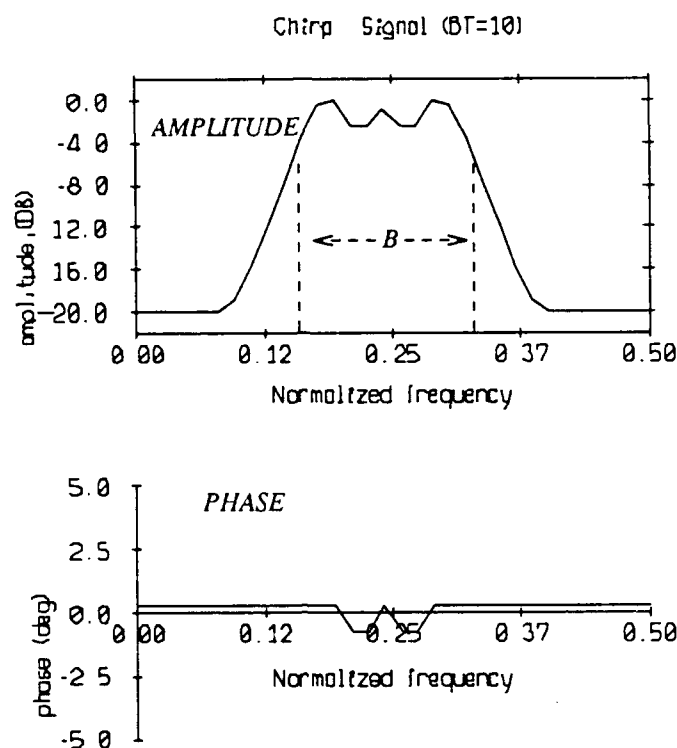


Figure 6.1 The spectrum and the phase of a chirp signal with  $BT = 10$

As an example of the performance of the chirp DPSK modulation scheme relative to other frequency diversity methods, let us consider a shallow water, short range underwater acoustic communication system. The available bandwidth is 10 kHz and the required data rate is 1 Kbit/sec. From measured data<sup>18</sup>, the frequency selectivity  $\rho_h$  is approximately 50 Hz. For this example, the time-bandwidth product ( $BT_c$ ) is  $10000 \text{ Hz} \times 1 \text{ msec} = 10$ ,  $L \leq 10$ , and  $K = \frac{10^4}{50} = 200$ .

In Figure 6.2 we present a comparison of various modulation schemes with 10 diversity branches and a chirp DPSK with 20 and 200 degrees of freedom. For all practical purposes, 200 degrees of freedom can be considered as infinite.

Comparison of different modulation performance  
using frequency diversity ( $L=10$ ) in a presence  
of selective Rayleigh fading

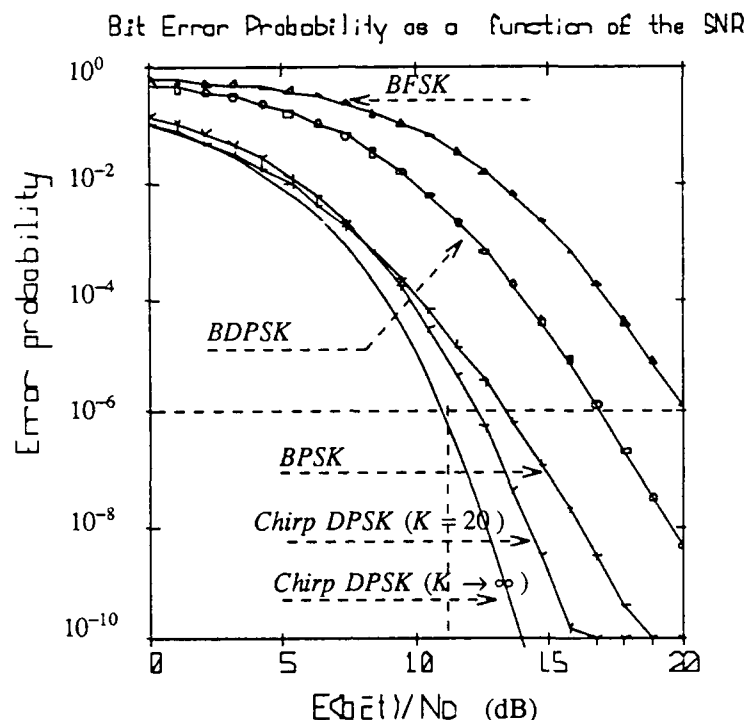


Figure 6.2 Comparison between various diversity methods and chirp DPSK modulation

Observing the plots, we see that in the presence of slowly time-varying, frequency selective fading, using chirp DPSK is superior to all other modulation schemes using frequency diversity and a gain of almost 10 dB in signal to noise ratio is achieved with respect to NBFSK with diversity of 10.

Another way to combat the fading channel is to use combinations of coding and modulation schemes. This method optimally combines diversity modulation and coding. A modified version of the combined coding and modulating approach that was proposed by Pieper at el<sup>71</sup> is used by a group at Woods Hole<sup>17</sup> in their telemetry system.

Comparing the performance of the chirp QPSK modulation with bandwidth expansion of 5 with several other combined coding and modulating schemes (Figure 3.10) having similar bandwidth expansion (4), shows that the QDPSK is superior over the other methods. A necessary condition for any DPSK scheme to be used, is that a high coherency between two adjacent symbols must exist. In the case of slowly time-varying fading and quasi-static terminals, the coherency between two adjacent symbols is almost one and the degradation in the system performance is negligible (Figure A.8)

An underwater channel for acoustic communication is a very tough channel in the sense of having disastrous interference caused by strong multipath signals. A necessary condition for reliable communication is to find methods which eliminate the effect of the multipaths. Although the results of sea experiments show that only one dominant path exists, it is a mistake to assume that this is the case in general. Hence, a way to prevent the huge ISI caused by the multipaths has to be found.

Multipath has two major properties that makes the equalizer implementation very difficult:

- (1) The delay between the direct path and the multipath signal can be on the order several thousand bits and hence an equalizer with many taps is required.
- (2) The intensity of one of the multipath signals can be much higher than the direct path signal, i.e. the channel is a nonminimum phase channel.

In this thesis, we propose an equalizer implementation which requires a minimum number of taps and overcomes the problem of the nonminimum phase of the channel impulse response. The proposed equalizer is a combination of forward and decision

feedback equalizers. In this configuration, the strongest signal (which is not necessarily the direct path) is assumed to be the reference signal and hence the channel changes to being a noncausal instead of a nonminimum phase channel. The forward filter approximates the part of the equalizer that equalizes the noncausal part of the channel and the feedback filter equalizes the causal part of the channel. The decision feedback configuration enables implementation the equalizer with the minimum number of taps. Although a nonconventional equalizer configuration is chosen, it is shown that using the mean square error optimization criterion leads to the well known Wiener-Hopf equation for the tap weights. An error propagation phenomena exists but it proves to be non-catastrophic with an average error propagation time of 2 bits. Some numerical simulation results are included which demonstrate the performance of the proposed equalization method.

The strong multipath phenomena results in bit synchronization being complicated. In order to achieve the best performance, the synchronization method was designed in such a way that the synchronizer is always locked to the strongest multipath. The intensity of the multipath signals change with time (especially the micro multipath) so in order to prevent the synchronizer from losing lock and locking onto another multipath, an average multipath intensity is calculated and the synchronizer is locked onto the maximum average multipath signal.

The telemetry system proposed and analyzed in this work is not a universal system. It is important to emphasize that the system performs optimally only under specific condition (source/reciever almost at rest and a slowly time varying channel). When the channel is not a slowly time-varying channel, the propopsed methods of equalization and bit synchronization do not work any longer and different methods must be found. Designing a telemetry systems for a fast time varying channel is a tough problem which has been not solved yet. Since the number of the mutipath

signals, their intensity and location varies rapidly, no reference exists for synchronization. Moreover, the rate of the multipath variation is so fast that the common adaptive equalization algorithm do not succeed in following the variation of the channel. New adaptive algorithms with a fast adaptation properties must be found. If the requirement of general telemetry system exists, the system probably will be much more complicated (and expensive) and will have worse performance than a system that has been designed to operate in a specific well-defined scenario.

### VI.1 Real data analysis

A stream of pseudo randomly selected ones and zeros was differentially modulated by a chirp signal and transmitted as a part of the at-sea experiments. A receiver implemented in software processed the data. Figure 6.3 shows a block diagram of the receiver.

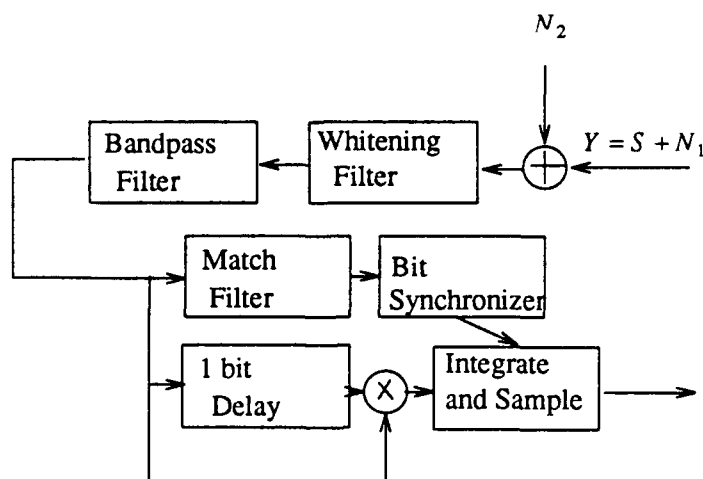


Figure 6.3 Implemented DPSK receiver - block diagram.

The ocean ambient noise is not white and has a power spectrum shown in Figure 6.4.

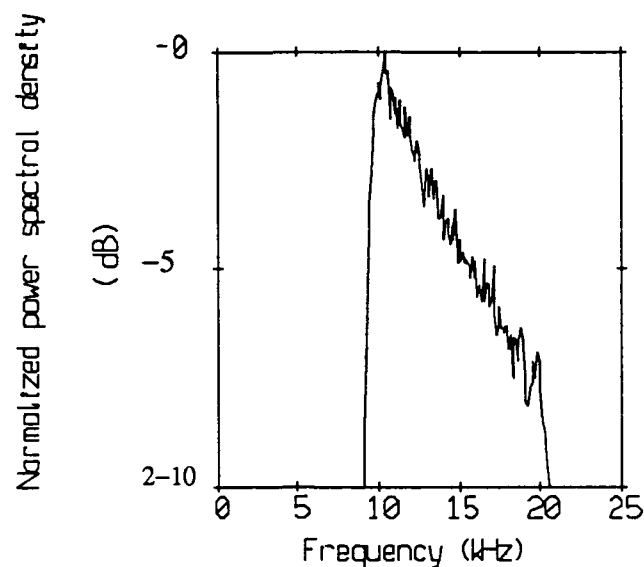


Figure 6.4 Power spectral density of the ambient noise (after bandpassing)

It can be approximated roughly as a single pole AR process. Therefore, the whitening filter was implemented as a simple derivative. The received signal-to-noise ratio ( $\bar{\gamma}_b$ ) was quite high (20 dB). In order to analyze the performance of the system, at several values of signal-to-noise ratio ambient noise ( $N_2$  measured at different time interval which was clean from any signal) was added artificially to the received signal ( $Y$ ).

A stream of  $6 \times 10^6$  bits was analysed. The achieved bit error and the theoretical bit error rate for DPSK modulation in the presence of AWGN are presented in Figure 6.5.

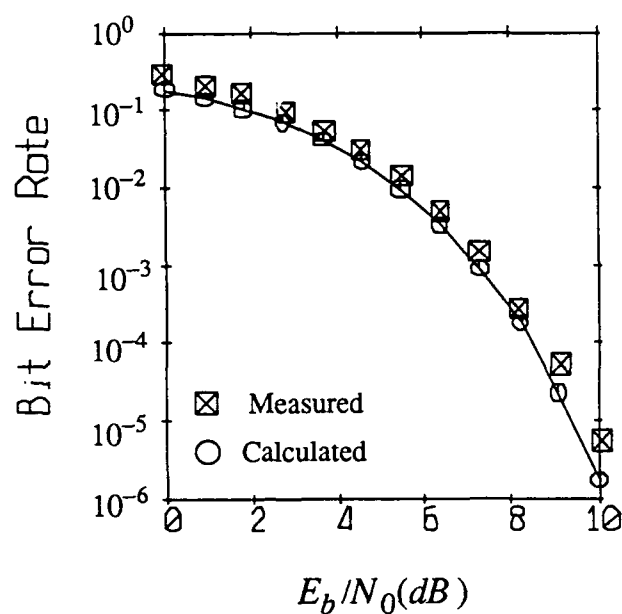


Figure 6.5 Comparison between theoretical and achieved bit error rate.

As shown in Figures 2.4, 2.5 and 2.6, the first multipath is much stronger than the direct signal and the other multipath signals. Therefore, the bit synchronizer was locked onto the first multipath. Since the first multipath was so large relative to the other signals, in the range of bit error rate that was analyzed, the absence of the equalizer did not affect the achieved results.

## **Appendix A - Chirp as a Frequency Diversity Technique**

### **Introduction**

The main idea behind all frequency diversity methods is to spread the spectrum of the signal as much as possible over the transmission bandwidth.<sup>123</sup> This is precisely the reason why spread spectrum communication is a useful diversity technique.

A simple and very useful spreading method is chirp carrier signal modulation. As with all familiar frequency diversity techniques, it is strongly desired to make use of as many branches as possible for a given frequency bandwidth.<sup>4</sup> Although the channel and the branches are designed (at least theoretically) to be orthogonal, choosing the branches too close together in the frequency domain results in of cross-talk and intersymbol interference between adjacent branches.

A chirp signal is the same as an isolated signal. Thus, no cross-talk between adjacent branches occurs. Moreover, the rectangular character of the chirp's power spectrum<sup>56</sup> (at least for time-bandwidth products much greater than one) minimizes the intersymbol interference problem. In this appendix we will analyze the performance of FSK and DPSK modulation schemes using a chirp as the carrier.

#### **A.1 Possible signal sets for binary chirp modulation**

In binary chirp modulation, when both mark and space occupy the same frequency region, three signal sets can be chosen. These are labeled (a), (b), and (c) and are given by

(a)

$$S_1(t) = \begin{bmatrix} \sin \\ \cos \end{bmatrix} (\omega_0 t + \frac{1}{2} \mu t^2) \quad (\text{A.1})$$

$$S_0(t) = \begin{bmatrix} \sin \\ \cos \end{bmatrix} (\omega_0 t - \frac{1}{2} \mu t^2) .$$

Here, the correlation coefficient,  $\rho$ , between the two signals  $S_1(t)$  and  $S_0(t)$  is defined as:

$$\rho = \frac{\int_{-\frac{1}{2}T}^{\frac{1}{2}T} S_1(t) S_0(t) dt}{\left[ \int_{-\frac{T}{2}}^{\frac{T}{2}} S_1^2(t) dt \int_{-\frac{T}{2}}^{\frac{T}{2}} S_0^2(t) dt \right]^{\frac{1}{2}}} = \frac{1}{2} \int_{-\frac{1}{2}T}^{\frac{1}{2}T} \left[ \cos(2\omega_0 t) + \cos(\mu t^2) \right] dt . \quad (\text{A.2})$$

(b)

$$S_1(t) = \begin{bmatrix} \sin \\ \cos \end{bmatrix} (\omega_0 t + \frac{1}{2} \mu t^2) \quad (\text{A.3})$$

$$S_0(t) = \begin{bmatrix} \cos \\ \sin \end{bmatrix} (\omega_0 t + \frac{1}{2} \mu t^2) .$$

The correlation coefficient,  $\rho$ , between  $S_1(t)$ , and  $S_0(t)$  is :

$$\rho = \frac{1}{2} \int_0^{\frac{1}{2}T} \left[ \cos(2\omega_0 t) \sin(\mu t^2) \right] dt . \quad (\text{A.4})$$

For appropriate values of  $\mu$  and  $\omega_0$ ,  $\rho$  vanishes and the two signals are orthogonal.

(c)

$$S_1(t) = \begin{bmatrix} \sin \\ \cos \end{bmatrix} (\omega_0 t + \frac{1}{2} \mu t^2) \quad (\text{A.5})$$

$$S_0(t) = \begin{bmatrix} \cos \\ \sin \end{bmatrix} (\omega_0 t - \frac{1}{2} \mu t^2) .$$

In this case :

$$\rho = \frac{1}{2} \int_{-\frac{T}{2}}^{\frac{T}{2}} \sin(\mu t^2) dt . \quad (\text{A.6})$$

## A.2 Detection of incoherent BFSK chirp modulation in the presence of AWGN and Rayleigh fading

Before analyzing the performance of binary chirp modulation in the presence of AWGN over a fading channel, let us start with the simple case of a channel distorted only by additive white Gaussian noise with two sided spectral density  $\frac{N_0}{2}$ .

For the following signal set, the receiver is a incoherent BFSK receiver as shown in Figure A.1.

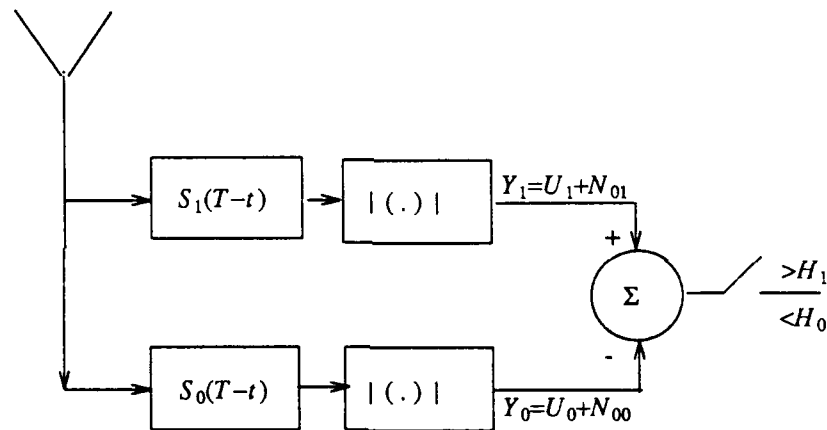


Figure A.1 Incoherent BFSK Receiver

In this figure,

$$S_1(t) = A \cos(\omega_0 t + \frac{1}{2}\mu t^2), \quad -\frac{T}{2} \leq t \leq \frac{T}{2} \quad (\text{A.7})$$

and

$$S_0(t) = A \cos(\omega_0 t - \frac{1}{2}\mu t^2), \quad -\frac{T}{2} \leq t \leq \frac{T}{2}.$$

Without any loss of generality, it can be assumed that  $S_1(t)$  is transmitted. It is easy to show (neglecting the high frequency terms) that

$$U_1\left(\frac{T}{2}\right) = \frac{AT}{2} \quad (\text{A.8})$$

$$U_0\left(\frac{T}{2}\right) = A \int_0^{0.5T} \cos(\mu t^2) dt \quad (\text{A.9})$$

and

$$\sigma_N^2 = \frac{N_0 T}{4} .$$

Then

$$P(y_1/s_1) = \frac{y_1}{\sigma_N^2} \exp\left\{-\frac{y_1^2 + U_1^2\left(\frac{T}{2}\right)}{2\sigma_N^2}\right\} I_0\left\{\frac{y_1 U_1\left(\frac{T}{2}\right)}{\sigma_N^2}\right\} \quad (\text{A.10})$$

and

$$P(y_0/s_1) = \frac{y_0}{\sigma_N^2} \exp\left\{-\frac{y_0^2 + U_0^2\left(\frac{T}{2}\right)}{2\sigma_N^2}\right\} I_0\left\{\frac{y_0 U_0\left(\frac{T}{2}\right)}{\sigma_N^2}\right\} . \quad (\text{A.11})$$

Define the probability of correct decision as  $P_c$  . Then [Helstrom<sup>41</sup> p. 431]

$$\begin{aligned} P_c &= \int_{y_0=0}^{\infty} \int_{y_1=y_0}^{\infty} P(y_1/s_1) P(y_0/s_1) dy_1 dy_0 \\ &= Q\left\{\sqrt{\gamma_1}, \sqrt{\gamma_0}\right\} - \frac{1}{2} \exp\left[-\frac{1}{2}(\gamma_0 + \gamma_1)\right] I_0\left[\sqrt{\gamma_1 \gamma_0}\right] \end{aligned} \quad (\text{A.12})$$

where:

$$\gamma_i = \frac{U_i^2\left(\frac{T}{2}\right)}{2\sigma_N^2}, \quad i = 0, 1$$

and  $Q(\alpha, \beta)$  is the Marcum Q function. The bit error probability  $P_e$  is given by

$$P_e = 1 - P_c .$$

### A.3 The Incoherent case in the presence of frequency selective, slowly time-varying Rayleigh fading

Due to the nature of the fading channel, the transmitted signal is strongly distorted in amplitude and phase when it arrives at the receiver. This distortion renders a coherent system absolutely useless in a strongly fading environment. For this reason, we present only the analysis of an incoherent system.

For the signal set in (A.7), the received signal is

$$y_1(t) = \text{Re} \left\{ \bar{y}_1(t) \exp(j\omega_0 t) \right\} , \quad (\text{A.13})$$

where (see (1.3))

$$\bar{y}_1(t) = \alpha A \bar{S}_1(t) + \int_{-\infty}^{+\infty} A \bar{S}_1(\tau) h(t-\tau; t) d\tau + n(t) \quad (\text{A.14})$$

and

$$\bar{S}_1(t) = \exp(j\mu t^2) \quad ; \quad -\frac{T}{2} \leq t \leq \frac{T}{2} .$$

The signal component,  $U_1(\frac{T}{2})$ , at the output of the receiver is:

$$U_1(\frac{T}{2}) = \frac{1}{2} \int_{-\frac{T}{2}}^{\frac{T}{2}} \left\{ A \alpha \bar{S}_1(t) \bar{S}_1^*(t) + \int_{-\infty}^{+\infty} A \bar{S}_1(\tau) h(t-\tau; t_1) d\tau \bar{S}_1^*(t) \right\} dt . \quad (\text{A.15})$$

where  $(\cdot)^*$  denotes the complex conjugate. For convenience, define  $r(t)$  as:

$$r(t) = A \int_{-\infty}^{+\infty} \bar{S}_1(\tau) h(t-\tau; t_1) d\tau . \quad (\text{A.16})$$

$r(t)$  also can be expressed as:

$$\begin{aligned} r(t) &= A \int_{-\infty}^{+\infty} \bar{S}_1(\omega) H(\omega; t_1) \exp(j\omega t) \frac{d\omega}{2\pi} \\ &= A \int_{-\infty}^{+\infty} |\bar{S}_1(\omega)| \exp(j\theta(\omega)) H(\omega; t_1) \exp(j\omega t) \frac{d\omega}{2\pi} . \end{aligned} \quad (\text{A.17})$$

For a time-bandwidth product much greater than one<sup>26</sup>

$$|\bar{S}_1(\omega)| \approx \text{const} = \frac{2\beta}{A}, \quad (\text{A.18})$$

and

$$\theta(\omega) \approx \text{const} = \theta.$$

Substituting (A.18) in (A.17) yields

$$r(t) \approx \beta \exp(j\theta) \int_{-\infty}^{+\infty} H(\omega; t_1) \exp(j\omega t) \frac{d\omega}{2\pi} = \beta \exp(j\theta) h(t; t_1). \quad (\text{A.19})$$

Substituting (A.19) into (A.15) gives

$$\begin{aligned} U_1\left(\frac{T}{2}\right) &= \frac{1}{2} \int_{-\frac{T}{2}}^{\frac{T}{2}} A \alpha \bar{S}_1(t) \bar{S}_1^*(t) dt + \int_{-\frac{T}{2}}^{\frac{T}{2}} \beta \exp(j\theta) h(\tau; t_1) \bar{S}_1^*(\tau) d\tau \\ &= \frac{1}{2} \alpha A T + \kappa\left(\frac{T}{2}\right), \end{aligned} \quad (\text{A.20})$$

where

$$\kappa\left(\frac{T}{2}\right) = \beta \exp(j\theta) \int_{-\frac{T}{2}}^{\frac{T}{2}} h(\tau; t_1) \bar{S}_1^*(\tau) d\tau.$$

As  $h(\tau; t)$  is a complex Gaussian process and  $\bar{S}_1^*(t)$  is only a phase shift,  $\kappa\left(\frac{T}{2}\right)$  is also a Gaussian random variable with zero mean and variance

$$\text{Var}(\kappa) = \frac{1}{2} E[\kappa(\tau) \kappa^*(\xi)] = \frac{\beta^2}{2} \int_{-\frac{T}{2}}^{\frac{T}{2}} \int_{-\frac{T}{2}}^{\frac{T}{2}} \bar{S}(\tau) \bar{S}^*(\xi) E[h(\tau; t) h^*(\xi; t)] d\tau d\xi, \quad (\text{A.21})$$

where  $E[\cdot]$  denotes the expectation of  $[\cdot]$ . Assuming

$$E[h(\tau; t) h^*(\xi; t)] = \sigma_h^2 \delta(\tau - \xi)$$

we have  $\text{Var}(\kappa) = \frac{\beta^2}{4} \sigma_h^2 T$ .

It is obvious that if  $\kappa\left(\frac{T}{2}\right)$  is a Gaussian random variable, then  $U_1\left(\frac{T}{2}\right)$  is also a

Gaussian random variable but with mean  $= \frac{1}{2} \alpha A T$  and  $\sigma_{U_1}^2 = \frac{\beta^2}{4} \sigma_h^2 T$ . Similarly, we find that

$$\begin{aligned}
 U_0\left(\frac{T}{2}\right) &= \frac{1}{2}\alpha A \int_{-\frac{T}{2}}^{\frac{T}{2}} \bar{S}_1(t) \bar{S}_0^*(t) dt + \int_{-\frac{T}{2}}^{\frac{T}{2}} \beta \exp(j\theta) h(\tau; t) \bar{S}_0^*(t) d\tau \\
 &= \frac{1}{2}\alpha A \int_{-\frac{T}{2}}^{\frac{T}{2}} \cos(\mu t^2) dt + \beta \exp(j\theta) \int_{-\frac{T}{2}}^{\frac{T}{2}} \cos(\mu \tau^2) h(\tau; t) d\tau.
 \end{aligned} \tag{A.22}$$

$U_0\left(\frac{T}{2}\right)$  also is a Gaussian random variable with mean  $= \frac{1}{2}\alpha A \int_{-\frac{T}{2}}^{\frac{T}{2}} \cos(\mu t^2) dt$  and:

$$\sigma^2 = \frac{\beta^2}{2} \sigma_h^2 \int_{-\frac{T}{2}}^{\frac{T}{2}} \cos^2(\mu t^2) dt. \tag{A.23}$$

For fixed values of  $U_0\left(\frac{T}{2}\right)$  and  $U_1\left(\frac{T}{2}\right)$ , the probability of correct decision  $P_c$  is given by

$$P_{c/U_0\left(\frac{T}{2}\right), U_1\left(\frac{T}{2}\right)} = Q\left\{\sqrt{\gamma_1}, \sqrt{\gamma_0}\right\} - \frac{1}{2} \exp\left[-\frac{1}{2}(\gamma_0 + \gamma_1)\right] I_0\left[\sqrt{\gamma_1 \gamma_0}\right], \tag{A.24}$$

where

$$\gamma_1 \equiv \frac{U_1^2\left(\frac{T}{2}\right)}{2\sigma_N^2}$$

and

$$\gamma_0 \equiv \frac{U_0^2\left(\frac{T}{2}\right)}{2\sigma_N^2}.$$

Then the marginal probability of correct decision then is:

$$P_c = \int_{-\infty}^{+\infty} \int_{-\infty}^{+\infty} P_{c/U_0\left(\frac{T}{2}\right), U_1\left(\frac{T}{2}\right)} P_{(U_1\left(\frac{T}{2}\right))} dU_1\left(\frac{T}{2}\right) P_{(U_0\left(\frac{T}{2}\right))} dU_0\left(\frac{T}{2}\right). \tag{A.25}$$

#### A.4 Chirp differential BPSK as an efficient diversity technique

A new modulation technique now will be presented. This technique combines the chirp waveform and the phase modulation approach. As mentioned previously, coherent detection in the presence of fading is useless. This especially is true when the data is transmitted in short bursts interspersed with long breaks. Even if the information could be sent coherently, phase synchronization would have to be performed on each burst. Since bursts are relatively short, it is difficult to achieve phase synchronization.

As the fading is very slowly time varying and the relative drift between the transmitter and the receiver is assumed to be very small, the phase difference between two consecutive bits also is small. Nevertheless, it must be taken into consideration.

In this section, we will prove that the new chirp differential BPSK (CDPSK) is identical to the conventional DPSK in the presence of AWGN. Then we will evaluate the performance of the receiver under the condition of fading. Two kinds of fading will be examined. The first is very slowly time-varying, frequency selective, Rayleigh fading and the second is non-random fading.

Let us define our signal set as

$$S_i(t) = \sin[\omega_0 t + \frac{1}{2}\mu t^2 + \phi_i(t) + \theta] \quad i = 0, 1, \quad (\text{A.26})$$

where  $\phi_i = \frac{\pi}{2}$  when a mark is transmitted and  $\phi_i = -\frac{\pi}{2}$  when a space is transmitted.

$\theta$  is random phase uniformly distributed between 0 and  $2\pi$ . Figure A.2 shows the block diagram of the receiver. The received signal plus noise is correlated bit by bit with a one-bit delayed version of the signal plus noise. The output of the correlator is compared with a threshold set at zero. A decision is made in favor of a 1 or a 0

depending on whether the correlator output is positive or negative.

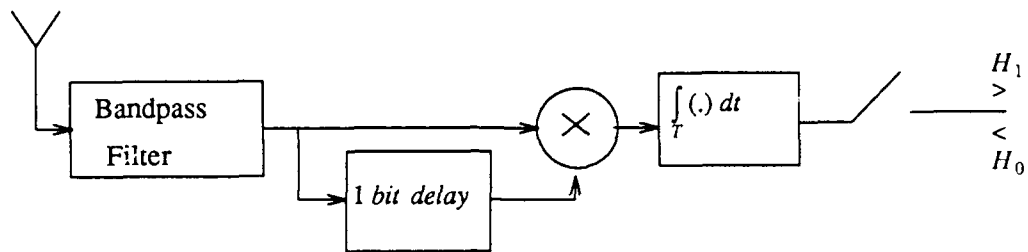


Figure A.2 Binary chirp DPSK demodulator.

In our analysis, we assume that a mark is transmitted and, without any loss of generality, we assume that  $\theta = 0$ . Hence, the received signal is

$$e_i(t) = A S_i(t) + n(t) , \quad (\text{A.27})$$

where

$$\begin{aligned} S_i(t) &= \sin[\omega_0 t + \frac{1}{2}\mu t^2 + \frac{\pi}{2}] \\ &= \cos[\omega_0 t + \frac{1}{2}\mu t^2] \end{aligned} \quad (\text{A.28})$$

and  $n(t)$  is additive narrow band Gaussian noise. In complex form this is given by

$$S_i(t) = A \operatorname{Re} \left\{ \bar{S}(t) \exp(j\omega_0 t) \right\} . \quad (\text{A.29})$$

Expressing  $e_1(t)$  and  $e_2(t)$  in their quadrature components yields

$$e_i(t) = \left[ A \cos(\frac{1}{2}\mu t^2) + n_{c/i}(t) \right] \cos(\omega_0 t) - \left[ A \sin(\frac{1}{2}\mu t^2) + n_{s/i}(t) \right] \sin(\omega_0 t) ; \quad i=1,2 \quad (\text{A.30})$$

Following Stein's proof,<sup>81</sup> we find

$$P_e = \frac{1}{2} \exp(-\gamma_b) . \quad (\text{A.31})$$

We see that in the absence of fading, the chirp DBPSK system has the same performance as the conventional DBPSK system.

For a fading channel we substitute  $r(t)$  in (A.31) instead of  $\bar{S}(t)$  where  $r(t)$  is

defined in (A.16). Again following Stein's proof<sup>81</sup>

$$e_i(t) = [r_i(t) + x_i(t)] \cos(\omega_0 t) - y_i(t) \sin(\omega_0 t) \quad i=1,2, \quad (\text{A.32})$$

where  $x_i(t)$  and  $y_i(t)$  are the quadrature components of the noise. The fading is assumed to be a slowly time-varying, frequency selective process, so at each frequency the fading is assumed to be constant for the relevant time period (i.e.  $H(f;t) \approx H(f)$ ).

As the frequency of the chirp signal is swept, the amount of fading varies accordingly. This actually is the reason why the amplitude of the received signal changes during a bit period. Since the channel is very slowly time-varying, the amplitudes are the same from bit to bit, i.e.

$$r_1(t) \approx r_2(t) = r(t) . \quad (\text{A.33})$$

Let us define  $\gamma_b$  as  $\gamma_b = \frac{E_b}{N_0}$ , where,

$$E_b = \frac{1}{2} \int_{-\frac{T}{2}}^{\frac{T}{2}} r(t) r^*(t) dt .$$

Assuming no intersymbol interference

$$\begin{aligned} E_b &= \frac{1}{2} \int_{-\infty}^{+\infty} r(t) r^*(t) dt \\ &= \frac{1}{2} \int_{-\infty}^{+\infty} H(f;t) \bar{S}(f) H^*(f;t) \bar{S}^*(f) df = \frac{1}{2} \int_{-\infty}^{+\infty} |H(f;t)|^2 |\bar{S}(f)|^2 df . \end{aligned} \quad (\text{A.34})$$

For  $BT \gg 1$ ,

$$|S(f)|^2 \approx \begin{cases} \frac{A^2 T}{2B} & |f| \leq \frac{B}{2} \\ 0 & \text{else} \end{cases} \quad (\text{A.35})$$

Then

$$E_b = \frac{1}{2} \frac{A^2 T}{B} \int_{-\frac{B}{2}}^{\frac{B}{2}} |H(f;t)|^2 df \quad (\text{A.36})$$

and

$$\gamma \equiv \frac{E_b}{N_0} = \frac{1}{2} \frac{A^2 T}{BN_0} \int_{-\frac{B}{2}}^{\frac{B}{2}} |H(f;t)|^2 df = \frac{\gamma_b}{B} \int_{-\frac{B}{2}}^{\frac{B}{2}} |H(f;t)|^2 df \quad (\text{A.37})$$

Since  $H(f;t)$  is a zero mean Gaussian random process,  $|H(f;t)|$  is a Rayleigh process with standard deviation  $2\sigma_H^2$ .

For  $H(f;t)$ , with  $\rho_H \ll B$  ( $\rho_H$  defined in section I.1),  $\gamma$  can be approximated by

$$\gamma \approx \frac{\gamma_b}{B} \sum_{n=0}^K |H(-\frac{B}{2} + n\rho_H)|^2 \rho_H = \sum_{n=0}^K \gamma_n \quad (\text{A.38})$$

where  $K$  is defined as the number of degrees of freedom of the channel and is equal to the largest integer which is smaller than  $\frac{B}{\rho_H}$  and:

$$\gamma_n = \frac{\gamma_b}{B} \rho_H |H(-\frac{B}{2} + nK)|^2 = \frac{\gamma_b}{2} \rho_H |H_n|^2.$$

Sampling  $|H(f;t)|$  at rate greater than or equal to  $\rho_H$  guarantees that the samples will be uncorrelated.

Assuming that  $|H_n|$  is a Rayleigh distributed random variable with variance equal to  $2\sigma_H^2$  and making the appropriate transformation, we find that

$$P(\gamma_n) = \frac{B}{\gamma_b \rho_H} \exp \left[ -\frac{B \gamma_n}{\gamma_b \rho_H} \right] U(\gamma_n) \quad (\text{A.39})$$

For a given sample of  $r(t)$ ,

$$P_{e|\gamma} = \frac{1}{2} \exp(-\gamma) \quad (\text{A.40})$$

and

$$P_e = \int_{-\infty}^{\infty} P_{e|\gamma} P(\gamma) d\gamma \quad (\text{A.41})$$

The characteristic function,  $\Phi(iu\gamma)$ , of  $\gamma$  when  $\gamma$  is defined as  $\gamma = \sum_{n=0}^{K-1} \gamma_n$ , is

$$\Phi(iu\gamma) = E[\exp(iu\gamma)] = \prod_{n=0}^{K-1} E[\exp(iu\gamma_n)] = \left[ \frac{B}{\gamma_b \rho_H \sigma_r^2} \right]^K \left[ iu + \frac{B}{\gamma_b \rho_H \sigma_r^2} \right]^{-K} . \quad (\text{A.42})$$

The probability density function of  $\gamma$  is the inverse Fourier transform of the characteristic function  $\Phi(iu\gamma)$ , and is given by

$$P_\gamma(\gamma) = \left[ \frac{B}{\gamma_b \rho_H \sigma_r^2} \right]^K \frac{\gamma^{K-1}}{(K-1)!} \exp\left(-\frac{B}{\gamma_b \rho_H \sigma_r^2} \gamma\right) U(\gamma) . \quad (\text{A.43})$$

Substituting  $\hat{\gamma}_b = \gamma_b \sigma_r^2$ , and  $K = \frac{B}{\rho_H}$  in (A.43) yields

$$P_\gamma(\gamma) = \left[ \frac{K}{\hat{\gamma}_b} \right]^K \frac{\gamma^{K-1}}{(K-1)!} \exp\left(-\frac{K\gamma}{\hat{\gamma}_b}\right) U(\gamma) . \quad (\text{A.44})$$

Figure A.3 gives the calculated density function of  $\gamma$  for various values of  $K$  and for  $\hat{\gamma}_b = 10 \text{ dB}$ . Figure A.4 compares the simulation results and the calculated results for  $K = 4$  and  $\hat{\gamma}_b = 10 \text{ dB}$ .

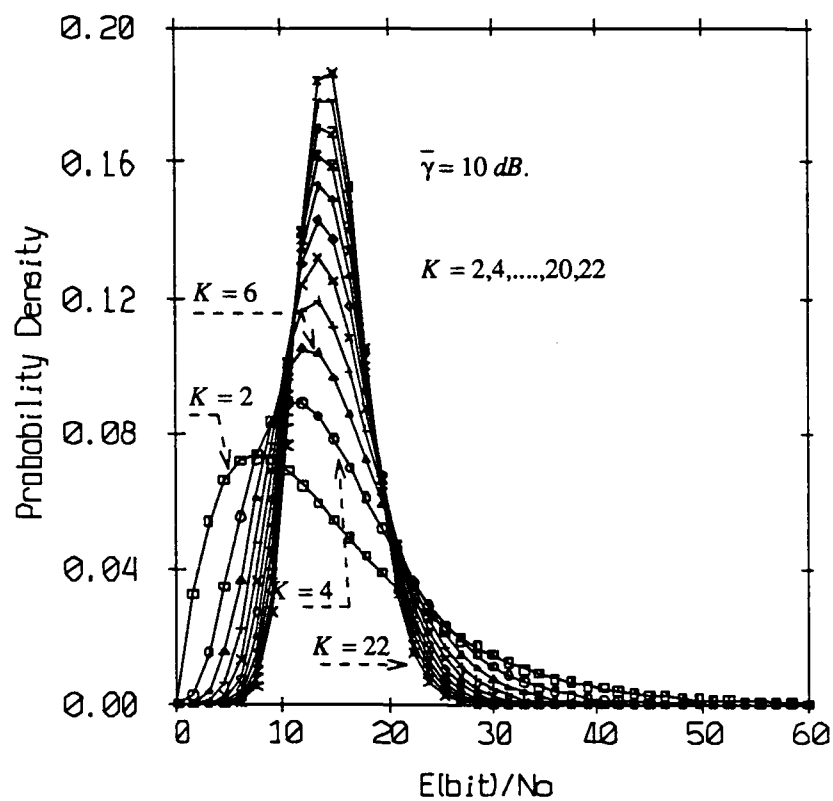


Figure A.3 The calculated probability density function of  $\gamma$  for various values of  $K$  and  $\gamma_b = 10 \text{ dB}$ .

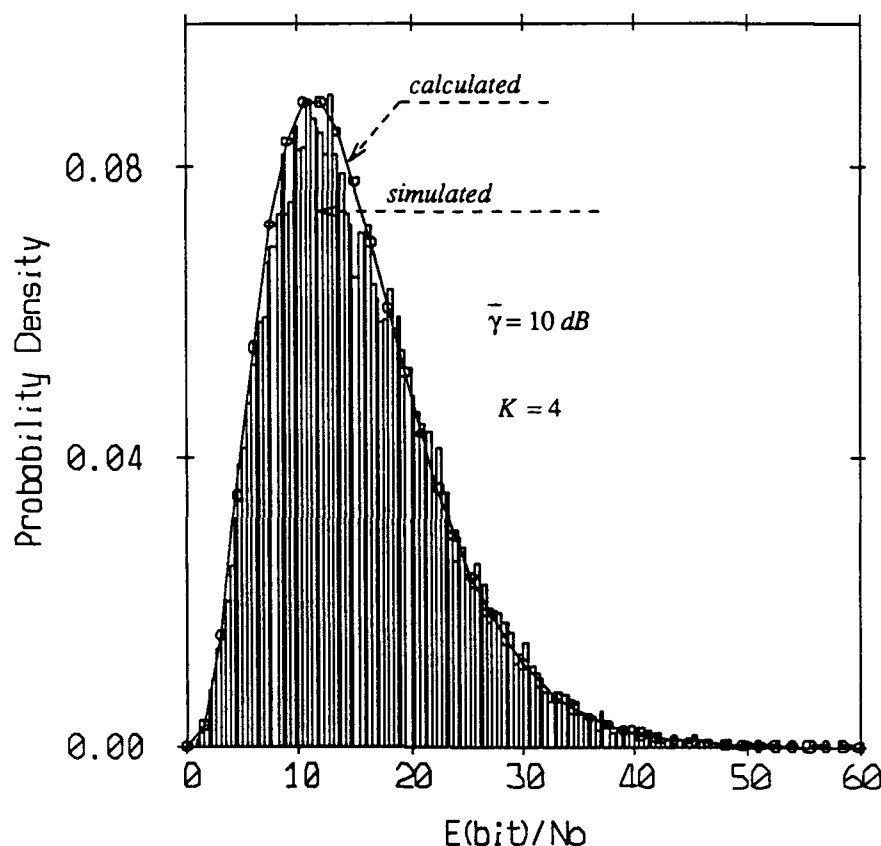


Figure A.4 The probability density function of  $\gamma$  for  $K = 4$  and  $\hat{\gamma}_b = 10 \text{ dB}$ . Comparison between calculated and simulated results.

Substituting (A.44) in (A.41), changing variables, and integrating yields

$$P_e = \frac{1}{2} \left\{ 1 + \frac{\hat{\gamma}_b}{K} \right\}^{-K} . \quad (\text{A.45})$$

As  $K \rightarrow \infty$  (uncorrelated process):

$$P_e = \frac{1}{2} \lim_{K \rightarrow \infty} \left\{ 1 + \frac{\hat{\gamma}_b}{K} \right\}^{-K} = \frac{1}{2} \exp(-\hat{\gamma}_b) . \quad (\text{A.46})$$

Figure A.5 gives the bit error probability of a chirp DPSK as a function of  $\hat{\gamma}$  for various values of  $K$ .

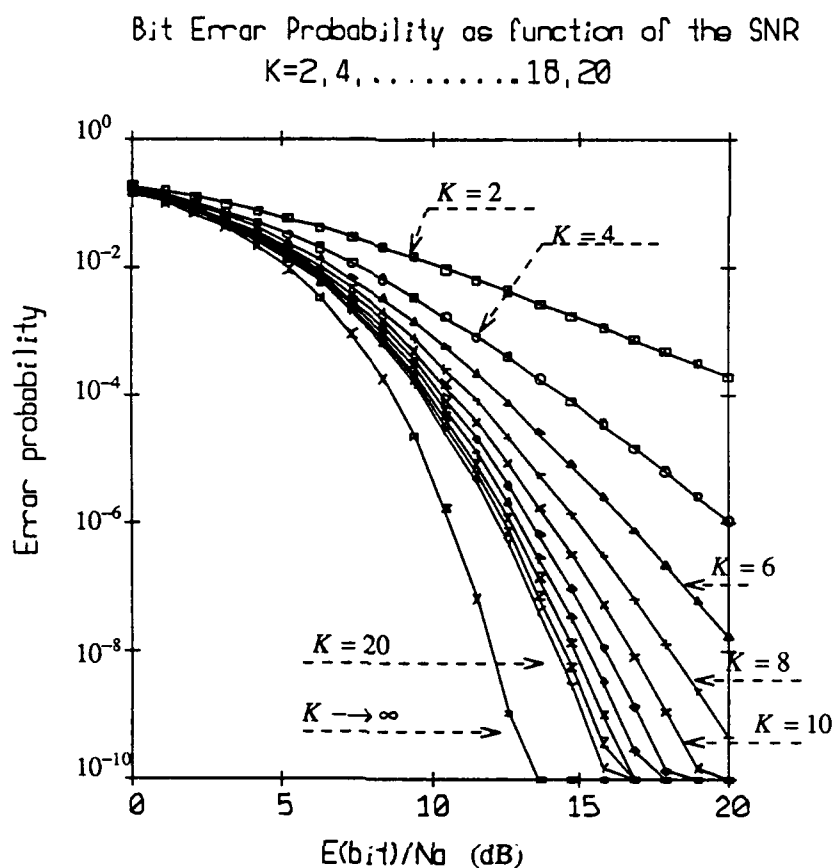


Figure A.5 The bit error probability of a chirp DPSK as a function of  $\hat{\gamma}$  for various values of  $K$ .

For a given signal to noise ratio, the probability of a binary bit error for 4 phase DPSK with Gray coding is given by<sup>75</sup>

$$P_{e,\gamma} = Q[a, b] - \frac{1}{2} I_0[a, b] \exp\left[-\frac{1}{2}(a^2 + b^2)\right], \quad (\text{A.47})$$

where

$$a = \sqrt{\frac{\gamma}{2}} (\sqrt{2+\sqrt{2}} - \sqrt{2-\sqrt{2}})$$

and

$$b = \sqrt{\frac{\gamma}{2}} (\sqrt{2+\sqrt{2}} + \sqrt{2-\sqrt{2}}).$$

After some algebraic manipulation, (A.47) is identical to

$$P_{e|\gamma} = \frac{1}{2} \exp(-2\gamma) \int_{\theta=0}^{2\pi} \frac{\sqrt{2} \exp[\sqrt{2} \gamma \cos(\theta)]}{2 - \sqrt{2} \cos(\theta)} \frac{d\theta}{2\pi} \quad (\text{A.48})$$

The marginal bit error probability  $P_e$  is given by (A.41) and  $P_\gamma$  is given by (A.44).

Substituting (A.44) and (A.48) into (A.41) and integrating with respect to  $\gamma$  yields

$$P_e = \frac{\sqrt{2}}{4\pi} \int_{\theta=0}^{2\pi} \left[ 2 + \frac{K}{\hat{\gamma}_b} - \sqrt{2} \hat{\gamma}_b \cos(\theta) \right]^{-K} (2 - \sqrt{2} \cos(\theta))^{-1} d\theta \quad (\text{A.49})$$

and as  $K \rightarrow \infty$ ,

$$P_e = \frac{\sqrt{2}}{4\pi} \int_{\theta=0}^{2\pi} (2 - \sqrt{2} \cos(\theta))^{-1} \exp[-\hat{\gamma}_b (2 - \sqrt{2} \cos(\theta))] d\theta \quad (\text{A.50})$$

Figure A.6 gives the calculated bit error probability as a function of the signal to noise ratio for various values of  $K$ .

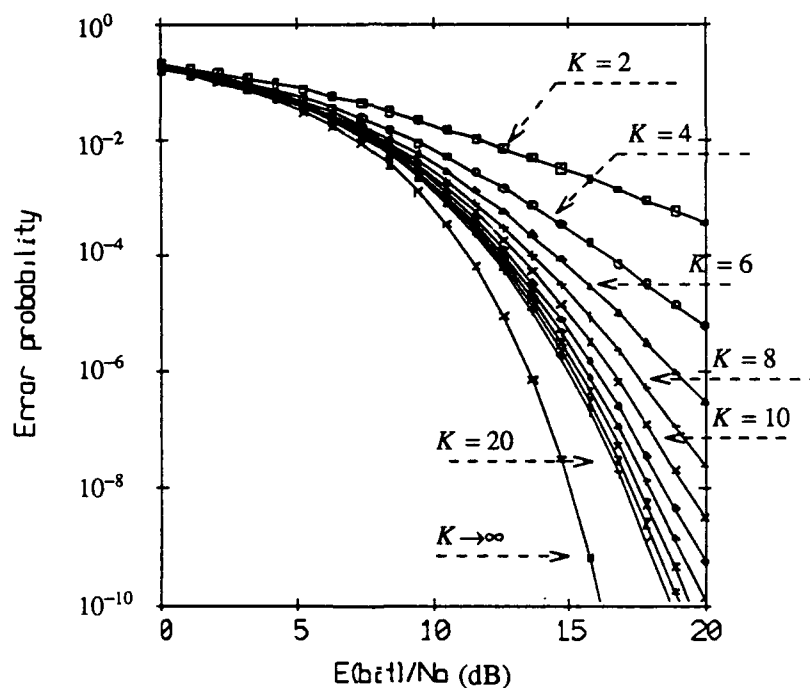


**Figure A.6** The bit error probability of a 4-Phase chirp DPSK as a function of  $\hat{\gamma}$  for various values of  $K$ .

For non-random fading, the received  $i$ -th signal is

$$S_i(t) = A [1 \sin(\omega_0 t + \frac{1}{2}\mu t^2 + \phi_i(t)) + \alpha \sin(\omega_0 \bar{t} + \frac{1}{2}\mu \bar{t}^2 + \phi_i(t) + \theta)] , \quad (\text{A.51})$$

where  $\bar{t} = t + t_d$ , and  $t_d$  is the time delay between the direct and indirect received signals.  $\alpha$  is the attenuation of the indirect signal and  $\theta$  is the phase difference between the direct and indirect signal caused by reflection and the difference in path length. Assuming  $t_d \ll T$ , and no intersymbol interference, the received  $(i-1)$ -th signal is given by

$$S_{i-1}(t) = A [\sin(\omega_0 t + \frac{1}{2}\mu t^2 + \phi_{i-1}(t)) + \alpha \sin(\omega_0 \bar{t} + \frac{1}{2}\mu \bar{t}^2 + \phi_{i-1}(t) + \theta)] \quad (\text{A.52})$$

and

$$S_i(t) = A [\sin(\omega_0 t + \frac{1}{2}\mu t^2 + \phi_i(t)) + \alpha \sin(\omega_0 \bar{t} + \frac{1}{2}\mu \bar{t}^2 + \phi_i(t) + \theta)] . \quad (\text{A.53})$$

For simplicity, let us define  $\xi(t) \equiv \frac{1}{2}\mu t^2$  and  $\zeta(t) \equiv \omega_0 t_d + \mu t t_d + \frac{1}{2}\mu t_d^2 + \theta$ .

Without any loss of generality, we can assume that  $i-1 = 1$ ,  $i=2$ , and  $\phi_1 = \phi_2 = \frac{\pi}{2}$ .

Rewriting (A.52) and (A.53) in their quadrature form yields:

$$e_1(t) = \left[ A [\cos(\xi(t)) + \alpha \cos(\zeta(t)) + n_{c1}(t)] \right] \cos(\omega_0(t)) - \left[ A [\sin(\xi(t)) + \alpha \sin(\zeta(t)) + n_{s1}(t)] \right] \sin(\omega_0(t)) \quad (\text{A.54})$$

and

$$e_2(t) = \left[ A [\cos(\xi(t)) + \alpha \cos(\zeta(t)) + n_{c2}(t)] \right] \cos(\omega_0(t)) - \left[ A [\sin(\xi(t)) + \alpha \sin(\zeta(t)) + n_{s2}(t)] \right] \sin(\omega_0(t))$$

It is convenient to rewrite (A.54) in terms of a another nonzero mean Gaussian process. Then,

$$e_i(t) = x_i(t) \cos(\xi(t)) - y_i(t) \sin(\xi(t)) = \text{Re} \left[ z_i \exp(j\xi(t)) \right] \quad i=1,2 . \quad (\text{A.55})$$

Again following Stein,<sup>81</sup> we find

$$P_e = \frac{1}{2} \exp(-\gamma) , \quad (\text{A.56})$$

where  $\gamma = \frac{\eta^2}{2N_0 T}$  and

$$\begin{aligned} \eta &= A \left\{ \int_{-0.5T}^{0.5T} [1 + \alpha^2 + 2\alpha \cos(\zeta(t))] dt \right\} \\ &= A T \left[ 1 + \alpha^2 + 2\alpha \cos(\omega_0 t_d + \frac{1}{2}\mu_d^2 + \theta) \text{sinc}(\frac{\mu_d T}{2}) \right] . \end{aligned} \quad (\text{A.57})$$

From (A.57) we can show that

$$\gamma = \gamma_b \left[ 1 + \alpha^2 + 2\alpha \cos(\omega_0 t_d + \frac{1}{2}\mu_d^2 + \theta) \text{sinc}(\frac{\mu_d T}{2}) \right]^2 . \quad (\text{A.58})$$

For a very short time delay for which  $\mu_d T$  is very small, we can write

$$\gamma = \gamma_b \left[ 1 + \alpha^2 + 2\alpha \cos(\omega_0 t_d + \theta) \right]^2 .$$

In this case,  $\gamma$  is periodic with respect to  $t_d$  with a period equal to  $T_c$ . For appropriate values of  $t_d$ ,  $\omega_0$ , and  $\theta$ ,  $\gamma$  is bounded by 0 and  $2\gamma_b$ , and

$$\frac{1}{2} \leq P_e \leq \frac{1}{2} \exp(-2\gamma_b) .$$

In most underwater acoustic channels, the dominant indirect signal is the component that is reflected from the sea surface. In this case  $\theta \approx \pi$ . Figure A.7 shows the effect of the indirect path on the bit error probability for various values of time delay,  $t_d$ , between the direct and the indirect path when  $\alpha = 0.5$ , and  $\theta = \pi$ .

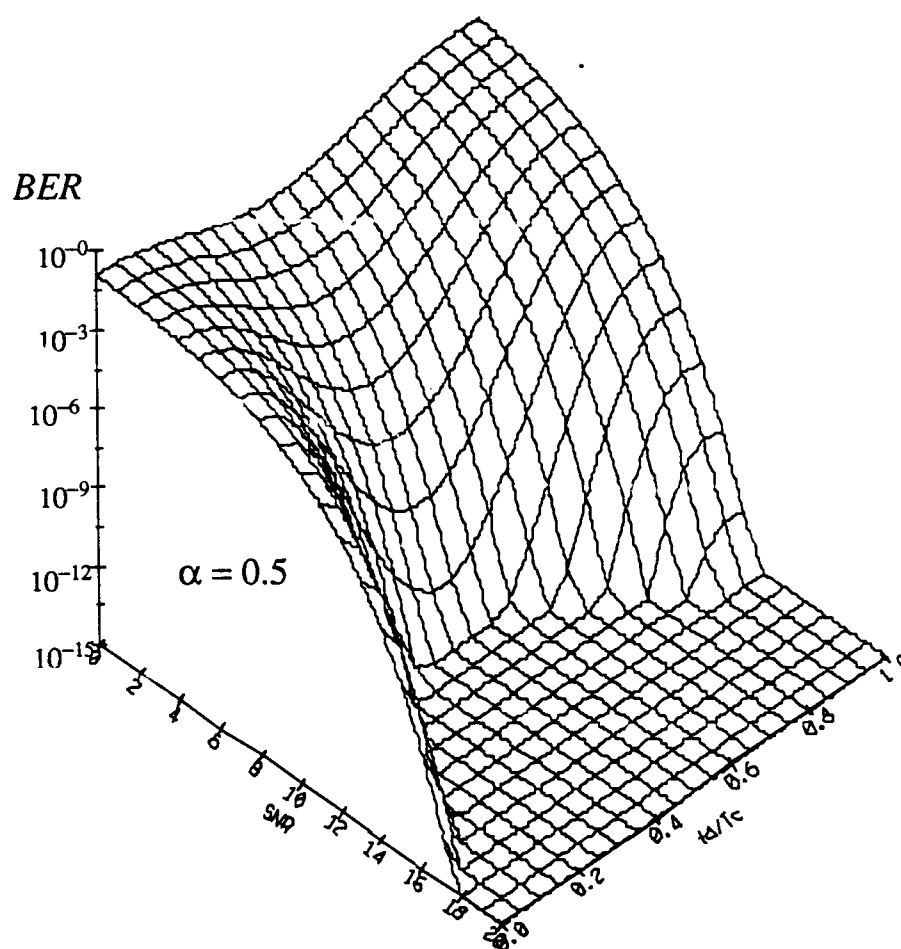


**Figure A.7** Indirect path effect on the BER of chirp BDPSK modulation for  $\alpha = 0.5$  and  $\theta = \pi$ .

Usually,  $t_d$  is such that  $\text{sinc}(\frac{\mu t_d T}{2}) \approx 0$ . In this case:

$$\gamma = \gamma_b (1 + \alpha^2)^2 \quad (\text{A.59})$$

From (A.59), one can see that when a chirp waveform is used as the carrier signal, a short delayed deterministic multipath does not cause any damage to the system.

### A.6.1 Motion effect on the performance of chirp DPSK

In most communication links, a relative motion between the receiver and the transmitter exists. In a communication link between several sonobuoys which are not moored, currents in the ocean cause a relative drift among the sonobuoys. Although the time drift between two successive bits caused by the distance difference is very small, it is a mistake to ignore this effect on the system performance. The drift is assumed to be much much smaller than the bit period.

Let us assume that the  $i$ -th received bit is  $S_i(t)$  and the  $(i-1)$ -th received bit is  $S_{(i-1)}(t)$ , and the time delay caused by the drift is much smaller than the bit period. Then,

$$S_i(t) = A_i(t) \sin [\omega_0 t + \frac{1}{2} \mu t^2 + \phi_i(t) + \theta] \quad (\text{A.60})$$

and

$$S_{i-1}(t) = A_{i-1}(t) \sin [\omega_0 t + \frac{1}{2} \mu t^2 + \phi_{i-1}(t) + \theta] .$$

For  $\zeta$  as defined in (A.52) and  $\xi = \omega_0 t_d + \mu t_d^2 + \frac{1}{2} \mu t_d^2 + \theta$

we find that

$$S_i(t) = A_i(t) \sin \xi(t) , \quad (\text{A.61})$$

and

$$S_{i-1}(t) = A_{i-1}(t) \sin [\xi(t) + \zeta(t)] .$$

From Pawula at el<sup>70</sup>. [(9) - (11)], we find that the bit error probability  $P_e$  is

$$P_e = P(\Phi_1 \leq \Phi \leq \Phi_2) = \begin{cases} F(\Phi_2) - F(\Phi_1) + 1 & ; \Phi_1 < \zeta(\frac{T}{2}) < \Phi_2 \\ F(\Phi_2) - F(\Phi_1) & ; \Phi_1 > \zeta(\frac{T}{2}) \text{ or } \Phi_2 < \zeta(\frac{T}{2}) \end{cases} \quad (\text{A.62})$$

where  $\Phi_1 = \frac{\pi}{2}$  and  $\Phi_2 = \frac{3\pi}{2} = -\frac{\pi}{2}$

and

$$F(\Phi) = \frac{\sin[\zeta(\frac{T}{2}) - \Phi]}{4\pi} \int_{-\frac{\pi}{2}}^{\frac{\pi}{2}} \frac{\exp\left[-\gamma[1 - \cos(\zeta(\frac{T}{2}) - \Phi)) \cos(t)]}{1 - \cos(\zeta(\frac{T}{2}) - \Phi)) \cos(t)} dt \quad (\text{A.63})$$

For  $\phi_i = \phi_{i-1}$ , a correct decision is made if  $\frac{\pi}{2} \leq \Phi \leq -\frac{\pi}{2}$ .

Define  $\bar{P}/\gamma$  as

$$\bar{P}/\gamma = F(-\frac{\pi}{2})/\gamma - F(\frac{\pi}{2})/\gamma = \quad (\text{A.64})$$

$$= \frac{\cos(\zeta(\frac{T}{2}))}{4\pi} \int_{-\frac{\pi}{2}}^{\frac{\pi}{2}} \left\{ \frac{\exp\left[-\gamma[1 - \sin(\zeta(\frac{T}{2})) \cos(t)]\right]}{1 - \sin(\zeta(\frac{T}{2})) \cos(t)} + \frac{\exp\left[-\gamma[1 + \sin(\zeta(\frac{T}{2})) \cos(t)]\right]}{1 + \sin(\zeta(\frac{T}{2})) \cos(t)} \right\} dt$$

The marginal probability  $\bar{P}$  is

$$\bar{P} = \int_{-\infty}^{\infty} \bar{P}/\gamma P(\gamma) d\gamma \quad (\text{A.65})$$

where  $P(\gamma)$  is given by (A.45). After some simple algebraic manipulation, one finds:

$$\bar{P} = \frac{\cos(\zeta(\frac{T}{2}))}{4\pi} \int_{-\frac{\pi}{2}}^{\frac{\pi}{2}} \sum_{i=1}^2 \frac{1}{a_i} \left[ 1 + \frac{\hat{\gamma}_b a_i}{K} \right]^{-K} dt, \quad (\text{A.66})$$

where

$$a_1 = 1 - \sin(\zeta(\frac{T}{2})) \cos(t)$$

and

$$a_2 = 1 + \sin(\zeta(\frac{T}{2})) \cos(t).$$

As  $K \rightarrow \infty$

$$\bar{P} = \frac{\cos(\zeta(\frac{T}{2}))}{4\pi} \int_{-\frac{\pi}{2}}^{\frac{\pi}{2}} \sum_{i=1}^2 \frac{1}{a_i} \exp(-\hat{\gamma}_b a_i) dt. \quad (\text{A.67})$$

From (A.61), we find that the bit error probability  $P_e$  is given by

$$P_e = \begin{cases} \bar{P} + 1, & \frac{\pi}{2} < \zeta(\frac{T}{2}) < \frac{3}{2}\pi \\ \bar{P}, & \frac{\pi}{2} > \zeta(\frac{T}{2}) \text{ or } \frac{3}{2}\pi < \zeta(\frac{T}{2}) \end{cases} \quad (\text{A.68})$$

When there is no delay,  $\zeta(\frac{T}{2}) = 0$ . Substituting this into (A.66) and (A.67) and integrating gives us (A.32). Figure A.8 shows the bit error probability as a function of the signal to noise ratio ( $\hat{\gamma}_b$ ) for various values of the delay  $\tau$ .

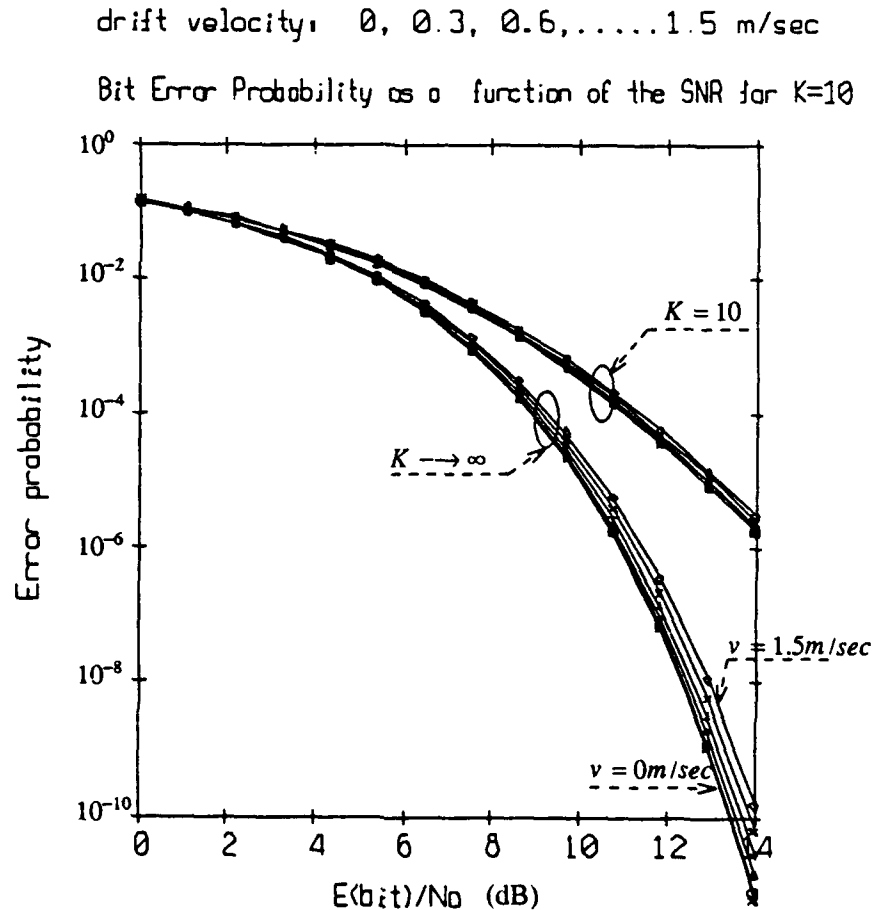


Figure A.8 Motion effect on the BER of chirp BDPSK modulation.

## Appendix B - Performance of several common error correction codes

The following plots taken from Odenwalder<sup>66</sup> show the performance of several common error correction codes.

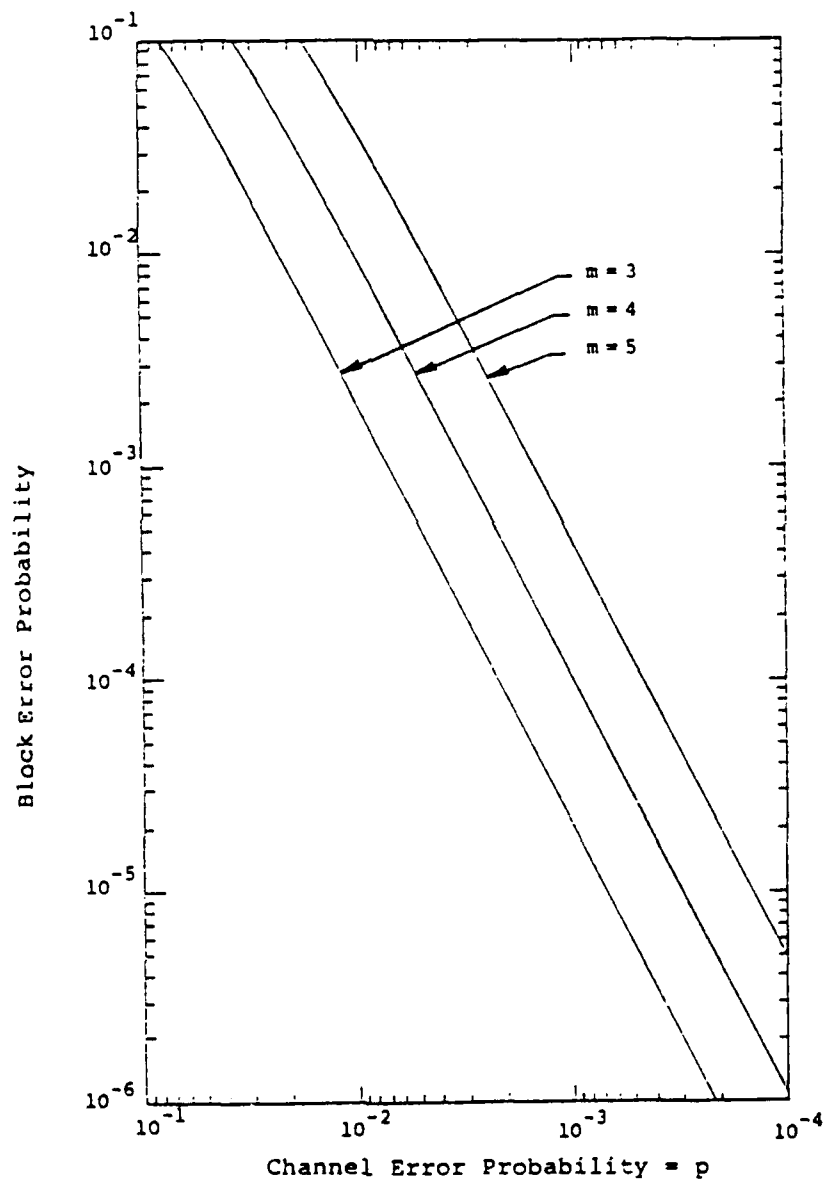


Figure B.1 Bit error probability versus channel error probability for block length  $n=2^m-1$  Hamming codes with  $m=3, 4$ , and  $5$

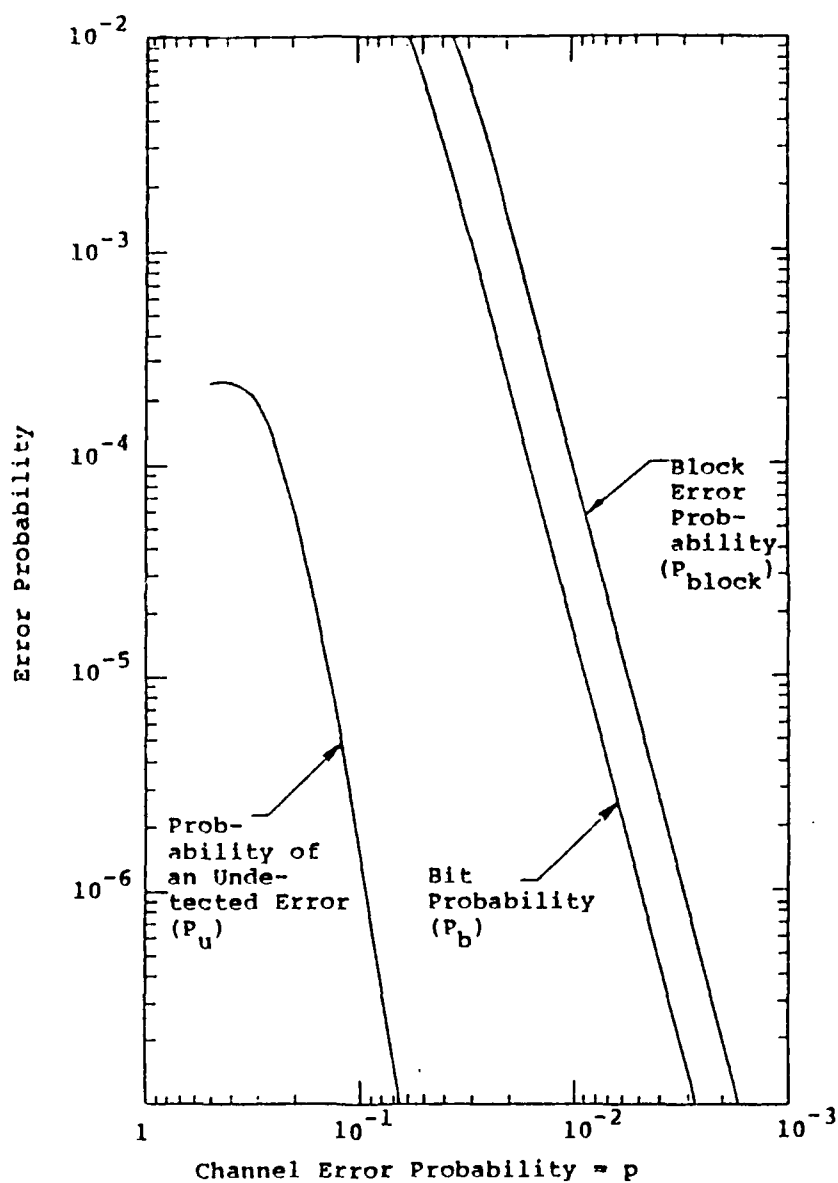


Figure B.2 Block, and bit error probabilities versus channel error rate with extended Golay coding.

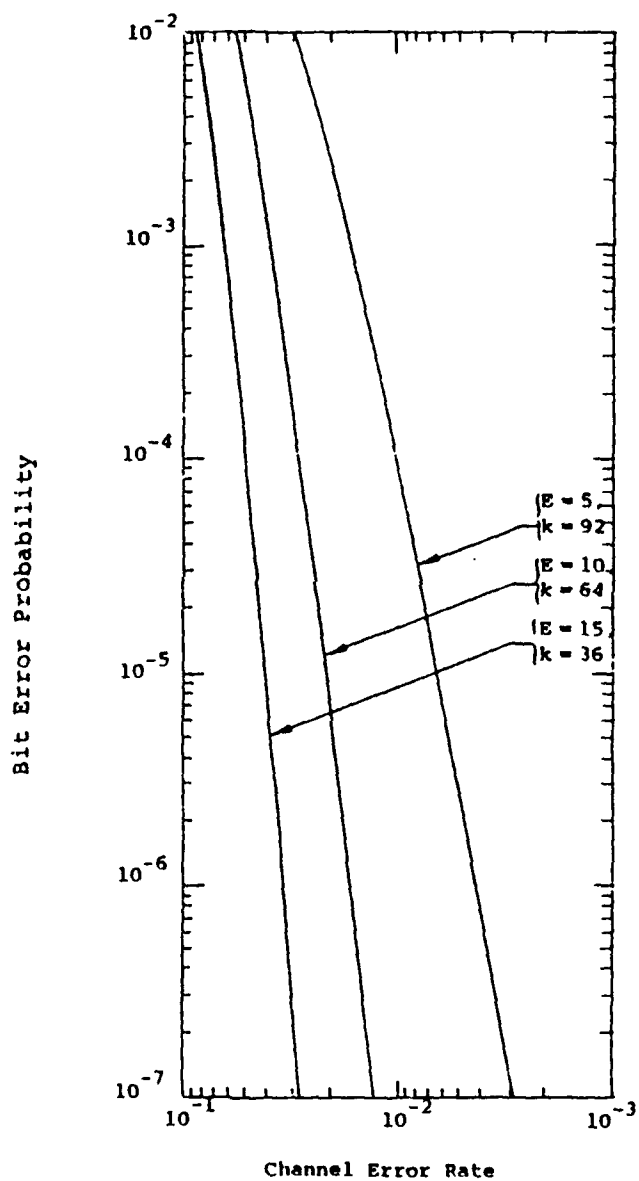


Figure B.3 Bit error probability versus channel error rate performance of several block length 127, BCH codes

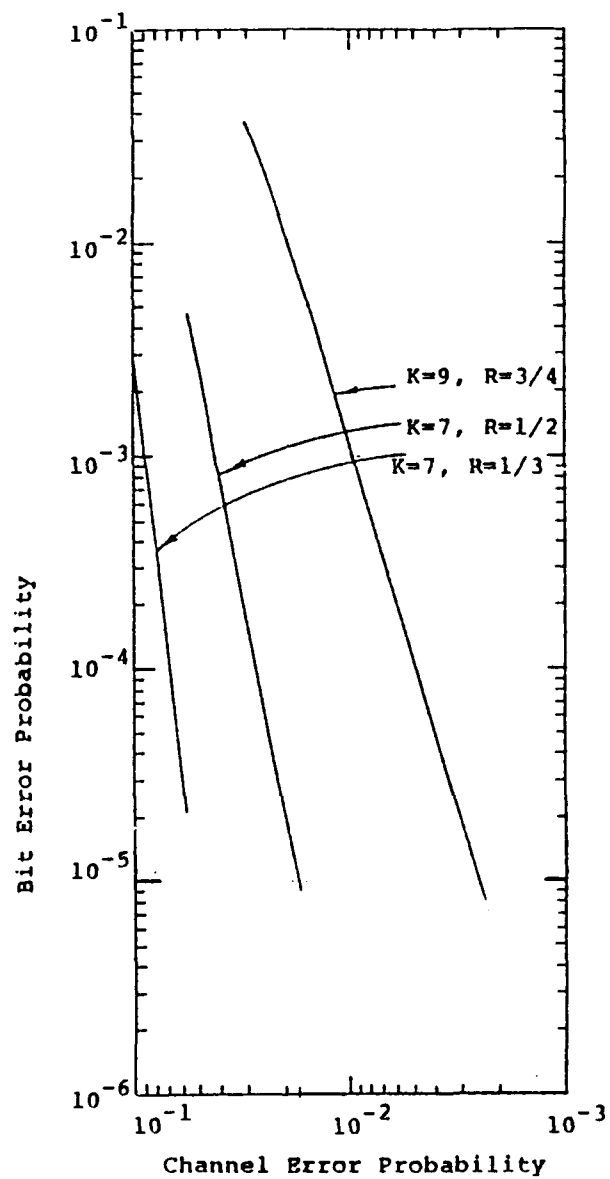


Figure B.4 Bit error probability versus channel error rate performance of several convolutional coding systems.

## Appendix C - Proof of Equation 3.16

The mean-square error,  $\epsilon^2$ , between the transmitted and the received data is

$$\epsilon^2 = E_j \left\{ [V(n) - \hat{V}(n)]^2 \right\} = \frac{1}{2^{2b}} E_j \left\{ \left[ \sum_{i=0}^{b-1} (c_{ij} - \hat{c}_{ij}) 2^i \right]^2 \right\} . \quad (C.1)$$

Changing order of summation and the expectation operation, we get

$$\epsilon^2 = \sum_{i=0}^{b-1} \sum_{n=0}^{b-1} E \left[ (c_{ij} - \hat{c}_{ij}) (c_{nj} - \hat{c}_{nj}) \right] 2^{i+n} . \quad (C.2)$$

For  $i \neq n$

$$E_{j,n} \left[ (c_{ij} - \hat{c}_{ij}) (c_{nj} - \hat{c}_{nj}) \right] = E_j \left[ (c_{ij} - \hat{c}_{ij}) \right] E_n \left[ (c_{in} - \hat{c}_{in}) \right] . \quad (C.3)$$

But

$$E_j \left[ (c_{ij} - \hat{c}_{ij}) \right] = 0 .$$

Since

$$E_j \left[ (c_{ij} - \hat{c}_{ij}) \right] = \frac{1}{4} \left[ p_i (1-0) + (1-p_i) (1-1) + p_i (0-1) + (1-p_i) (0-0) \right] = 0 ,$$

where  $p_i$  is the probability that the  $i$ -th bit was incorrectly detected. In the same way, we get for  $i = n$ ,

$$E_j \left[ (c_{ij} - \hat{c}_{ij})^2 \right] = p_i$$

and hence

$$\epsilon^2 = \frac{1}{2^{2b}} \sum_{i=0}^{b-1} p_i 2^{2i} . \quad (C.4)$$

Q.E.D

## Appendix D - Optimal Power Assignment

A set of  $p_i$  is to be found such that the function  $\epsilon^2$  given by

$$\begin{aligned}\epsilon^2 &= \frac{1}{2^{2b}} \sum_{i=0}^{b-1} p_i 2^{2i} \\ &= \frac{1}{2^{2b}} \sum_{i=0}^{b-1} f(\gamma_i) 2^i ,\end{aligned}\tag{D.1}$$

will be minimized under the constraint of a given value of word energy. Let  $p_i$  be the probability of incorrect detection of the  $i$ -th bit in the word (W). It is a function of the appropriate signal to noise ratio  $\gamma_i$ . In other words, we want to minimize

$$\eta = \sum_{i=0}^{b-1} f(\gamma_i) 2^i \tag{D.2}$$

under the constraint

$$\theta = \sum_{i=0}^{b-1} \gamma_i - \gamma = 0. \tag{D.3}$$

where  $\gamma = \frac{E_w}{N_0}$  and  $E_w$  is the word energy. Using Lagrange multipliers, we define

$$\psi = \eta - \lambda \theta \tag{D.4}$$

Then the set of  $\gamma_i$  that satisfies

$$\begin{cases} \frac{\partial \psi}{\partial \gamma_i} = 0 & i = 0, \dots, b-1 \\ \theta = 0 \end{cases} \tag{D.5}$$

is the set that minimizes (D.2). In our case ,

$$\frac{\partial \psi}{\partial \gamma_i} = 2^{2i} \frac{\partial f(\gamma_i)}{\partial \gamma_i} + \lambda . \tag{D.6}$$

For binary DPSK where

$$f(\gamma_i) = \frac{1}{2} \exp(-\gamma_i) , \tag{D.7}$$

the optimal  $\gamma_i$  are

$$\gamma_i = \frac{\gamma}{b} + (2i + 1 - b) \ln 2, \quad \gamma > b(b - 1) \ln 2. \quad (\text{D.8})$$

Substituting (D.8) in (D.1) we get

$$\varepsilon_{opt}^2 = \frac{b 2^{2-1}}{[2^b - 1]^2} p \ln 2, \quad \gamma > b(b - 1) \ln 2 \quad (\text{D.9})$$

where:

$$p = \frac{1}{2} \exp\left(-\frac{\gamma}{b}\right)$$

## References

1. Amos, D. E. and L. H. Koopmans, *Tables of the Distribution of the Coefficient of Coherence for Stationary Bivariate Gaussian Processes*, SCR 483, Mathematics and Computers, TID 4500, march 1963.
2. Baggeroer, A. B., D. E. Koelsh, K. von der Heydt, and J. Catipovic, "DATS - A Digital Acoustic Telemetry System for Underwater Communication," *OCEANS 81*, pp. 55-59, IEEE, Boston, Massachusetts, Sep. 16-18 1981.
3. Barton, D. K., *Pulse Compression*, Raytheon Company, Bedford, Mass., 1975.
4. Bendat, J. S. and A. G. Piersol, *Random Data: Analysis and measurement procedures*, John Wiley & Sons, 1971 (second ed. 1986).
5. Berkta, H. O. and B. K. Gazy, "Communication Aspects of Underwater Telemetry," *Telecommunication*, pp. 28-34, Jan. 1968.
6. Berni, A. J. and W. D. Gregg, "On the Utility of Chirp Modulation for Digital Signaling," *IEEE Trans. on Communication*, pp. 748-751, june 1973.
7. Bhargava, V. K., D. Haccoun, R. Matyas, and P. P. Nuspl, *Digital Communication by Satellite*, John Wiley & sons, New-york, 1981.
8. Boyarinov, I. M. and G. L. Katsman, "Linear Unequal Error Protection Codes," *IEEE Trans. on Information Theory*, vol. Vol. IT-27, No. 2, pp. 168-175, March 1981.
9. Brockwell, P. J and R. A. Davis, *Time Series Theory and Methods*, Springer Verlag, 1987.
10. Burrows, D. W., "Cableless Underwater Television Link Design and Test," *Oceanology International*, Brighton, England, 1969.
11. Carter, G. C., "Bias in Magnitude Squared Cohererence Estimation Due to Misalignment," *IEEE Trans. on ASSP*, vol. ASSP 28, No 1, pp. 97-99, Feb. 1980.
12. Carter, G. C., C. Knapp, and A. H. Nuttall, "Estimation of the Magnitude Squared Coherence Function Via Overlapped Fast Fourier Transform Processing," *IEEE Trans. on Audio and Electroacoustics*, vol. AU-21, No. 4, pp. 337-344, Aug. 1973.
13. Carter, G. C., C. H. Knapp, and A. H. Nuttall, "Statistics of the Estimate of the Magnitude Coherence Function," *IEEE Trans. on Audio and Electronics*, pp. 388-389, Aug. 1973.

14. Carter, G. C. and A. H. Nuttall, "Statistics of The Estimate of Coherence," *Proceedings of the IEEE*, pp. 465-466, April 1972.
15. Catipovic, J. and L. Freitag, "WHOI Acoustic Telemetry Project, Interim Report 12/1/88 - 6/1/89," *Tevhnical Report WHOI-89-21*, Woods Hole, July 1989.
16. Catipovic, J., L. Freitag, M. Deffenbahgh, and D. Frye, "An Acoustic Telemetry System For Deep Ocean Mooring Data Acquisition and Control," *Ocean 89*, pp. 887-892, IEEE, Seattle, Washington, Sep. 18-21 1989.
17. Catipovic, J. A. and L. E. Freitag, "High Data Rate Acoustic Telemetry for Moving ROVs in a Fading Multipath Shallow Water Environment," *Proceedings of the Symposium on Autotntomous Underwater Vehicle Technology*, pp. 296-303, IEE, Washington, DC, June 5-6, 1990.
18. Catipovitc, J. A., *Design and Performance Analysis of Digital Acoustic Telemetry System*, Massachusetts institute of Technology, Feb. 2 1988. PHD thesis
19. Chan, Y. T. and R. K. Miskowicz, "Estimation of Coherence and Time Delay with ARMA Models," *IEEE Trans. on ASSP*, vol. ASSP-32, No 2, pp. 295-303, April 1984.
20. Chiu, J. H. and L. S. Lee, "The Minimum Liklihood - A New Concept for Bit Synchronization," *IEEE Trans. on Communication*, vol. Vol Com-35 No 5, pp. 545-549, May 1987.
21. Churgin, J. and S. J. Halminski, *Temperature, Salinity, Oxygen, and Phosphate in Waters off the United States*, 3, National Oceanographic Data Center, 1974.
22. Chyi, G. T., J. K. Proakis, and C. M. Keller, "Diversity Reception over a Rayleigh-Fading Multipath Channel," *Proceedings of the 22nd Conference on Information Science and System*, pp. 420-425, Department of Engineering Princeton University, Princeton, New Jersy 08544, March 16-18 1988.
23. Collins, J. S. and J. L. Galloway, "Acoustic Telemetry of Video Information," *Proceedings OCEANS 83*, vol. I, pp. 163-166, IEEE, San Francisco, Aug. 29-Sep 1 1983.
24. Cook, C. E. and M. Bernfeld, *Radar Signals, an introduction to theory and application*, Academic Press, 1967.
25. Cook, C. E., "Linear FM Signals Formats for Beacon and Communication Systems," *IEEE Trans .on AES*, vol. AES-10, No 4, pp. 471-478, July 1974.

26. Cook, C. E., "Pulse Compression, Key to More Efficient Radar," *proc. IRE*, vol. 48, No. 3, pp. 320-316, March 1960.
27. Dashen, R., W. H. Munk, K. M. Watson, F. Zachariasen, and S. M. Flatte (Editor), *Sound Transmission Through a Fluctuating Ocean*, Cambridge University Press, Cambridge, 1979.
28. Dotan, A. and W.S. Hodgkiss, "Coherence of transients," *MPL TM-422*, San-Diego, July 1990.
29. Dow, W., "A Telemetering Hydrophone," *Deep Sea Research*, vol. 7, pp. 142-147, 1960.
30. Dunbar, R. M., A. Settery, D. R. Carmichael, and I. Anderson, "Cable-less Communication for Underwater Inspection, Engineering and Autonomous ROVs," *Underwater System Design*, pp. 21-27, Jan., Feb. 1987.
31. Duttweiler, D. L., J. E. Mazo, and D. G. Messerschmitt, "An Upper Bound on the Error Probability in Decision-Feedback Equalization," *IEEE Trans. on Information Theory*, vol. VOL. IT-20 No. 4, pp. 490-497, July 1974.
32. Fay, J. W., "Confidence bound for Signal to Noise Ratios from Magnitude Squared Coherence Estimates," *IEEE Trans. on ASSP*, vol. ASSP 28, No 6, pp. 758-760, Dec. 1980.
33. Flewellen, C. G., "PASTY: The Pulsed Acoustic Telemetry System," *Proceedings of the Institute of Acoustics*, vol. 9 part 4, pp. 79-85, Norwich, England, Dec. 17-18 1987.
34. Franks, L. E., "Carrier and Bit Synchronization in Data Communication A Tutorial Review," *IEEE Trans. on Communication*, vol. Vol. Com-28, No. 8, pp. 1107-1121, Aug. 1980.
35. Garber, F. and M. B. Pursley, "Performance of Differentially Coherent Digital communication over Frequency Selective Fading Channels," *IEEE Trans. on Communication*, vol. 36. No 1, pp. 21-31, Jan 1988.
36. Garrood, D. J., "Application of the MFSK Acoustical Communications System," *OCEANS 81*, pp. 61-66, IEEE, Boston, Massachusetts, Sep. 16-18 1981.
37. Gott, G. F. and J. P. Newsome, "H.F. Data Transmission Using Chirp Signals," *Proc. IEEE*, vol. 118, No 9, pp. 1162-1166, Sept. 1971.
38. Hannan, E. J., *Time Series Analysis*, 1970.
39. Haykin, S., *Adaptive Filter Theory*, Prentice-Hall, 1986.

40. Hearn, P. J., "Underwater Acoustic Telemetry," *IEEE Trans. on Communication*, vol. vol COM-14, No 6, pp. 839-843, 1966.
41. Helstrom, C. W., *Signal Detection and Estimation*, Department of Electrical Engineering and Computer Science, UCSD, San Diego, 1985.
42. Hill, W., G. Chaplin, and D. Nergaad, "Deep Ocean Tests on an Acoustic Modem Intensive to Multipath Distortion," *IEEE*, pp. 275-282, 1988.
43. Hodgkiss, W.S., "A Modular Approach to Exploratory Data Analysis," *Proc. OCEANS' 89*, pp. 1100-1104, 18-21 Sept. 1989.
44. Holland-Moritz, E. K., J. C. Dute, and D. R. Brundage, *Swept Frequency Modulation*, pp. 469-474.
45. Holmes, J. K., *Coherent Spread Spectrum Systems*, John Wiley & Sons, 1982.
46. Hummels, D. R., "The Capacity of a Model for the Underwater Acoustic Channel," *IEEE Trans. Sonic and Ultrasonics*, vol. Vol. SU-19, pp. 350-353, July 1972.
47. Jacobsen, H. P., K. Vestgard, and F. T. Knudsen, "Acoustic Control System," *OCEANS 82*, pp. 106-110, IEEE, Washington, D.C., Sep. 20-22 1982.
48. Kay, S. M. and S. L. Marple, "Spectrum Analysis - A Modern Perspective," *Proceedings of the IEEE*, vol. 69 No. 11, pp. 1380-1419, Nov. 1981.
49. Kay, S. M., *Modern Spectral Estimation*, Prentice-Hall, 1988.
50. Kearney, P. O. Jr and C. A. Laufer, "SONALINK - A Deep Ocean High Data Rate, Adaptive Telemetry System," *OCEANS 84*, pp. 49-53, IEEE, Washington, D.C., Sep. 10-2 1984.
51. Leduc, B. and G. Ayela, "TIVA a Self Contained Image/Data Acoustic Transmission System for Underwater Application," *Marine Instrumentation '90, Conference proceedings*, pp. 211-214, West Star Production, San Diego, Feb. 27-March 1, 1990.
52. Lee, E. A. and D. G. Messerschmitt, *Digital Communication*, Kluwer Academic Publishers, Boston, 1988.
53. Lee, P. F., "An Algorithm for Computing the Cumulative Distribution for Magnitude Squared Coherence Estimats," *IEEE Trans. on ASSP*, vol. ASSP 29 No 1, pp. 117-119, Feb. 1981.

54. Lindsey, W. C. and M. K. Simon, *Telecommunication Systems Engineering*, Prentice-Hall, Inc., 1973.
55. Lord, G. E. and T. D. Plemons, "Characterization and Simulation of Underwater Acoustic Signals Reflected from the Sea Surface," *J. Acoust. Soc. Am.*, vol. 63(2), pp. 378-384, Feb 1978.
56. Mackenzie, K. V., "Nine term equation for sound speed in the oceans," *J. Acoust. Soc. Am.*, vol. 70(3), 1981.
57. Marple, S. L., *Digital Spectral Analysis with Applications*, Prentice-Hall, 1987.
58. Marple, S. L. and A. H. Nuttall, "Experimental Comparison of Three Multichannel Linear Prediction Spectral Estimation," *IEE Proc.*, vol. 130, part F, pp. 218-229, April 1983.
59. Marple, S. L., "Performance of Multichannel Autoregressive Spectral Estimators," *ICASSP-86*, vol. 5.8.1, pp. 197-200, Tokyo, Japan, 1986.
60. Masnick, B and J. Wolf, "On Linear Unequal Error Protection Codes," *IEEE Trans. on Information Theory*, vol. IT-3, No. 4, pp. 600-607, ocober 1967 .
61. Meyers, M. H. and L. E. Franks, "Joint Carrier Phase and Symbole Timing Recovery for PAM Systems," *IEEE Trans. on Communication*, vol. vol. com-28 N0. 8, pp. 1121-1129, Aug. 1980.
62. Morgan, D. R., "Adaptive Multipath Cancellation for Digital Data Communications," *IEEE Trans. on Communication*, vol. Vol. COM.- 26. No. 9, pp. 1380-1390, Sept. 1978.
63. Murray, W., *Numerical methods for Unconstrained Optimization*, Academic Press, New-York, 1972.
64. Nuttall, A. H. and C. C. Carter, "Bias of the Estimate of Magnitude Squared Coherence," *IEEE Trans. on ASSP*, pp. 582-583, Dec. 1976.
65. Nuttall, A. H., "Direct Coherence Estimation via a Constrained Least Squares Linear Prediction Fast Algorithm," *ICASSP 82, Proceedings*, vol. 2, pp. 1104-1107, IEEE, Paris, France, 3-5 May 1982.
66. Odenwalder, J. P., *Error control coding handbook*, Linkabit corporation 10453 Roselle st., San-Diego, CA. July,15 1976.
67. Oppenheim, A. V. and R. W. Schafer, *Digital Signal Processing*, Prentice-Hall, 1975.

68. Papoulis, A., *Probability Random Variables and Stochastic Processes*, McGraw Hill, 1984.
69. Park, L. H. JR., "On Binary Dpsk Detection," *IEEE Trans. on Communication*, vol. VOL. COM-26, No.4, pp. 484-486, April 1978.
70. Pawula, R. F., S. O. Rice, and J. H. Roberts, "Distribution of the Phase Angle Between Two Vectors Perturbed by Gaussian Noise," *IEEE Trans. on Communication*, vol. COM-30 No 8, pp. 1828-1841, Aug. 1982.
71. Pieper, J. F., J. G. Proakis, R. R. Reed, and J. K. Wolf, "Design of Efficient Coding and Modulation for a Rayleigh Fading Channel," *IEEE Trans. on Information Theory*, vol. IT-24, No 4, pp. 457-469, July 1978.
72. Pierce, J., "Theoretical diversity improvment in FSK," *Proc. IRE*, vol. 46, pp. 903-910, may 1958.
73. Prada, K. E., K. von der Heydt, and T. F. O'Brien, "A versatile Multi-Channel Data acquisition System For Seismic and Acoustic Application," *OCEANS 81*, pp. 43-47, IEEE, Boston, Massachusetts, Sep. 16-18 1981.
74. Priestley, M. B., *Spectral Analysis and Time Series*, Academic Press, 1987.
75. Proakis, J., *Digital communications*, McGraw Hill, 1989.
76. Qureshi, S. U. H., "Adaptive Equalization," *Proc. of the IEEE*, vol. Vol. 73, No 9, pp. 1349-1387, Sept. 1985.
77. Sakai, H. and H. Tokumaru, "Statistical Properties of Multivariate Autoregressive Spectral Analysis," *Proc. IFAC 8th Triennial World Congress*, vol. 1, pp. 707-712, Kyoto, Japan, 24-28, Aug, 1981.
78. Sakai, H. and H. Tokumaru, "Statistical Properties of Coherence and Power Contribution Ratios via Multivariate Autoregressive Modeling," *ICASSP 85, Proceedings*, vol. 2, pp. 628-631, IEEE, Tampa, Florida, 26-29 March, 1985.
79. Scally, D. R., D. E. Ryerson, and T. L. Towles, "Acoustic Telemetry in an Automated System for Long-Term Ocean Data in Real Time," *OCEAN 84*, vol. 2, pp. 748-751, IEEE, Washington,D.C., Sep. 10-12 1984.
80. Scannel, E. H. and G. C. Carter, "Confidence Bound for Magnitude Squared Coherence Estimates," *IEEE Trans. on ASSP*, vol. ASSP 26, No 5, pp. 475-477, Oct. 1978.
81. Schwartz, M., W. Bennet, and S. Stein, *Communication systems and techniques*, McGraw Hill, 1966.

82. Spilker, J. J., *Digital Communication by Satellite*, Prentice-Hall, 1977.
83. Stearns, S. D., "Error surfaces of recursive adaptive filters. ( Special issue on adaptive Systems)," *IEEE Trans, Circuits Syst.*, vol. vol. CAS-28, 1981.
84. Stein, S., "Fading channels issues in system engineering," *IEEE Journal on Selected Areas in Communication*, vol. SAC-5, No 2, pp. 68-89, Feb. 1987.
85. Urick, R. J., *Principles of Underwater sound*, McGraw Hill, 1983. 3d edition
86. Urkowitz, H., *Signal theory and random processes*, p. 331, Artech House, 1983.
87. Wainwright, R. A., "On the Potential Advantege of a Smearing-Desmearing Filter Technique in Overcoming Impulse-Noise Problems in Data Systems," *IRE Trans. on Communication Syst.*, pp. 362-366, Dec. 1961.
88. Wax, D. W., "MFSK - The Basic For Robust Acoustical Communication," *OCEANS 81*, pp. 61-66, IEEE, Boston, Massachusetts. Sep. 16-18 1981.
89. Wax, M., "Order Selection for AR Models by Predictive Least Squares," *IEEE Trans. on ASSP*, vol. 36, No 4, pp. 581-588, April 1988.
90. Weinberg, H., "Generic Sonar Model," *NUSC Technical Document 5971D*, Naval Underwater Systems Center, Newport, Rhode Island/New London, Connecticut, June 6 1985.
91. Widrow, B. and M. E. Hoff, "Adaptive Switching circuits," *IRE WESCON Conv. Rec.*, pp. 96-104, 1960.
92. Widrow, B. and S. D. Stearns, *Adaptive Signal Processing*, Prentice-Hall, Englewood Cliffs, N.J, 1985.
93. Winkler, M. R., "Chirp Signals for Communication," *IEEE WESCON*, p. 14.2, Los Angeles, Aug. 21-24, 1962.
94. Wintz, P. A. and E. J. Luecke, "Performance of Optimum and Suboptimum Synchronizers," *IEEE Trans. on Communication Technology*, vol. com-17, No 3, pp. 380-389, June 1969.
95. Youn, Dae Hee, N. Ahmed, and G. C. Carter, "Magnitude Squared Coherence Function Estimation An Adaptive Approach," *IEEE Trans. on ASSP*, vol. ASSP 31, No 1, pp. 137-142, Feb. 1983.
96. Zaytsev, D. L. and V. I. Zhuravlev, "Noise Immunity of Digital Data System Using Linearly Frequency-Modulated Signals," *Telecommunication*,

vol. 22. No 4, pp. 13-17, 1968.

97. Ziemer, R. E. and R. L. Peterson, *Digital Communication and Spread Spectrum Systems*, MacMillan, New York, 1985.

## ONR/MPL GENERAL DISTRIBUTION LIST

Chief of Naval Research  
Department of the Navy  
Arlington, Virginia 22217-5000  
Code 12, 122(2), 125  
1121, 112, 1122,  
1123, 1125, 1125 OA,  
1125 GG, 23

ONRDET  
Stennis Space Center  
Bay St. Louis, Mississippi 39529-5004  
Code 125

Commander  
Naval Sea Systems Command  
Washington, D. C. 20362  
Code 63DB, 933A

Commanding Officer  
Naval Ocean Research and  
Development Activity  
Stennis Space Center  
Bay St. Louis, Mississippi 39529-5004  
Code 100, 110, 300, 330,  
200, 220, 240, 250, 270,  
320, 360, 350

Commander  
U.S. Naval Oceanographic Office  
NSTL Station  
Bay St. Louis, Mississippi 39522-5004  
Attn: Bill Jobst

Assistant Secretary of the Navy  
(Research Engineering & Systems)  
Department of the Navy  
Washington, D. C. 20350

Defense Advanced Res. Proj. Agency  
TTO - Tactical Technology Office  
1400 Wilson Boulevard  
Arlington, Virginia 22209-2308  
Attn: John N. Entzminger

National Oceanic & Atmospheric  
Administration  
Ocean Engineering Office  
6001 Executive Boulevard  
Rockville, Maryland 20852

Commander  
Space and Naval Warfare  
Systems Command  
Washington, D. C. 20360-5100  
Code PMW-180T, PMW-180-S

Commander  
Naval Ship Res. & Dev. Center  
Bethesda, Maryland 20084

Executive Secretary  
Naval Studies Board  
National Academy of Sciences  
2101 Constitution Avenue, N.W.  
Washington, D.C. 20418

Director  
Strategic Systems Proj. Ofc.  
Department of the Navy  
Washington, D. C. 20361  
Code NSP-20

Commander  
Naval Ocean Systems Center  
San Diego, California 92152  
Code 00, 01, 16, 94,  
54, 541, 605, 71, 72, 701

Commander  
Submarine Development Group ONE  
139 Sylvester Road  
San Diego, California 92106

Commanding Officer  
Civil Engineering Laboratory  
Naval Construction Battalion Center  
Port Hueneme, California 93043  
Code L40, L42

Commanding Officer  
Naval Underwater Systems Center  
Newport, Rhode Island 02844  
Attn: E.L. Sullivan

Officer in Charge  
Naval Underwater Systems Center  
New London Laboratory  
New London, Connecticut 06320  
Code 900, 905, 910, 930, 960

Director of Research  
U.S. Naval Research Laboratory  
Washington, D. C. 20375  
Code 2620, 2627, 5000, 5100, 5800

Officer in Charge  
Naval Surface Warfare Center  
10901 New Hampshire Avenue  
White Oak Laboratory Detachment  
Silver Spring, Maryland 20903-5000  
Attn: E232 Tech Library

Commanding Officer  
Naval Coastal Systems Laboratory  
Panama City, Florida 32401

STOIA  
Battelle Columbus Laboratories  
505 King Avenue  
Columbus, Ohio 43201

Commander  
Naval Air Systems Command  
Washington, D. C. 20361  
Code 370

Commanding Officer  
U.S. Naval Air Development Center  
Attention: Bruce Steinberg  
Warminster, Pennsylvania 18974

Director  
Defense Documentation Center  
(TIMA), Cameron Station  
5010 Duke Street  
Alexandria, Virginia 22314

Institute for Defense Analyses  
1801 North Beaugard Street  
Arlington, Virginia 22311

Superintendent  
U.S. Naval Postgraduate School  
Monterey, California 93940

Chief Scientist  
Navy Underwater Sound Reference Div.  
U.S. Naval Research Laboratory  
P.O. Box 8337  
Orlando, Florida 32806

Supreme Allied Commander  
U.S. Atlantic Fleet  
ASW Research Center, APO  
New York, New York 09019  
Via: ONR 100 M, CNO OP092D1,  
Secretariat of Military,  
Information Control, Committee

Director  
Institute of Marine Science  
University of Alaska  
Fairbanks, Alaska 99701

Director  
Applied Physics Laboratory  
Johns Hopkins University  
Johns Hopkins Road  
Laurel, Maryland 20810  
Attn: J. R. Austin

Director  
College of Engineering  
Department of Ocean Engineering  
Florida Atlantic University  
Boca Raton, Florida 33431

Director  
Marine Research Laboratories  
c/o Marine Studies Center  
University of Wisconsin  
Madison, Wisconsin 53706

Director  
Applied Research Laboratory  
Pennsylvania State University  
P.O. Box 30  
State College, Pennsylvania 16802

Director  
Applied Physics Laboratory  
University of Washington  
1013 NE 40th Street  
Seattle, Washington 98195

Director  
The Univ. of Texas at Austin  
Applied Research Laboratory  
P.O. Box 8029  
Austin, Texas 78712

Director  
Lamont-Doherty Geological Observatory  
Torrey Cliff  
Palisades, New York 10964

Director  
Woods Hole Oceanographic Institution  
Woods Hole, Massachusetts 02543

Director  
Inst. of Ocean Science Engineering  
Catholic University of America  
Washington, D.C. 20017

National Science Foundation  
Ocean Sciences Division  
Washington, D. C. 20550

Office of Naval Research  
Resident Representative  
c/o Univ. of California, San Diego  
Mail Code 0023  
La Jolla, California 92093

University of California, San Diego  
Marine Physical Laboratory  
Branch Office  
La Jolla, California 92093